YAEC-1126

MITNE-194

MASSACHUSETTS INSTITUTE OF TECHNOLOGY

DEPARTMENT OF NUCLEAR ENGINEERING

CAMBRIDGE, MASSACHUSETTS 02139

REACTOR PHYSICS CALCULATION OF BWR FUEL BUNDLES CONTAINING GADOLINIA

BY

Diego Morales
David D. Lanning
Edward E. Pilat*

January 1977

* Yankee Atomic Electric Company

REACTOR PHYSICS CALCULATION OF BWR FUEL BUNDLES CONTAINING GADOLINIA

by

Diego Morales
David D. Lanning
Edward E. Pilat

Abstract

A technique for the calculation of the neutronic behavior of BWR fuel bundles has been developed and applied to a Vermont Yankee fuel bundle. The technique is based on a diffusion theory treatment of the bundle, with parameters for gadolinia bearing pins generated by transport theory, and converted to effective diffusion theory values by means of blackness theory. The method has been used to examine the dependence of various bundle average parameters on control rod insertion history.

ACKNOWLEDGEMENTS

The work described in this report has been performed primarily by the principal author, D. E. Morales, who has submitted substantially the same report as partial fulfillment of the requirements for the degree of Master of Science in Nuclear Engineering at MIT.

The principal author would like to especially thank those most responsible for organizing the project, namely Professor David Lanning and Dr. Edward E. Pilat. Their advice and guidance were invaluable throughout this work.

The project was developed with and supported by the Yankee Atomic Electric Company. Sincere thanks is given to the Yankee Reactor Physics Group for their help, especially D. VerPlanck, R. Cacciapouti, G. Solan, D. Denver, and A. Sarja.

Special thanks to NUS Corporation for supplying the NUCELL computer code and to Yankee for the CHIMP program.

Thanks to G. Shea for his technical assistance and D. Mulkern and N. Kelley for typing.

The principal author deeply appreciates the support of Ibernuclear, S.A. Madrid for his masters work at MIT.

TABLE OF CONTENTS

Table of Contents
(continued)

LIST OF TABLES

LIST OF FIGURES

LIST OF FIGURES

(continued)

LIST OF FIGURES

(continued)

1.0 INTRODUCTION AND OBJECTIVES

The analysis of boiling water reactors for core follow and licensing is based on reactor physics calculations to determine gross power distributions, local power distributions, and control rod worths. The initial step in all these analyses is development of a calculational model to predict the reactor physics behavior of individual BWR fuel bundles. This task is considerably more complicated than the corresponding task for PWR bundles because:

- BWR bundles contain several groups of fuel rods, differing in enrichment, compared to the generally identical enrichments used for the rods in PWR bundles.
- BWR bundles contain water slots around the outside, to allow space for the insertion of cruciform control rods. This causes considerably more spatial inhomogeneity than in PWR bundles, where individual control rodlets which replace fuel rods are distributed nearly uniformly throughout the bundle.
- BWR bundles usually include several fuel rods which contain gadolinia as a burnable poison. The gadolinia is a much stronger poison than the boron typically used in PWR's, and it requires a true transport theory analysis to predict its neutronic behavior correctly.

For these reasons, the neutronic analysis of BWR fuel bundles is often based on methods which are time consuming, require elaborate computer codes, and are expensive.

The objective of this work is to develop a method which yields reasonable accuracy in predicting the neutronic behavior of BWR fuel bundles at a minimum of complication and expense. It was therefore decided

to use only existing computer codes. This method allows the calculation of the following bundle characteristics as a function of bundle burnup:

- Infinite multiplication factor, k_∞, for the whole bundle, with the control rod either inserted or removed.
- Local (rod by rod) relative power distribution within the bundle, with the control rod inserted or removed.
- Bundle isotopics, the concentrations of fissile and fertile isotopes.
- Few group, flux weighted diffusion parameters for the bundle.

The method has been demonstated and tested by application to one of the fuel bundle types in use at the Vermont Yankee boiling water power plant. The licensing docket for this plant provides data with which local power peaking results can be compared. Private discussions with Vermont Yankee personnel indicate that results for values of k_∞ and isotopics are also reasonable. The actual demonstration was performed using a so-called 8D219 bundle (described in Chapter 2), at a constant void fraction of 40%. This is sufficient to demonstrate the usefulness of the methods described herein. More complex situations can be analyzed by obvious extensions of the same methods.

2.0 OUTLINE OF DATA AND METHODS

2.1 Description of the Fuel Bundle

The subject of this report is a BWR fuel bundle consisting of a square 8 x 8 array of fuel rods having an average enrichment of 2.19 w/o U-235. Each fuel rod consists of UO_2 pellets encased in a zircaloy cladding. The dimensions, constituents and operating conditions are shown in Table 2-1 and Figure 2-1.

There is one control rod for each four fuel bundles. The dimensions and constituents of the control rods are given in Table 2-2.

2.2 Outline of Methods

Figure 2-2 is a flow chart outline of the methods used here. The calculation of bundle neutronic behavior is carred out with the PDQ-7 multigroup diffusion program. This requires input in the form of diffusion theory parameters for each unit fuel cell, and for the non-fuel regions of the bundle. In this representation, each fuel cell is treated as a homogeneous region whose cross sections have been adjusted to account for the actual heterogenities present in the cell. By means of the HARMONY program, cross sections are used in tabular form, as a function of local fuel rod burnup. Cross sections for regions other than fuel cells are constant (Chapter 3 contains computer code descriptions and references).

The preparation of unit fuel cell cross sections for use in the diffusion calculation takes two different forms, depending on whether or not gadolinia is present. When gadolinia is not present, flux weighted cross sections are obtained directly from the LEOPARD program using unit cell depletions in which the neutron spectrum is recomputed at each time step. These cross sections are processed by the CHIMP program into the proper form for use by HARMONY.

When gadolinia is present, the NUCELL version of the LASER program is used, as it accounts more accurately for the spatial inhomogeneities which occur within the gadolinia bearing fuel rod. Again, depletions are performed in which the neutron spectrum is recomputed at each time step. Because the gadolinia causes a large flux dip in the fuel pin, the resulting flux weighted cross sections are adjusted using blackness theory so that they yield the correct reaction rates when used in a diffusion theory calculation, and are then converted manually to the proper HARMONY format.

Cross sections for control rods are obtained from blackness theory as implemented in the RODWORTH program. This requires that the control rod be treated as a slab, but subsequent corrections are made based on measured data to account for the actual "picket fence" nature of the control rod.

TABLE 2-1

8D219 FUEL BUNDLES

Fuel Assembly	
Geometry	8 x 8
Rod Pitch (in.)	0.640
Water to Fuel Volume Ratio	2.60
Heat Transfer Area (ft^2)	97.6
Weight of UO_2 (Kg)	207.9
Weight of U (Kg)	183.3
Average Enrichment (w/o U-235)	2.19
Fuel Rods	
Active Fuel Length (in.)	144.0
Gas Plenum Length (in.)	16
Fill Gas	helium
Fuel	
Material	sintered UO_2
Pellet Diameter (in.)	0.416
Pellet Length (in.)	0.420
Pellet Immersion Density (% TD)	95.0
Stack Density (%TD)	~94.0
Cladding	
Material	Zr-2
Outside Diameter (in.)	0.493
Thickness (in.)	0.034
Water Rod	
Material	Zr-2
Outside Diameter (in.)	0.493
Thickness	0.034
Spacers	
Material	Zr-4 with Inconel X-750 Springs
Number per Bundle	7
Fuel Channel	
Material	Zr-4
Outside Dimension (in.)	5.438
Wall Thickness (in.)	0.080

Table 2-1 (continued)

Operating Conditions

Core Average Pressure (psia)	1032
Core Inlet Enthalpy (btu/lb)	519.8
Core Inlet Temperature (^{o}F)	526.5
Average Power per Assembly (Mwt)	4.329

TABLE 2-2

MOVABLE CONTROL RODS

Shape	Cruciform
Pitch (in.)	12.0
Stroke (in.)	144.
Width (in.)	9.75
Control Length (in.)	143.0
Control Material	B_4C granules in stainless steel tubes and sheath
Number of Control Material Tubes per Rod	84
Tube Dimensions	0.188 in. OD 0.025 in. wall

Figure 2-1 8d219 Fuel Bundle

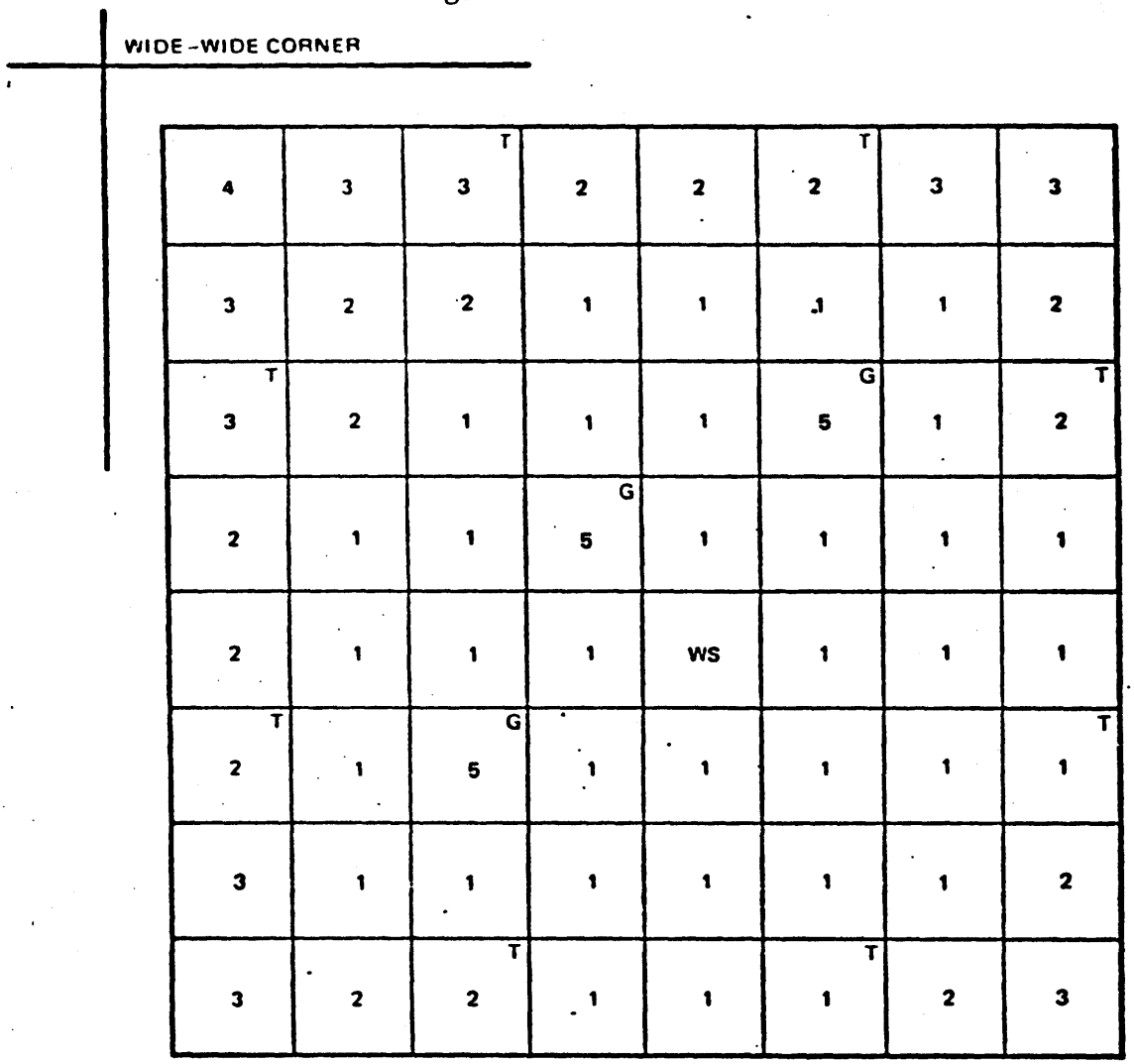

ROD TYPE	ENRICHMENT wt % U-235	NUMBER OF RODS
1	2.50	35
2	1.90	15
3	1.49	9
4	1.18	1
5	2.50	3
WS	–	1

WS – SPACER CAPTURE WATER ROD
T – TIE RODS
G – GADOLINIUM RODS

FIGURE 2-2

CALCULATION FLOW CHART

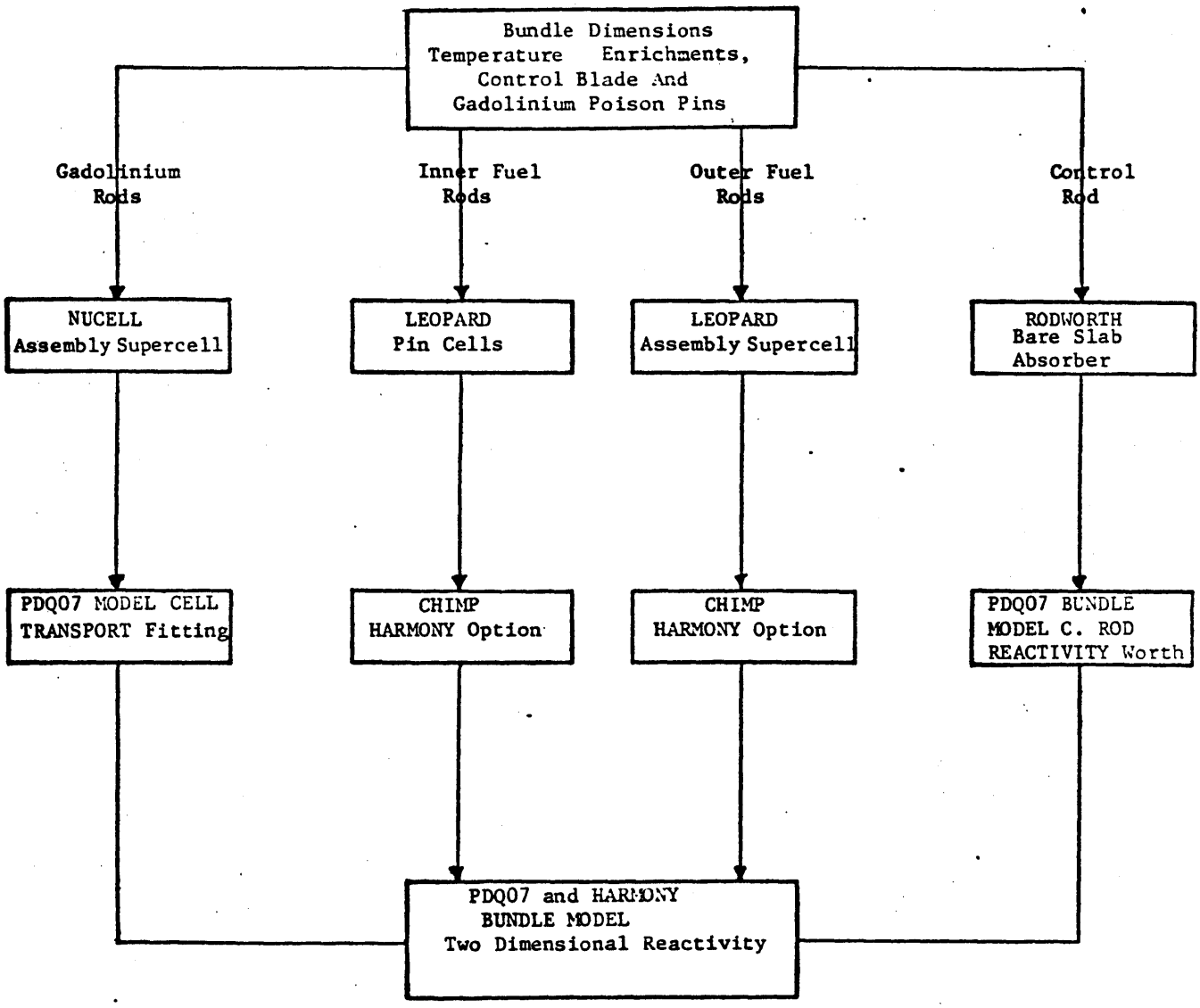

3.0 DESCRIPTION OF COMPUTER CODES

3.1 The LEOPARD Program

LEOPARD[4] is a zero-dimensional criticality and depletion code which determines fast and thermal neutron spectra using a modified MUFT-SOFOCATE [5,6] model. The code performs a multigroup calculation of the space-averaged flux spectrum, assuming that thermal leakage and fast leakage are both adequately represented by a single value of the buckling, B^2. After the spectrum has been calculated, broad group cross sections are evaluated and the value of k_{eff} is determined from them. In order to accurately predict criticality, it is necessary to average the cross sections over the spectrum characteristic of a system in the steady state. In LEOPARD, such a spectrum is obtained by varying the value of the buckling until a k_{eff} of unity results. In practice, this is done only for the nonthermal spectrum, because the thermal spectrum is insensitive to the value of the buckling. If the value of the average power density is known, the code calculates the change in the density of each nuclide present at a number of discrete time steps, and repeats the spectrum calculations at each step so that broad group cross sections are calculated as a function of burnup.

The reactor core is represented as an infinite array of unit cells, each consisting of fuel, cladding, moderator, and an "extra" region which accounts for water slots, followers, and other items in the core that are not part of the fuel unit cells. Cross sections are calculated for four broad energy groups - three fast and one thermal. In the present work, the three fast groups have been combined into one. One hundred seventy-two fine energy groups are used in the

thermal energy range (0 to 0.625 ev) and fifty-four energy groups in the nonthermal range (0.625 ev to 10 mev). Table 3-1 shows the group structure used for the nonthermal calculation. Cross sections for each fine, nonthermal group are computed by volume averaging the actual number densities of the constituents. Such an averaging procedure is valid because the mean free paths for most nonthermal interactions are much larger than the dimensions of any heterogeneous constituent of the system. The only exceptions in which heterogeneity might be important are in the calculation of the fast fission effect and resonance absorption. The heterogeneous contribution to the fast fission effect has been shown to be minor in systems of this type[7].

Resonance absorption in U-238 is treated by using in each fine group a fictitious smooth cross section which is equivalent to the homogeneous resonance integral for that group, and multiplying this by a self-shielding factor, L, to account for the reduction in cross section because of the heterogeneity of the actual system. The self-shielding factor is evaluated on the reasonable assumption that it is independent of the presence or absence of nuclides other than U-238 and H. When these two nuclides are the only ones present, an analytical formula for the resonance escape probability can be written as:[8]

$$P = e^{-\frac{N^{28} I^{28}}{\xi \Sigma_s}} \qquad (3.1)$$

where I^{28} is the heterogenous resonance integral of U-238 corrected for Doppler and Dancoff effects, and N^{28} and $\xi\Sigma_s$ are the homogenized number density of U-238 and the homogenized slowing down power. The self-shielding factor is determined as that value of L which causes a MUFT calculation of the same system (U-238 and H) to give the same value of the resonance escape probability as that resulting from Equation (3.1). The identical self-shielding factor is then used in a final MUFT calculation in which all the proper nuclides are included.

The MUFT calculation provides a solution, accurate to terms of order P1 in a Legendre polynomial expansion, of the equation:

$$\mu \frac{\partial \Phi}{\partial x}(x,u,\mu) + \Sigma(u)\Phi(x,u,\mu) = \int_0^\infty du' \int_{-1}^{1} \frac{d\mu'}{2} \Sigma_s(u',u,\mu_0)\Phi(x,u',\mu') + S_0 \cos Bx \qquad (3.2)$$

This is the Boltzmann equation describing slowing down and spatial transport of neutrons in a bare slab of half-thickness $\frac{\Pi}{2B}$, with a neutron source having a fundamental mode shape. The parameters appearing in Equation (3.2) are:

Φ = angular neutron flux

x = spatial coordinate perpendicular to the face of the slab

μ = cosine of the angle between the x axis and the neutron's direction of travel.

u = lethargy

$\Sigma(u)$ = total cross section at lethargy u

Σ_s (u', u, μ_o) = differential cross section for scattering a neutron from lethargy u' to lethargy u through an angle whose cosine is μ_o.

Implicit in the use of Equation (3.2) is the assumption that the resulting neutron energy spectrum will be nearly the same as that in the actual reactor as long as the correct value of the buckling, B^2, is used, regardless of the actual shape of the region. This approximation is valid for systems of more than a few mean free paths extent.

In the thermal range, the mean free paths are short enough so that cross sections at all energies must be appropriately weighted. It is unnecessary to calculate the spectrum at each point of the cell, since it is desired only to obtain correct values of the total thermal reaction rates averaged over all thermal energies and over the complete unit cell. It suffices to calculate an average spectrum for the cell by using cross sections which have been averaged over the cell according to the relative flux in each constituent of the cell. Weighting factors for the nuclides in the real unit cell are computed at each of the 172 energy groups by the method of Amouyal, Benoist, and Horowitz[9]. An arbitrary group independent weighting factor may be applied to the nuclides in the "extra" region to account for flux peaking (or dipping) there. The flux weighted cross sections are used in the SOFOCATE code to obtain an average spectrum in the cell based on the assumption that the scattering properties of the moderator are adequately represented by those of a monatomic gas. The equations describing this situation were first derived by Wigner and Wilkins,[10] who showed that the equation describing the neutron

thermalization was reducible to a second order, differential equation. The solution of this equation is provided by the SOFOCATE program. Although the effect of chemical binding in the H_2O molecule is neglected in the Wigner-Wilkins formalism, the resulting reaction rates and disadvantage factors agree very well[7] with the values predicted by more sophisticated models such as THERMOS. This occurs because the Wigner-Wilkins scattering model simultaneously underestimates the total scattering cross section and overestimates the energy transfer, with the result that simultaneous averages over both space and energy are well predicted.[11]

The output parameters available from LEOPARD include:

- Value of the resonance escape probability;
- Values of microscopic cross sections for transport, absorption, removal, and fission for each broad energy group for each element;
- Values of relative thermal and nonthermal absorption rates in each element;
- Values of the diffusion coefficient and macroscopic cross sections for removal, absorption, and fission in each broad group;
- Values of the thermal self-shielding factor for each nuclide.

3.2 The NUCELL Program

3.2.1 General Description

NUCELL is a one-dimensional (cylindrical), multi-energy (50 fast and 35 thermal) lattice program that is based on the MUFT and THERMOS codes and has capabilities of criticality search and depletion. It is

an improved and expanded version of the LASER program which was originally developed by C. G. Poncelet.

Following is the list of improvements and modifications that have been incorporated into the LASER program by NUS corporation in generating NUCELL:

1. The maximum allowable value for the total space points is 24, and the maximum allowable space points in fuel region is 10.
2. A non-lattice region (non-depletable) containing U-235, U-238, Pu-239, H(or D) O, and Zr (or SS or Al) can be specified next to the moderator region.
3. Variable mesh spacings can be used for each material region by assigning more than one geometrical region. A total of up to 20 geometrical regions can be assigned to the cell.
4. The burnup step length can be varied from step to step.
5. Gd-155 and Gd-157 can be present in the fuel region as burnable poisons.
6. Adjustment of thermal neutron flux to simulate a critical condition at each burnup step without time consuming buckling or poison search.
7. Use of the previously converged thermal neutron fluxes as initial flux guess for succeeding burnup steps or for poison search iterations.
8. Calculation and edit of average microscopic cross sections and associated thermal disadvantage factors (more precisely, G factors) separately for pure cell and super cell).
9. The built-in maximum allowable number for THERMOS iteration was changed to 250 and 300 (from 150 and 200) for the iteration with

extrapolation and the iteration without extrapolation, respectively. A summary of iteration data is printed for each THERMOS iteration instead of the final iteration only.

10. Listing input data as they appear in the input data cards.

For the detailed description of theory in NUCELL and LASER, the code user must refer to Reference 12.

The MUFT code used for non-thermal calculations in the NUCELL code is essentially identical to that in the LEOPARD code.

3.2.2 Thermal Calculations in NUCELL

The space-dependent thermal neutron spectrum is calculated with THERMOS.[13] THERMOS computes the scalar neutron flux as a function of energy and position in a lattice by solving numerically the multi-thermal-group integral transport equation for isotropic scattering:

$$v\,N(\bar{r},v) = \int T(\bar{r},\bar{r}',v)\; H(\bar{r}',v)\; d\bar{r}' \tag{3.3}$$

$$H(\bar{r}',v) = S(\bar{r}',v) + \int_0^{v^*} P(\bar{r}',v,v')\; N(\bar{r}',v')\,dv' \tag{3.4}$$

In these equations, N ($\bar{r}$, v) is the neutron density, T ($\bar{r}$, $\bar{r}'$, v) is the transport kernel, P ($\bar{r}$, v, v') is the scattering kernel, S ($\bar{r}$, v) is the slowing down source, and v* is the velocity corresponding to the cutoff energy for the thermal region. The above equations are converted to a matrix form by dividing the $\bar{r}$ space into k finite volumes, V_n, and the velocity space into j discrete points, v_i. In matrix form:

$$N_{ni} = \sum_k T_{nki}\; H'_{ki} \tag{3.5}$$

$$H'_{ki} = S'_{ki} + \sum_j P'_{kij} N_{kj} \qquad (3.6)$$

where the primes indicate that the quantities have been divided by v. The transport kernel T_{nki} is defined as the average uncollided flux of neutrons of velocity v_i in the volume V_n due to a uniform volumetric source of neutrons of velocity v_i uniformly distributed in a volume V_k. In slab geometry, the transport kernel is simply expressed in terms of exponential integrals. In cylindrical geometry, the kernels are computed by a numerical ray-tracing procedure. Only cell type (reflecting) boundary conditions are available.

The scattering kernels used in THERMOS are defined by

$$P_n(v' \to v) = 2k_o T_o v v' \Sigma_{sn}(E' \to E) \qquad (3.7)$$

$$\Sigma_{sn}(E' \to E) = 2\pi \int_{-1}^{1} \Sigma_s(E' \to E, \mu) P_n(\mu) d\mu \qquad (3.8)$$

where $kT_o = 0.0253$ ev

μ is the cosine of the scattering angle

$P_n(\mu)$ is the Legendre polynomial or order n

If the energy of an incident neutron is large compared with the chemical for which at energies below 1 ev, chemical binding causes a rapid increase in the cross section over the constant free atom values. There is a second effect which causes an increase in the scattering cross section for low energy neutrons. This effect is temperature dependent and follows a 1/v law. Due to the thermal motion of the molecules, even zero energy neutrons which are struck by moving molecules can be scattered in spite of the absence of an apparent (laboratory) neutron current. In using THERMOS, it is important that the low energy cross section variation and its

temperature dependence be accurately represented by the scattering kernel employed.

The THERMOS code has been designed to use any tabulated scattering kernel. The frequently used Brown and St. John modified free gas kernel [14] can be calculated by THERMOS. However, to adequately account for the effects of molecular binding on the effective scattering cross section for hydrogen bound in H_2O, use was made of a more refined physical model. This was the modified Nelkin model described by Koppel [15] and calculated by the GAKER code [13].

In the Nelkin [16] model, the motions of hydrogen atoms in water are considered in terms of the H_2O molecule as the basic dynamical unit. It is assumed that a classification of the atomic motions into vibrations, hindered rotations, and hindered translations of the molecule gives an adequate description of the proton motion in the liquid. The approximation is made that the various degrees of freedom carry-out simple harmonic oscillations. The Nelkin model has been very successful in predicting neutron spectra in infinite media of aqueous solutions, but gives too high a value of the scattering cross section at very low energies. For media with large admixtures of absorbing nuclei the experimental spectra are systematically harder than those predicted by the Nelkin model.

In approximating two-dimensional cells by using cylindrical cell geometry with a reflecting outer boundary condition, significant errors can be introduced in calculations of the thermal disadvantage factor. Honeck [17] has pointed out that the desirable boundary condition of isotropic return of neutrons at the cell boundary can be obtained with the existing THERMOS code through the artifice of adding

a heavy scattering region at least two mean free paths thick outside the cylindrical cell and placing the reflecting boundary condition outside this extra region. Although this effect is important only in tightly packed lattices, the heavy scattering region was used for all THERMOS cylindrical cell calculations.

In the THERMOS calculations, a thermal energy group structure with 35 energy groups was used (see Table 3.2). Results were edited over 0.625 ev and 1.855 ev cutoffs.

3.2.3 Definition of Microscopic Cross Sections

The NUCELL output gives several different types of microscopic cross sections. They are listed below:

a. Region-averaged microscopic cross section

$$\overline{\sigma}_R = \int_R (\sigma\phi)_r \, dV_r \Big/ \overline{\phi}_R V_R \qquad (3.9)$$

R: region index

b. Effective microscopic cross section

$$\overline{\sigma}_{eff} = \int_{cell} (\sigma\phi)_r N_r dV_r \Big/ \overline{\phi}_{cell} \overline{N}_{cell} V_{cell} \qquad (3.10)$$

c. Cell average thermal absorption cross section

$$\overline{\sigma}_a = \int_{cell} (\sigma\phi)_r \, dV_r \Big/ \overline{\phi}_{cell} V_{cell} \qquad (3.11)$$

d. Thermal disadvantage factor (G)

$$G = \overline{\sigma}_{eff,a} \Big/ \overline{\sigma}_a \qquad (3.12)$$

3.2.4 Cross Section Library for Gadolinium Isotopes

The fast group microscopic cross sections for natural gadolinium in the MUFT-5 library were divided by the combined abundance of Gd-155 and Gd-157 to obtain equivalent cross sections per atom of Gd-155 and Gd-157. For the thermal group microscopic absorption cross sections for Gd-155 and Gd-157, the resonance data by Moller, Shore and Sailor (Reference 18) were used to calculate the cross sections for individual isotopes. Cross sections for Gd-155 and Gd-157 other than absorption cross sections were set to zero because the concentrations of Gd isotopes for practical cases will be too small to have any significant effect on cell neutron cross sections other than absorption. These calculations were carried out by NUS Corporation.

3.3 The RODWORTH Program

RODWORTH was programmed by United Nuclear Corporation to determine effective few group parameters by blackness theory methods, for use in the diffusion theory representation of control rods.

Given the absorber thickness and boron-10 number density RODWORTH calculates the multigroup values of α and β which account for spatial self-shielding within each of the microgroups. These microgroup values are calculated using the methods in Reference 19.

3.4 The PDQ HARMONY Programs

The eigenvalue or k_∞ for a particular bundle configuration was determined by means of a diffusion theory calculation of one bundle in the horizontal plane. This calculation was done with the PDQ program[20], which solves the few group neutron diffusion equations:

$$-\nabla \cdot D^g(x) \nabla \phi^g(x) + \left[\Sigma_a^g(x) + \Sigma_r^g(x) + D^g(x)(B_T^g)^2\right]\phi^g(x) = \frac{\chi^g}{\lambda}\psi(x) + \Sigma_r^{g-1}(x)\phi^{g-1}(x)$$

$$(g = 1,2) \qquad (3.13)$$

where:

x		represents spatial coordinate
g		represents energy group number
D	=	diffusion coefficient
Σ_a	=	macroscopic absorption cross section
Σ_r	=	macroscopic removal cross section
$(B_T)^2$	=	transverse buckling
χ^g	=	fraction of fission neutrons appearing in energy group g
ϕ	=	neutron flux
λ	=	eigenvalue (k_{eff})
ψ	=	fission source = $\sum_j (\nu\Sigma_f)_j \phi_j$
ν	=	neutrons produced per fission
Σ_t	=	macroscopic cross section for fission
Σ^o	=	0

The region of solution is rectangular and is composed of subregions whose interfaces must be parallel to the outer boundaries

of the rectangle. The solution is obtained at a set of selected points by solving the finite difference equivalent of Equation (3.14). The points are the intersections of a nonuniform grid of mesh lines which is imposed on the rectangular region of solution in such a way that each line is parallel to a boundary of the rectangle and extends from one outer boundary to the opposite boundary. The intervals between mesh lines are chosen so that both the boundaries of the region of solution and the interfaces between subregions exactly coincide with mesh lines. The solution is effected by using the "power method:"[21,22] inner (flux) iterations are accelerated by Chebyshev extrapolation.

The output consists of the eigenvalue (k_{eff}), pointwise power and fluxes over desired regions, and regionwise macroscopic parameters for desired regions. The values of regionwise output parameters are obtained by flux-averaging the pointwise values within the region. The value of the group independent buckling for each region is calculated by equating to zero the determinant of the coefficients of the flux in the set of equations:

$$\left[\overline{D}^g B^2 + \overline{\Sigma}_a^g + \overline{\Sigma}_r^g + \overline{D^g (B_T^g)^2} \right] \phi^g - \frac{\overline{\chi^g \psi}}{\lambda} - \overline{\Sigma}_r^{g-1} \phi^{g-1} = 0 \qquad (g=1,2) \tag{3.14}$$

where:

B^2 = group independent buckling;

A bar over any quantity indicates that it is flux averaged over the region being considered;

All other symbols are defined in the list following Equation (3.13)

Note that a bar over the product of two quantities indicates that the product, rather than each individual quantity, is flux averaged. Equation (3.14) is just Equation (3.13) with the leakage term, $-\nabla \cdot D^g(x)\nabla\phi^g(x)$ replaced by $D^g B^2$. The group dependent buckling is also obtained from equation (3.14), but in this case the equation for each group is solved individually to give a B^2 for each group. For this purpose, the ϕ^g's in Equation (3.14) are replaced by the integral of the flux over the region being considered. Finally, the value of k_∞ is found by putting both B^2 and $(B_t^g)^2$ to zero in Equation (3.14) and then equating to zero the determinant of the coefficients of the fluxes, in which λ is now considered the variable whose value is to be determined. These region-averaged parameters are suitable for use in studies of other aspects of the problem, such as diffusion theory calculations in the axial direction and lifetime analyses of the core.

The HARMONY[23] system enables depletion of the PDQ diffusion theory model. Depletion equations solved by the program are specified by the user. This specification identifies (1) how each nuclide is formed (radioactive decay or capture) from previous nuclides in the chain, (2) whether or not the nuclide is a direct product of the fission process, and (3) how the nuclide is destroyed (radioactive decay and/or absorption).

Any of the cross sections or shielding factors used in the spatial or depletion calculation may be represented as time dependent. This time dependence is attained by representing the cross section as a function of as many as three nuclide concentrations. The dependence on nuclide concentration is attained through the use of interpolating tables.

3.5 The CHIMP Program

The original CHIMP program was written by Yankee Atomic to handle the tremendous amount of number manipulations and input preparation associated with reload core analysis. CHIMP-II is an extensive modification of the original program to automate more of the number transfer from one computer program to another. CHIMP-II is composed of six parts and performs the following:

A. Prepares two-group macroscopic cross sections for the fueled regions of PDQ-7.

B. Prepares two-group macroscopic cross sections for the unfueled regions of PDQ-7.

C. Prepares complete sets of input, including two-group macroscopic cross sections, for FOG(a 1-D diffusion theory code)

D. Prepares complete sets of input, including pellet number densities, for LEOPARD.

E. Prepares microscopic and macroscopic cross section table sets for HARMONY.

F. Prepares the polynomial fit constants for the two-group macroscopic cross sections used in SIMULATE.

The basic cross section and number density information required by CHIMP-II is obtained from LEOPARD. CHIMP-II has the ability to read this information from either cards, tape or disk. The use of tape or disk alleviates the handling of massive input cross section decks. In addition, if the user obtains all the possible punched output from LEOPARD, CHIMP-II can sort through this data to obtain the necessary input for each part.

Only Part E of CHIMP was used in this study. This portion of the CHIMP-II program prepares macroscopic and microscopic cross section tables for HARMONY. The program accepts as input, the microscopic cross sections as punched by LEOPARD. The LEOPARD input to CHIMP-II for each isotope, contains the volume weighted number density, assembly ratio, pin cell and super cell ratios, kappa, fast and thermal nu, the cross section for fast removal, and fast and thermal-MND cross sections for fission, absorption, and transport. From this data, the program can punch HARMONY tables for any of the isotopes contained in LEOPARD.

The program sets up all but the mask cards for a HARMONY table set input. For a specific isotope, the program allows the user to punch cards for any of the tables mentioned below. These tables will contain cross sections only for isotopes the user requests. In turn, the cross sections for each isotope can be assigned to specific tables by the table assignment number.

Table Assignment Number	Table
1	Master Macro
2	Macro Interpolating
3	Master Micro
4	Micro Interpolating
5	Reversed Micro Interpolating

For each group and cross section type, the code will sum over the isotopes, all those cross sections assigned to the master macroscopic table by the table assignment number 1. Each summation (macroscopic cross section) is of the following form:

$$\sum_i N_i G_i \sigma_i^{t,g} \qquad (3.15)$$

i = isotope

N_i = volume weighted number density for i

G_i = the ratio of flux weighted to volume weighted number densities for isotope i (G_i = 1 for fast group). This may be taken from LEOPARD pin cell, LEOPARD supercell or user input.

$\sigma_i^{t,g}$ = the microscopic cross section for i, type t, and group g.

For the macroscopic interpolating tables, the microscopic cross sections at a given burnup are multiplied by the number densities at that burnup. Thermal cross sections are also multiplied by the G factor.

The list of HARMONY and LEOPARD nuclides available is given in Table 3-3.

TABLE 3-1

FAST MICROGROUP STRUCTURE USED IN LEOPARD

Micro-Group Number	Lower Energy (ev)	Lethargy	Lethargy Width
0	10×10^6	0	
1	7.79	0.25	0.25
2	6.07	0.50	
3	4.72	0.75	
4	3.68	1.00	
5	2.86	1.25	
6	2.23	1.50	
7	1.74	1.75	
8	1.35	2.00	
9	1.05	2.25	
10	821×10^3	2.50	
11	639	2.75	
12	498	3.00	
13	387	3.25	
14	302	3.50	
15	235	3.75	
16	183	4.00	
17	143	4.25	
18	111	4.50	
19	86.5	4.75	
20	67.4	5.00	0.25
21	40.9	5.50	0.50
22	24.8	6.00	
23	15.0	6.50	
24	9.12	7.00	
25	5.53	7.50	
26	3.35	8.00	
27	2.03	8.50	
28	1.23	9.00	
29	750	9.50	
30	454	10.00	
31	275	10.50	
32	167	11.00	0.50
33	130	11.25	0.25
34	101	11.50	
35	78.7	11.75	
36	61.3	12.00	
37	47.8	12.25	0.25
38	37.2	12.50	
39	29.0	12.75	
40	22.6	13.00	
41	17.6	13.25	
42	13.7	13.50	
43	10.7	13.75	
44	8.32	14.00	

Table 3-1 (Continued)

45	6.50	14.25	
46	5.10	14.50	
47	3.97	14.75	
48	3.06	15.00	
49	2.38	15.25	
50	1.855	15.50	0.25
51	1.440	15.7538	0.2538
52	1.125	16.00	0.2462
53	0.835	16.30	0.3000
54	0.625	16.5884	0.2884

TABLE 3-2

NUCELL Thermal Energy Mesh

i	Speed[a] v_i	Mesh Width[a] Δv_i	Energy E_I (ev)	E_{int} (ev)
1	.2	.2	.001012	.002277
2	.4	.2	.004048	.006325
3	.6	.2	.009108	.012397
4	.8	.2	.016192	.020493
5	1.0	.2	.0253	.030613
6	1.2	.2	.036432	.042757
7	1.4	.2	.049588	.056925
8	1.65	.3	.068879	.081972
9	1.95	.3	.096203	.11157
10	2.25	.3	.12808	.14573
11	2.55	.3	.16451	.18444
12	2.85	.3	.20550	.22770
13	3.075	.15	.23923	.25104
14	3.21	.12	.26069	.27053
15	3.33	.12	.28055	.29075
16	3.42	.06	.29592	.30113
17	3.505	.11	.31081	.32064
18	3.66	.2	.33891	.35768
19	3.91	.3	.38679	.41704
20	4.26	.4	.45913	.50326
21	4.715	.51	.56245	.62493
22	5.265	.59	.70132	.78211
23	5.845	.57	.86435	.95070
24	6.23	.2	.98197	1.01374
25	6.275	.09	1.02821	1.04277
26	6.435	.03	1.04765	1.05254
27	6.465	.03	1.05744	1.06236
28	6.495	.03	1.06728	1.07222
29	6.55	.08	1.08543	1.09873
30	6.69	.2	1.13233	1.16645
31	6.99	.4	1.23616	1.30791
32	7.39	.4	1.38169	1.45748
33	7.765	.35	1.52547	1.59500
34	8.10	.32	1.65993	1.72616
35	8.41135	.3027	1.79000	1.85500

a unit = 2200 m/sec

TABLE 3-3

HARMONY AND LEOPARD NUCLIDES

HARMONY INDEX	LEOPARD INDEX	ELEMENT
1	1	Hydrogen
2	2	Oxygen
3	3	Zirconium-2
4	4	Carbon
6	6	Iron
7	7	Nickel
9	9	Aluminum
11	11	Chromium
15	15	Manganese
235	18	Uranium-235
236	19	Uranium-236
238	20	Uranium-238
239	21	Plutonium-239
240	22	Plutonium-240
241	23	Plutonium-241
1492	26	Samarium-149
1352	27	Xenon-135
900	28	Fission Prd.
29	29	Boron-10
37	38	Deuterium
232	62	Thorium-232
65	65	Protactinum-233
233	50	Uranium-233
234	51	Uranium-234
242	24	Plutonium-242

4.0 TREATMENT OF NON-GADOLINIA BEARING FUEL

4.1 Introduction

Input parameters for these cells were obtained by considering two different treatments in LEOPARD, one for the twenty eight outer fuel cells (more affected by the water of the water gap) and another for the thirty two (thirty five minus three gadolinia bearing fuel cells) inner fuel cells, with a harder thermal spectrum which results from being more than one mean free path away from the water gap.

4.2 LEOPARD Treatment for the Outer Fuel Cells

For the outer fuel cells, separate LEOPARD assembly supercell problems were run for each enrichment. The supercell consisted of a central pin cell with the pitch, pellet outer diameter, and clad thickness typical of the bundle and a moderator of water at 40% void fraction. The extra (non-lattice) region of the supercell was assumed to consist of 1/63 of the gap water, Zr-4 channel, voided film water and water tube (containing water, Zr clad and void). With these LEOPARD supercell problems, a good representation for the fast spectrum and a reasonable representation for the complicated softer thermal spectrum of these fuel cells is obtained.

From the fuel pin cell edit of these problems, two group cross sections (MND cross sections for the thermal range) were obtained for each of the four enrichments used in these 28 outer fuel cells. The removal cross section was obtained from a special removal treatment developed in this study and shown later.

4.3 LEOPARD Treatment for the Inner Fuel Cells

For the inner fuel cells, two LEOPARD problems were run, one for each enrichment. The cell representation is the same as for the outer pin cell of the supercell problems.

With these LEOPARD cell problems a good representation of the harder thermal spectrum of these fuel cells is obtained. The effect of using the fast cross sections from this cell model which neglects the extra region has been found to be small when the special removal treatment is applied.

4.4 Options Used

In all the LEOPARD problems, the material buckling was searched to simulate the burnup of the fuel with a critical spectrum. Additionally, the U-238 L factor for a square cell was searched to obtain the proper U-238 absorption. The power density (watts/cc) was input based on the average w/cm per rod (187.8706) and the problem volume (cell or supercell). In all LEOPARD depletions, regular time steps of 2000 MWD/MTU were used to reach 36,000 MWD/MTU. These regular time steps were preceded by two steps of 50 and one of 400 MWD/MTU (to accurately represent the Xe-135 and Sm-149 buildup), one of 500 and one of 1000 MWD/MTU to reach the first 2000 MWD/MTU condition. Number densities, two-group macroscopic and microscopic cross-sections from selected LEOPARD burnup steps were stored on disk to be used as CHIMP input to obtain PDQ tablesets.

4.5 Non-Lattice Peaking Factor Calculation

To account for the higher thermal flux in the bundle non-fuel regions than in the fuel regions, LEOPARD allows the user to input the ratio of the average thermal flux value in the extra region to that in the moderator of the unit cell i.e., NLPF = $(\phi \text{ extra}/\phi \text{ mod})^{TH}$.

To estimate a bundle average NLPF for use in the LEOPARD assembly supercell problems, a PDQ bundle calculation without gadolinia and at BOL conditions was run. The fuel cross-sections were obtained from the LEOPARD treatment described above, using an estimated NLPF of 1.35. From PDQ non-fuel region and fuel region edits, the ratio $(\overline{\phi}\text{extra}/\overline{\phi}\text{ fuel})$ was determined to be 1.500 for the thermal flux. Then, the NLPF was determined as follows:

$$NLPF = \frac{\overline{\phi}_{extra}}{\overline{\phi}_{mod}} = \frac{\overline{\phi}_{extra}}{\overline{\phi}_{fuel}} \cdot \frac{\overline{\phi}_{fuel}}{\overline{\phi}_{mod}}$$

$$\simeq \frac{\overline{\phi}_{extra}}{\overline{\phi}_{fuel}} \cdot \frac{1}{G_c^{Ni}} = 1.423 \qquad (4.1)$$

where $\overline{\phi}\text{extra}/\overline{\phi}\text{fuel} = 1.500$ and G_c^{Ni} is the cell edit of the ABH disadvantage factor for nuclide i obtained from a LEOPARD assembly 2.19 w/o supercell, 40% void with only a sample of nuclide i in the moderator region (volume fraction in the moderator equal to 0.000001) and NLPF = 1.35.

The following conclusion was obtained from NLPF sensitivity studies performed with LEOPARD assembly supercells:

At BOL and depletion conditions, the fuel cell average two group macroscopic cross-sections (MND scheme) do not depend on the NLPF used.

Then, the average bundle NLPF was used in all the LEOPARD supercell calculations for BOL and depletion conditions.

4.6 Representation of Cross Sections for Lumped Fission Products

In LEOPARD, the cross sections for the lumped fission products are represented by a polynomial function of burnup. The Yankee Atomic LEOPARD version allows one to input the coefficients of the polynomials. These coefficients were obtained from data published by Celnik[24] for the pseudo fission product thermal and epithermal cross sections as a function of burnup for typical water moderated power reactors. Celnik states that for a UO_2 fueled BWR:

a) the thermal fission product cross section is increased by 20% when the average void content is increased from 0 to 60 vol %. The fission product epithermal cross section after 10,000 MWD/MTU exposure is decreased by 5% for this same variation.

b) The cumulative reactivity worth of fission products at 25,000 MWD/MTU is 11.2% $\Delta K_\infty/K_\infty$,

Thus, a correct fission-product cross section representation is essential.

Table 4-1 compares the design of the BWR fuel used to obtain the fission product cross sections in Reference 24 with the design of the fuel calculated here.

As the average enrichment and the water to metal ratio are very similar (independent of voids and power density) the Celnik plots were used to compute the following polynomial fits by using a standard

least square curve fitting procedure which is included in the CHIMP II program:

$$\bar{\sigma}_a^{MND} = A_0 + A_1X + A_2X^2 + A_3X^3 \qquad (X = \text{burnup}) \quad (10^3 \text{MWD/MT})$$

$$A_0 = 98.3202 \qquad A_2 = 0.0615938$$
$$A_1 = -2.77998 \qquad A_3 = -0.000557621 \qquad (4.2)$$

$$\bar{\sigma}_a^{3/3} = B_0 + B_1X + B_2X^2$$

$$B_0 = 26.1813 \qquad B_2 = 0.00277768$$
$$B_1 = -0.325141 \qquad (4.3)$$

where $\bar{\sigma}_a^{MND}$ = 2200 m/sec absorption cross section of the pseudo fission product (standard deviation 0.25244)

$\bar{\sigma}_a^{3/3}$ = constant epithermal absorption cross section of the pseudo fission product (standard deviation 0.13834)

Figures 4-1 and 4-2 show the pseudo fission product polynomial fits used in this study.

4.7 Removal Cross-Section Treatment

Since the distance a fast neutron travels from the point at which it is born until it becomes thermalized is on the order of the assembly dimensions, the fast group cross-sections should be generated with a spectrum representative of the fuel bundle and its associated non-fuel regions. To simulate this spectrum, LEOPARD supercell problems for every enrichment can be run to obtain fast cross sections, but as stated before, separate LEOPARD cell problems were run to obtain fast and thermal cross sections for the inner fuel cells

only, giving in this way more importance to the simulation of their harder thermal spectrum.

However, the error involved in this procedure of obtaining fast cross sections for the inner fuel cells has been found to be small when the removal cross sections for all the fuel cells were computed by using the LEOPARD supercell model. This means that the slowing down of the neutrons throughout the bundle is very dependent on the amount of water (or H) associated with the bundle.

Two treatments for computing removal cross sections for the fuel cells have been used in this study, both based on matching the assembly supercell removal cross section calculated with the converged MUFT spectrum.

4.7.1 Treatment 1 (Spatial Removal Treatment)

This treatment is based on the following three facts:

a) The slowing down of the neutrons within the bundle is a very strong function of the amount of water associated with the bundle.

b) Neutrons in their slowing down process (especially those on the verge of being thermalized) scatter mostly with hydrogen.

c) A good computation of the bundle removal cross section can be performed by running a LEOPARD assembly supercell 2.19% (average enrichment) at 40% voids (because this problem has the right water and the MUFT treatment simulates very well the fast spectrum).

Defining fast microscopic effective removal cross-sections for the isotopes contained in this LEOPARD assembly supercell (2.19% at 40%) as follows:

$$\sigma^{H}_{r,eff} = \Sigma_{rs} / N^{H}_{s} \quad \text{and} \tag{4.4}$$

$$\sigma_r^{j} = 0 \qquad \text{for all other isotopes } j \tag{4.5}$$

Then, the macroscopic removal cross section Σ_{rc} for a unit cell is:

$$\Sigma_{rc} = N^{H}_{c}\, \sigma^{H}_{r,eff} = \Sigma_{rs} \left(\frac{N^{H}_{c}}{N^{H}_{s}} \right) \tag{4.6}$$

where N^{H}_{c} is the cell average number density for hydrogen and Σ_{rs} is the macroscopic removal cross section obtained from MUFT supercell calculations.

4.7.2 Treatment 2

The calculation of the removal cross section for the fuel cell in LEOPARD can be based on the assumption that the microscopic removal cross-section for all constituents except hydrogen can be found from

$$\sigma_r^{g,i} = \xi^{i} \sigma_s^{g,i} / \Delta U^{g} \tag{4.7}$$

where the subscript i refers to the particular isotope, ΔU^{g} is the lethargy width of the group through which the neutron slows down, $U = \ln E^{o} / E^{g}$, with E^{o} = 10 Mev and g denoting a particular fast energy group.

The microscopic removal cross-section for hydrogen is then computed using the equation presented below and dropping the group index as follows:

$$\sigma_r^H = \frac{\Sigma_{rs} - \sum_{i \neq H} N_s^i \sigma_r^i}{N_s^H} \qquad (4.8)$$

where Σ_{rs} is the removal cross section computed for the supercell by LEOPARD and N_S^H (or N_S^i) is the concentration of isotope H (or i) in the supercell

As our model is based on only one broad fast group, a collapsing is needed, namely in terms of three fast groups,

$$\Sigma_{rs} = \frac{\Sigma_{rs}^{3/3} \phi^{3/3}}{\phi^{1/3} + \phi^{2/3} + \phi^{3/3}} \qquad (4.9)$$

where $\phi^{i/3}$ are the fast groupwise fluxes calculated by LEOPARD on a supercell basis.

A comparison of the Σ_r predicted by Treatment 1 and 2 for two selected burnup steps of the LEOPARD problem (assembly supercell 2.19 w/o, 40% void) is presented in Table 4-2. As the difference found was very small and constant, it was decided to use in this study the removal cross sections predicted by Treatment 1 (SRT) since fewer hand calculations were required to determine Σ_r .

For PDQ bundle calculations at BOL, the fuel cell removal macroscopic cross section was determined using the SRT with Σ_{rs} obtained from LEOPARD assembly supercell calculations with 2.19 w/o fuel at 40% voids. Later, for PDQ bundle depletion calculations an improvement was achieved by applying the SRT to each one of the LEOPARD assembly supercell problems, obtaining in this way an enrichment dependent, fuel cell removal cross-section.

TABLE 4-1

Comparison of 8D219 Fuel With Fuel Used
To Obtain Fission Product Cross Section

	Celnik	8D219
Average enrichment (w/o U-235)	2.18	2.19
Fuel pellet OD (in.)	0.482	0.418
Water/full volume ratio	2.3	2.25
Void fraction (%)	28	40
Power density	40.9	50.96
Cladding material	Zircaloy	Zircaloy

TABLE 4-2

Comparison of Generated Removal Cross Sections for BWR Lattice Cells

Assembly Burnup (GWD/MTU)	Macroscopic Removal Cross Section (cm^{-1}) in unit cell by Method 1	Method 2	Percent (%) Difference
0	0.9992-2	0.1012-1	1.25
16	0.9853-2	0.9981-2	1.29

Figure 4-1 **THERMAL** FISSION-PRODUCT CROSS SECTION VS AVERAGE FUEL EXPOSURE

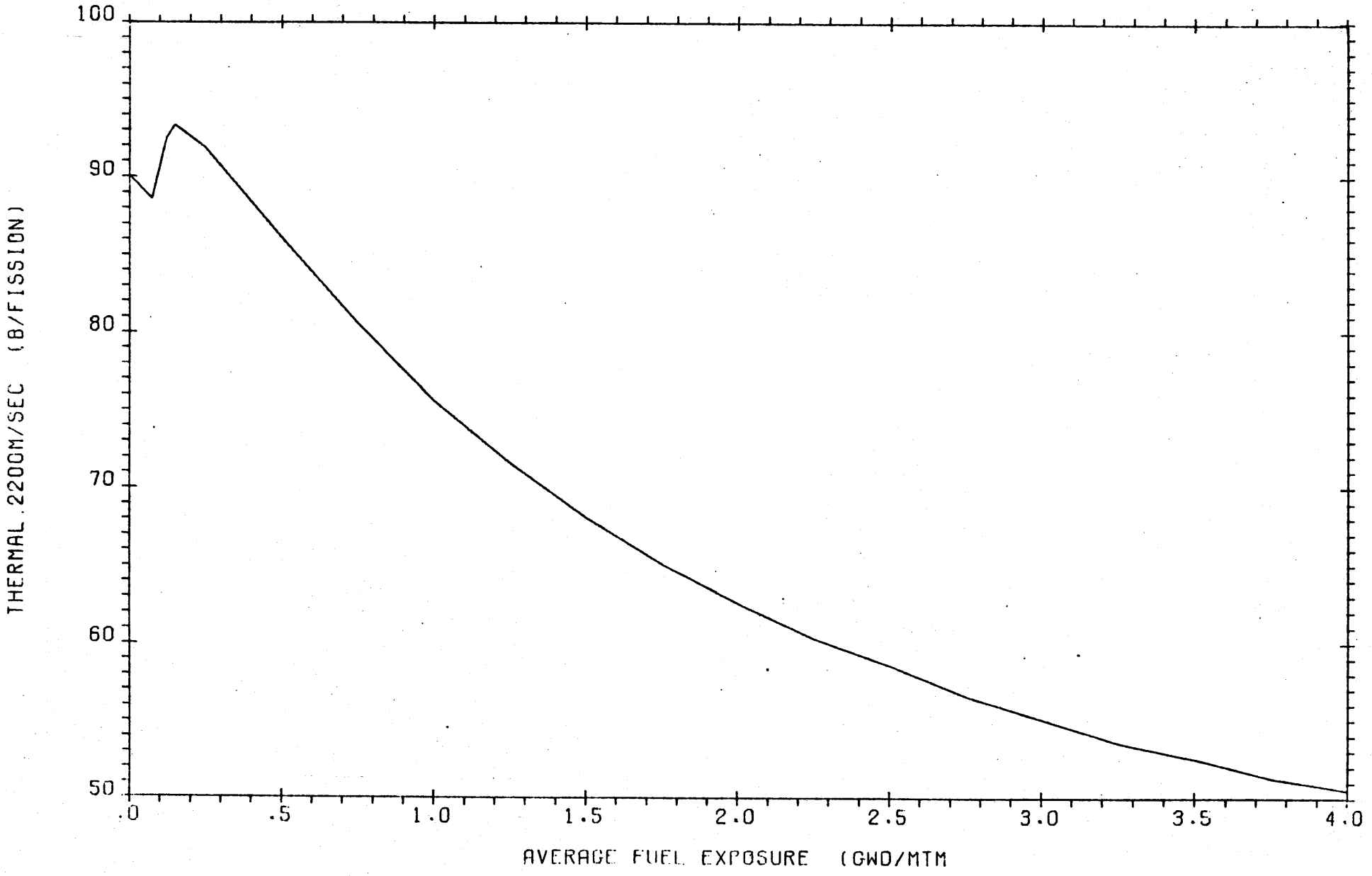

Figure 4-2 **EPITHERMAL** FISSION-PRODUCT CROSS SECTION VS AVERAGE FUEL EXPOSURE

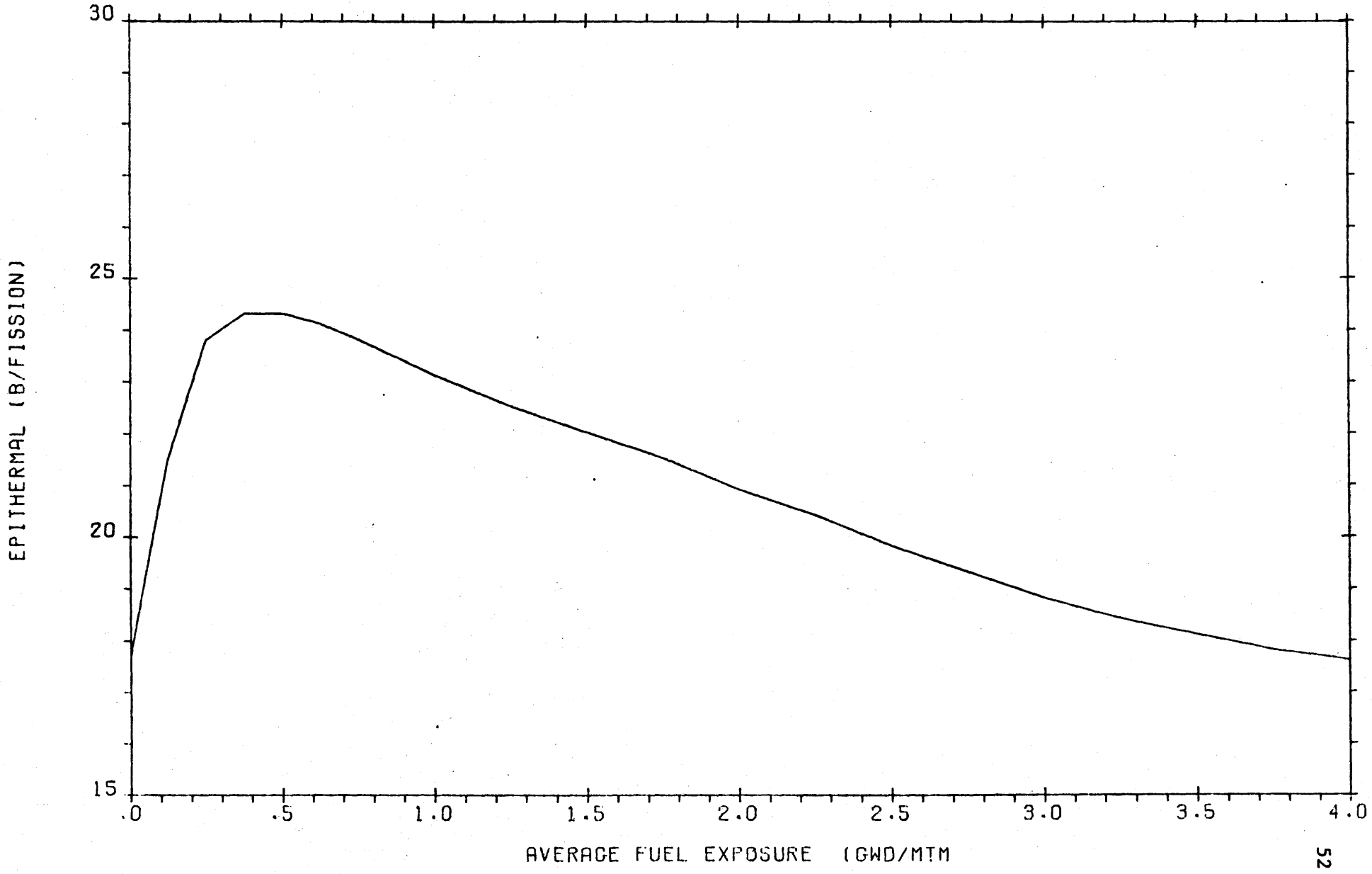

5.0 TREATMENT OF GADOLINIA BEARING FUEL

5.1 Introduction

The NUCELL code was used to determine absorption and fission reaction rates versus burnup for the gadolinia poison pin cells. These results were used to generate effective diffusion theory constants which will reproduce the NUCELL predicted reaction rates when used to represent the gadolinia poison pin cells in two dimensional PDQ bundle calculations - namely, a "fitting" procedure.

This "fitting" is essential because diffusion theory alone is known to be inadequate for regions with large absorption cross sections, since it tends to overestimate the flux (and hence the absorption rate) in such regions, resulting in an increase in their reactivity worth. For example, when uncorrected NUCELL two group cross sections for gadolinia poison pin cells were input into a two dimensional PDQ bundle calculation at BOL, an increase of 7% was observed in the bundle k_{∞}.

Such fitting has been treated extensively in the nuclear design literature by Rampolla [25], Radkowsky [26], Henry [27], Klotzken [28], and others. The theoretical bases of this procedure are some of the properties of the Boltzmann equation, as stated in the article published by Rampolla. These properties and their proofs are contained in this article, but to give more theoretical consistency to the use of this procedure they are going to be enumerated here.

As defined in the article published by Rampolla, we will call from now on:

-The new diffusion constants as "fitted constants"

-The ratios of fitted to original constants as "fitting factors"

-And the entire procedure as "fitting"

To understand better the properties of the Boltzman equation, we now consider it. Any approximation to the fixed-source Boltzman equation, as well as the fixed-source Boltzman equation itself, can be written symbolically as

$$D\phi + \Sigma^A\phi = S \tag{5.1}$$

where

ϕ is the solution vector

S is the source term

D is the transport and scattering operator

Σ^A is Sn absorption operator

We will assume that ϕ exists and has any required continuity properties.

Property 1: The solution vector ϕ is everywhere positive except possibly at the boundaries where it may vanish because of imposed boundary conditions

Property 2: Given an increase (decrease) in Σ^A in any finite, not necessarily connected volume R^t in phase space, then:

a) ϕ decreases (increases) everywhere except possibly at the boundaries where it may remain fixed because of imposed boundary conditions.

b) The capture rate in R^t given by $\int_{R^t} \Sigma^A \phi \, dV$ increases (decreases) while the capture rate in any region outside of R^t and the leakage from the solution space both decrease (increase). Note that

a negative leakage term implies that the leakage is into the solution space (or out of the space outside the solution space) and that any references to "increases" or "decreases" in leakage out of the solution space refer to algebraic increases or decreases.

c) If $\Delta\Sigma^A$ represents the change in Σ^A in R^t, then the change in capture rate in R^t is smaller in magnitude than $\left| \int_{Rt} (\Delta\Sigma^A)\ \phi\ dV \right|$

The development of the fitting procedure is based on the observation that, when it is desired to change the capture rate in some region, Property (2b) indicates the direction of the required change in Σ^A in that region, while Property (2c) guarantees an upper bound to the magnitude of the change induced by a given change in Σ^A.

In Reference 25 can be found a proof of these properties for a finite difference approximation (in Cartesian geometry) of the fixed-source Boltzmann equation, similar to that used in deriving the equations for the PDQ series of programs, giving in this way, a strong theoretical support to what we will do later.

Radkowsky, in the Naval Reactor Physics Handbook, calls this procedure "Empirical Blackness Theory". On pages 612 and 613, empirical blackness theory is described as follows:

Empirical blackness coefficients are defined directly in terms of effective diffusion theory constants (D and Σa)... The property of the desired Σa_{eff} is, when Σa_{eff} is used with the remainder of the design representation, that the proper absorption in the absorber (relative to that in some "normalizing region") will be

> calculated, the proper absorption rates being determined from more exact transport calculations... To determine Σa_{eff} which will adequately approximate the absorption in the lumped absorber, a "model cell geometry" is chosen for empirically determining Σa_{eff} by comparing a "high order transport theory calculation" to diffusion theory design type calculations in which Σa_{eff} is varied until the relative absorption rate in the design type calculation equals that of the high order transport calculation.

Henry, in Reference 27, calls this procedure "Equivalent Constants Found by Matching Particular Reaction Rates", and describes the procedure on pages 449, 450 and 451.

5.2 The Method of Transport Theory Fitting for Gadolinia Bearing Fuel Cells

Our bundle has properties such that 2-group diffusion theory can adequately describe its neutronics behavior except for the fuel bearing gadolinia pin cells. Here fussion theory cannot be trusted to yield good results because of the highly absorbing gadolinium 155 and 157 isotopes. If detailed information about these regions were desired, a direct transport theory approach might be desirable, but impractical because of the following considerations. To adequately determine what takes place neutronically within these gadolinia cells, the surrounding fuel cells and non-fuel regions of the bundle must be represented well enough for the gadolinia cells to see the proper incoming neutron spectrum, proper flux gradient, etc. Thus, one must perform an expensive 2-dimension transport theory calculation for the whole bundle. Furthermore, to adequately deplete the bundle very short steps must be taken to account for the high burn-out rate of the

gadolinium 155 and 157 in the fuel bearing cells. Because the cost of the 2-D transport theory depletion calculation is directly proportional to the number of mesh points used to represent the bundle and the number of time steps taken in the depletion, the expense makes this direct approach generally impractical from an economic standpoint.

The consideration of expense leads to the application of the transport theory fitting approach used here. In our approach, a gadolinia cell is represented accurately in a transport theory calculation surrounded with just enough bundle region to produce the proper incoming neutron-flux spectrum. A two-group diffusion theory representation of the gadolinia cell, with the same amount of bundle region and same boundary conditions, is also calculated. In the next step, the transport theory calculation is compared to diffusion-theory results, and then two-group diffusion theory cross sections are adjusted until the diffusion-theory absorptions and fissions of the gadolinia fuel bearing cell match the transport theory predictions. The fitted cross sections are then used in a full bundle diffusion calculation, with the gadolinia fuel bearing cells represented precisely as in the transport theory comparison case. If it is true that diffusion-theory is an adequate model for the basic bundle and since we have forced the gadolinia cells by cross-section modification to be predictable by diffusion theory, then the full-bundle diffusion calculation will yield information about as accurate as that obtained if a direct 2D transport theory calculation were used. The computer expense, however, will be much less.

One word of caution is in order. If the fitting approach is to force absorptions and fissions of the gadolinia fuel bearing cell to match the transport theory predictions, one should expect to obtain transport theory accuracy for the absorptions and fissions of the gadolinia fuel bearing cells from the full-bundle diffusion calculation. However, other "unfitted" facets of nuclear behavior may be grossly inaccurate.

In this study, the transport theory representation of a gadolinia cell and the two-group diffusion theory calculation of the same problem were carried out by using NUCELL and PDQ, respectively.

5.3 Representation of the Gadolinia Bearing Fuel Cell in NUCELL

In NUCELL a gadolinia fuel bearing cell is modeled by defining a gadolinia fuel bearing cylindrical pellet, a metallic clad, a moderator region, an extra region and an outer pure scattering region. As mentioned before, the gadolinia unit cell should be surrounded with at least enough bundle region to reproduce the bundle incoming neutron spectrum, the bundle thermal flux gradient or thermal leakage (produced by a dip in the thermal flux when going from the outer fuel to the gadolinium fuel cell), etc. All these conditions can be simulated by using two different cylindricized extra regions in our NUCELL problem; one extra region of twenty homogenized fuel unit cells (this is the proportion of regular fuel pin cells to gadolinia fuel cells that exist in the overall bundle) which serves principally as spectrum modifier, and another extra region including the fraction of the bundle that is not fuel cells (1/3 of the water gaps, channel, voided film and water tube) which serves principally as thermal flux gradient modifier. As the NUCELL code only allows one extra region,

the gadolinia fuel cell was surrounded by an extra region which is a homogenization of both above extra regions expecting to represent, on the average, a modification of the spectrum and the thermal flux gradient. The decision to consider this extra region instead of one including only the eight fuel units cells, which physically surrounding every gadolinia fuel cell in the bundle, is based on the following reasoning:

a) This representation allows the gadolinia fuel cell to see the proper incoming neutron spectrum, proper thermal flux gradient, etc.

b) This NUCELL assembly supercell problem simulated the depletion of the gadolinia cells in the bundle much more reasonably

c) During depletion of the NUCELL, criticality of this bundle array can be performed by a buckling search which simulates the fast leakages to or from the neighboring bundles. The NUCELL supercell problem with a non-lattice region which only included eight homogenized fuel unit cells is subcritical (negative buckling) for all exposures, and in reality, becomes critical by thermal inleakage, which is not easily represented in NUCELL.

d) The nine-cell model does not include the non-lattice extra region, and therefore, yields a smaller water-to-metal ratio than that of the actual bundle. This adversely affects the flux spectrum and gadolinia burnup rate.

e) The full-bundle procedure produces more realistic absolute flux levels for computing burnup, Xe-135 and Sm-149

concentrations, Pu-239 concentrations, secondary heating characteristics, etc. In this way, the NUCELL bundle supercell problem will predict more realistic two group macroscopic X-sections for the gadolinia cell (or pellet) and better absorption and fission reaction rates to match.

f) By using SRT, this NUCELL bundle supercell for fuel with 2.50 w/o U-235 + 4% Gd_2O_3 at 40% void problem predicts regionwise macroscopic removal valves which give agreement with the LEOPARD bundle supercell for the same problem. This is very important because removal is the parameter which controls the number of neutrons that are absorbed by the gadolinia pellet and thus it controls the gadolinia burnout rate.

5.3.1 Options Used

The following specific characteristics of the gadolinium fuel bearing are essential when selecting the NUCELL input options:

a) The gadolinium fuel cells approximately have a relative average power of ∿0.4 at BOL and, ∿1.0 when all the gadolinia is gone.

b) As a result, the average fuel temperature in the gadolinia rods goes from 755.51 degrees F to 1103.08 degrees F leading to a progressive decrease in reactivity due to a U-238 and Pu-240 Doppler broadening effect.

c) The sharp change in spectrum, flux level and burnup rate within the gadolinium fuel cells as a function of time lead to fission product buildup cross-sections (represented in this study by a lumped FP vs. burnup) and reactivity effect

different from the case of a regular, non-gadolinia fuel cell.

In this NUCELL problem, the material buckling was searched to simulate criticality by fast leakage to the neighboring bundles. A maximum of 10 iterations and a loose convergence criterion of 10^{-3} were specified for this buckling search. As we were not interested in K_{eff} a very small and arbitrary geometrical buckling was input, 0.0000001.

In this NUCELL problem, the L factor for U-238 was not searched either in the depletion calculations or at BOL conditions, because the presence of U-238 treated both heterogeneously in the gadolinia fuel pellet and homogeneously in the extra region makes the shelf-shielding iteration procedure (L approach) used in NUCELL inadequate for this problem. Instead, the following approach was taken:

A LEOPARD assembly supercell problem with the appropriate enrichment and effective resonance temperature has a very similar fast and epithermal spectrum to our NUCELL assembly supercell, because they have the same lattice geometry, water to uranium ratio and supercell average number densities (the important things are U-238 and H_2O). The L factor for U-238 was therefore obtained from a LEOPARD bundle supercell and input into NUCELL. As NUCELL does not allow variations in L factor with Gd cell burnup, (or with gadolinia cell power peaking) the LEOPARD problem was run at BOL with an effective resonance temperature of 920.84 degrees F, corresponding to an estimated average of the gadolinium fuel local power peaking while the gadolinia is present. The resulting L^{238} = 0.683999 which is very close to L^{238} = 0.675099 (0.693206) computed at 755.51 degrees F

(1103.09 degrees F). Since the maximum $\Delta K^{\infty}/K^{\infty}$ predicted by LEOPARD for this temperature difference is 0.2%, then the error made by inputting the L factor corresponding to the average power peaking condition is minor. The L factors for the other nuclides were input as 1.0. Additionally, the standard THERMOS iteration without extrapolation was used and the Nelkin kernel for water was selected since it has been shown to be reasonably accurate.

Since NUCELL calculates absolute fast fluxes on a supercell basis, as a consequence, watts/cm should be calculated on a problem (supercell) basis, i.e., as average watts/cm per rod multiplied by the 21 fuel rods present in the problem. As NUCELL requires a single value which does not reflect the gadolinia cell power change with burnup, an average value was used. This average input watts/cm was calculated as 0.704 multiplied by the average watt/cm per rod where 0.704 is an estimation of the average gadolinia power peaking during depletion.

The effective fuel temperature, EFTEMP, (used to Doppler broaden the U-238 resources) is defined as that temperature which gives the correct doppler reactivity. The NUCELL variable TEMP would be defined in an analogous fashion except that it would be concerned with the Pu-240 effect on the power coefficient.

The experimental information needed to accurately determine these two quantities was not available either for regular fuel or gadolinia bearing fuel, so the volume average fuel temperature, was used as an approximate value. To be consistent with the approach used in this study to calculate the L factor for U-238, both temperatures were set

at 920.89 degrees F (766.8 degrees K). As the L for U-238 was input, no U-238 resonance iteration calculation is performed by NUCELL.

A total of 22 space points were specified for our NUCELL problem (See Figure 5-1). Using the NUCELL notation, the region mixtures and space point distribution used for this NUCELL problem are the following:

Mixture No.	Constituent	# of Regions	# of Space Points
1	Gadolinia-uranium oxide	10	10
2	Zircaloy-2	1	1
3	H_2O (40% Voided)	1	4
4	Homogenized 1/3 of non-gadolinia fuel cells	1	5
5.	Heavy scatterer	1	2

The maximum permissible by NUCELL, ten space points in the pellet, was used to have continuity (or to avoid discontinuity) in the pointwise thermal fluxes. This leads to a very detailed shape of the isotopic pointwise thermal reaction rates through the pellet. This is needed to accurately calculate effective microscopic cross sections for the isotopes present in the pellet.

The thickness of each one of the ten pellet regions (with one space point per region) was adjusted so that they all had equal volumes. This is a desirable approach since gadolinia burns as a cylinder with decreasing radius leading to a depleted outer region and a relative fresh inner region of high optical thickness. This makes it difficult to maintain continuous details in the pellet pointwise thermal fluxes as the depletion proceeds, using a fixed number of regions and region structure in pellet.

The mass of fuel in a cell (MTU/cm) was calculated on a problem basis (as NUCELL requires) as:

$\{ (7.619) + 20\ (7.931) \}\ 10^{-6}$ at hot conditions. (5.2)

where 7.619 is the hand calculated value of the g/cm in the gadolinia fuel cells

and 7.931 is the LEOPARD calculated value of the g/cm in the regular fuel cells.

To account for the high burn-out rate of the 155 and 157 gadolinium isotopes, twenty three depletion steps were performed to reach 15,900 (MWD/MTU) for the problem: initial time steps of 50 and 250, followed by time steps of 300 to accumulate an exposure of 2700, 600 to accumulate 7500, 1200 to accumulate 11,100 and 2400 MWD/MTU to 15,900 (MWD/MTU). The length of these time steps in seconds was calculated using the equation in NUCELL to calculate problem burnups corresponding to the successive input lengths in seconds. As NUCELL depletion can only be controlled by the whole problem seconds (or whole problem exposure) the above small steps were taken to account for the high burn-out rate of the gadolinium. To avoid this difficulty, NUCELL should be modified to be controlled by the cell exposure.

NUCELL, like all codes based on the LASER code, requires the spatial distribution of epithermal captures in U-238 as input. This distribution accounts for the non-uniform buildup of Pu-239 in the fuel and is normalized by NUCELL such that the cell total capture rate using the input distribution is equal to the cell total capture rate calculated with MUFT. There is an uncertainty in how this normalization is done by NUCELL when the extra region contains U-238.

Such a distribution is best obtained from a Monte Carlo calculation. Mertens[29] and Momsen[30] used the results of a Monte Carlo calculation for the spatial distribution of U-238 in the Yankee Rowe Core I fuel. It is not clear if this spatial distribution is or is not pellet diameter dependent. To avoid this uncertainty, the Manfred Wagner (31) analytic approach to this problem was used, but it is in the best case an approximation because experimental information or Monte Carlo calculation for the spatial distribution of U-238 in gadolinium bearing fuel was not available.

The spatial distribution input values were obtained by determining the relative resonance absorption in every one of the 10 equal volume regions in the pellet, where the resonance absorption is given by the Manfred Wagner universal function f(K), K being Ri/Rpellet with Ri the pellet region's outside radius. The result is given below:

Fuel Space Point Number	Relative Resonance Capture Rate
1	1.080043
2	1.089913
3	1.030124
4	1.199772
5	1.200276
6	1.399930
7	1.499865
8	1.699796
9	2.200154
10	3.900273

(5.3)

The adaptation of LEOPARD fission product cross section representation to NUCELL was based on the following fact:

When the thermal cutoff is raised to 1.885 eV, one or both of the LEOPARD lumped fission product cross section expressions must be changed; it seems best to keep the thermal unchanged and to modify the

epithermal in such a way that the total fission product absorption in a 1/E spectrum remains the same, whether the cutoff is 0.625 or 1.855 eV. The result is given as:

$$\bar{\sigma}_a^{MND} = A_0 + A_1 X + A_2 X^2 + A_3 X^3 \quad (X = \text{burnup})$$

$(10^3 MWD/MT)$

(same values as Eqn. 4.2)

$$\bar{\sigma}_a^{epi} = B_0 + B_1 X + B_2 X^2 + B_3 X^3$$

$B_0 = 27.6791$ $\qquad B_2 = 0.00186335$

$B_1 = -0.$ $\qquad B_3 = 0.00001169722$

(5.4)

5.4 The Fitting Approach

In this study, the transport theory fitting for the gadolinia bearing fuel pellet was performed in the following steps:

1) The following parameters were calculated from selected NUCELL depletion steps

   - Two group macroscopic cross sections for the gad bearing pellet, the clad plus moderator plus extra region.
   - The ratios

   $$RA = \frac{\text{Thermal absorption rate in pellet}}{\text{Thermal absorption rate in clad plus moderator}}$$

   $$RF = \frac{\text{Thermal fission rate in pellet}}{\text{Thermal absorption rate in clad plus moderator}}$$

2) A PDQ representation of the NUCELL problem was set up (Figure 5-2) using rectangular geometry, with the macroscopic cross sections edited from the NUCELL problem.

3) For each burnup step selected from the NUCELL problem, Σ_a^{MND} and $\nu\Sigma_f^{MND}$ of the pellet were adjusted simultaneously until the PDQ problem gave the same values of the ratios RA and RF as did the NUCELL problem.

The cross sections resulting from step 3 were used directly in the PDQ bundle problem, because it has the same representation of the gad pellet unit cell. This treatment accounts for differences in both geometric shape and mesh spacing between the NUCELL and PDQ representations. Figure 5-3 shows flux distributions from the NUCELL problem at 3 times in life, to emphasize the importance of gadolinia burnup.

Figures 5-4 and 5-5 show the ratios RA and RF. Figure 5-6 shows the fitting factor (i.e., the ratio by which the NUCELL cross sections

must be multiplied to force agreement in the PDQ problem. Figures 5-7 through 5-13 show the resulting fitted cross sections for the pellet.

Figure 5-1

Nucell Assembly Supercell Geometry

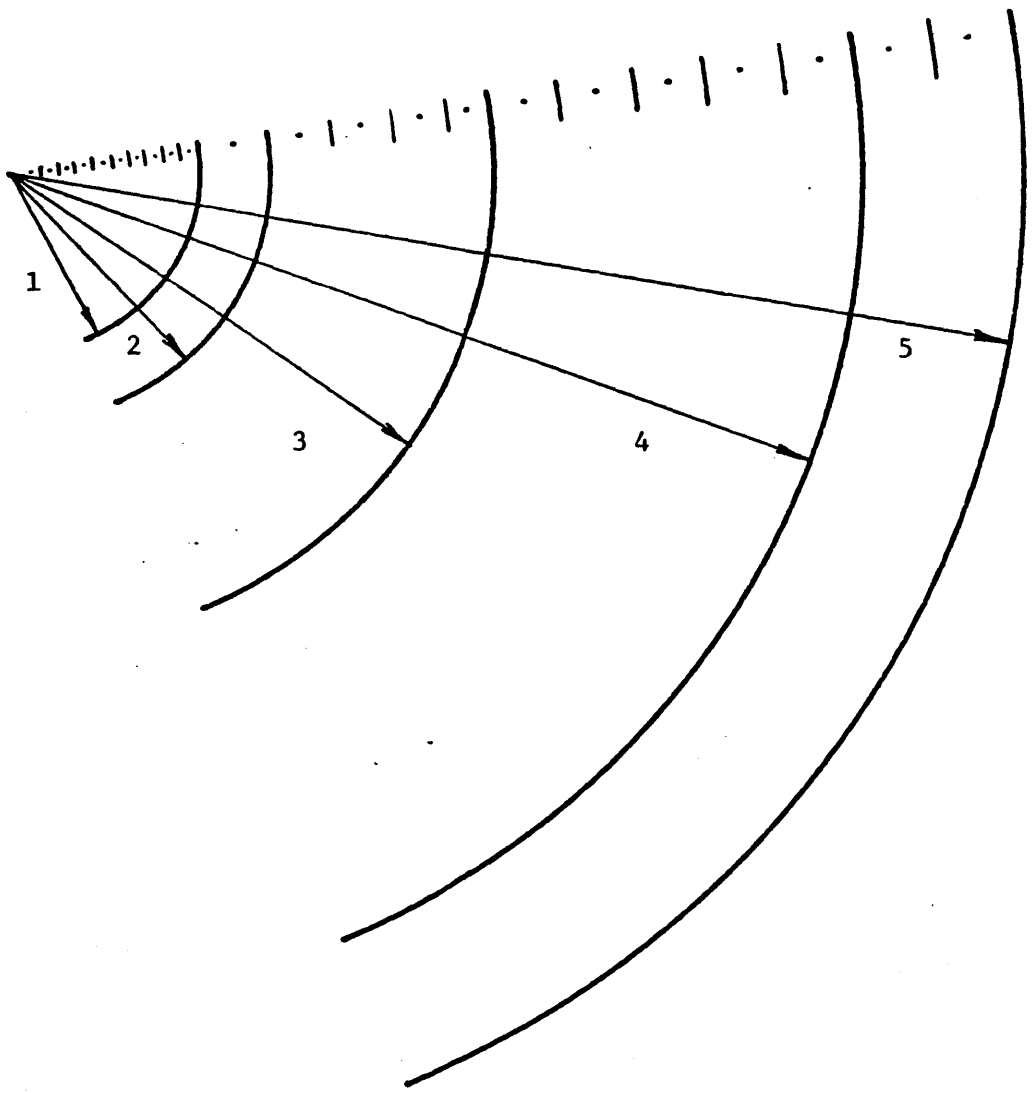

1	Gad Pellet.....	0.53085 cm
2	Clad	0.62713 cm
3	Voided H_2O	0.91872 cm
4	Homogenized Extra Region.	4.9720 cm
5	Heavy Scatterer	6.5933 cm

Figure 5-2

Equivalent PDQ Cell Geometry

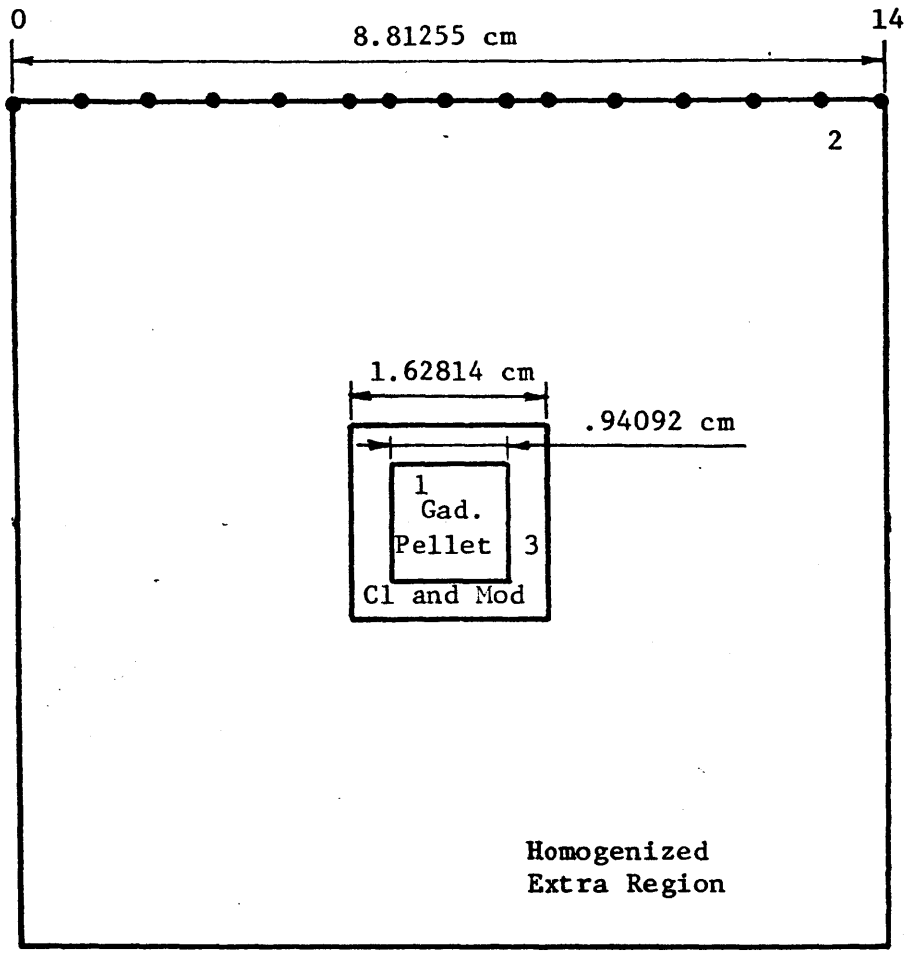

Figure 5-3

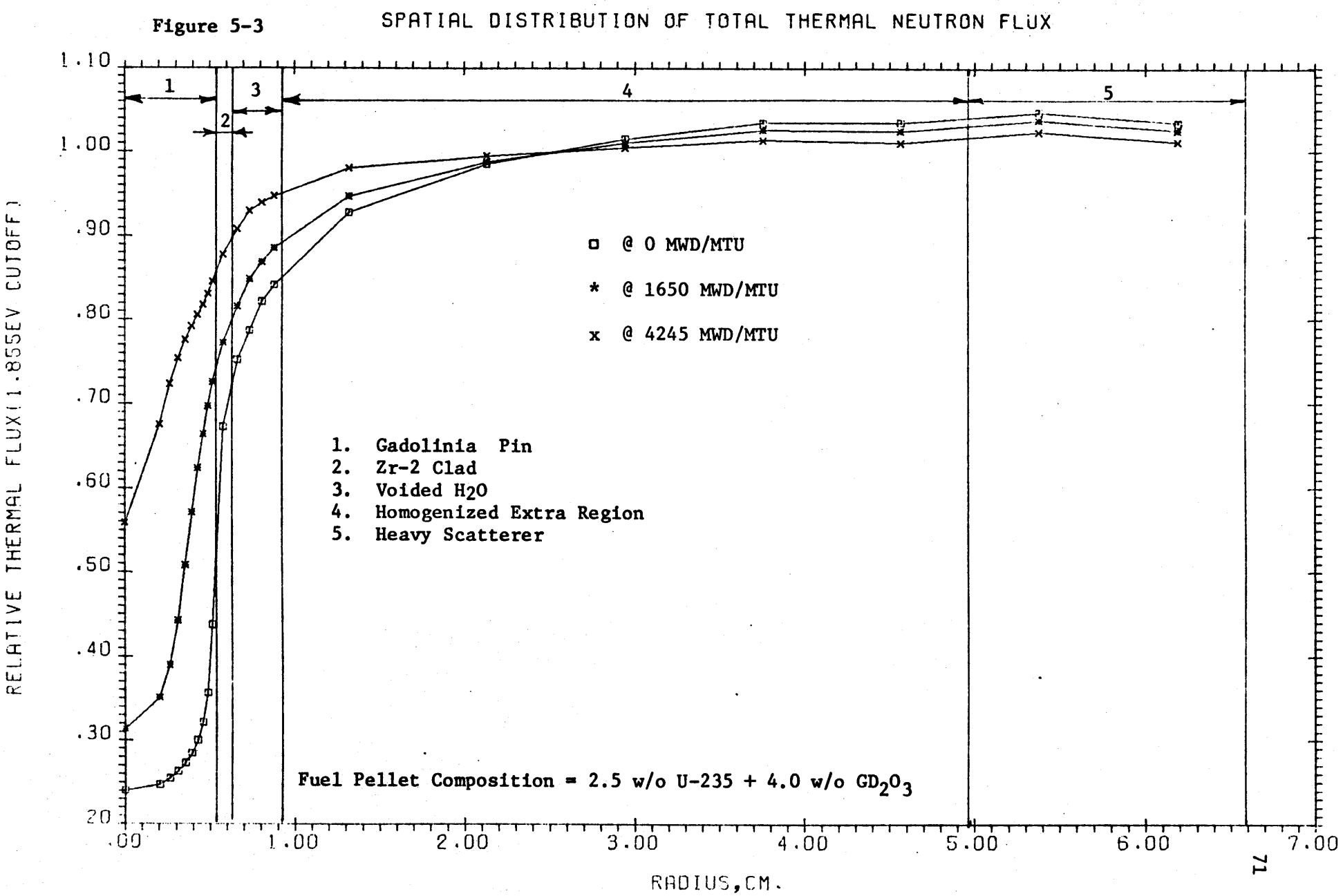
SPATIAL DISTRIBUTION OF TOTAL THERMAL NEUTRON FLUX
RELATIVE THERMAL FLUX(1.855EV CUTOFF)
RADIUS,CM.
1.10
1.00
.90
.80
.70
.60
.50
.40
.30
.20
.00
1.00
2.00
3.00
4.00
5.00
6.00
7.00
1
2
3
4
5
□ @ 0 MWD/MTU
* @ 1650 MWD/MTU
x @ 4245 MWD/MTU
1. Gadolinia Pin
2. Zr-2 Clad
3. Voided H2O
4. Homogenized Extra Region
5. Heavy Scatterer
Fuel Pellet Composition = 2.5 w/o U-235 + 4.0 w/o GD2O3

Figure 5-4

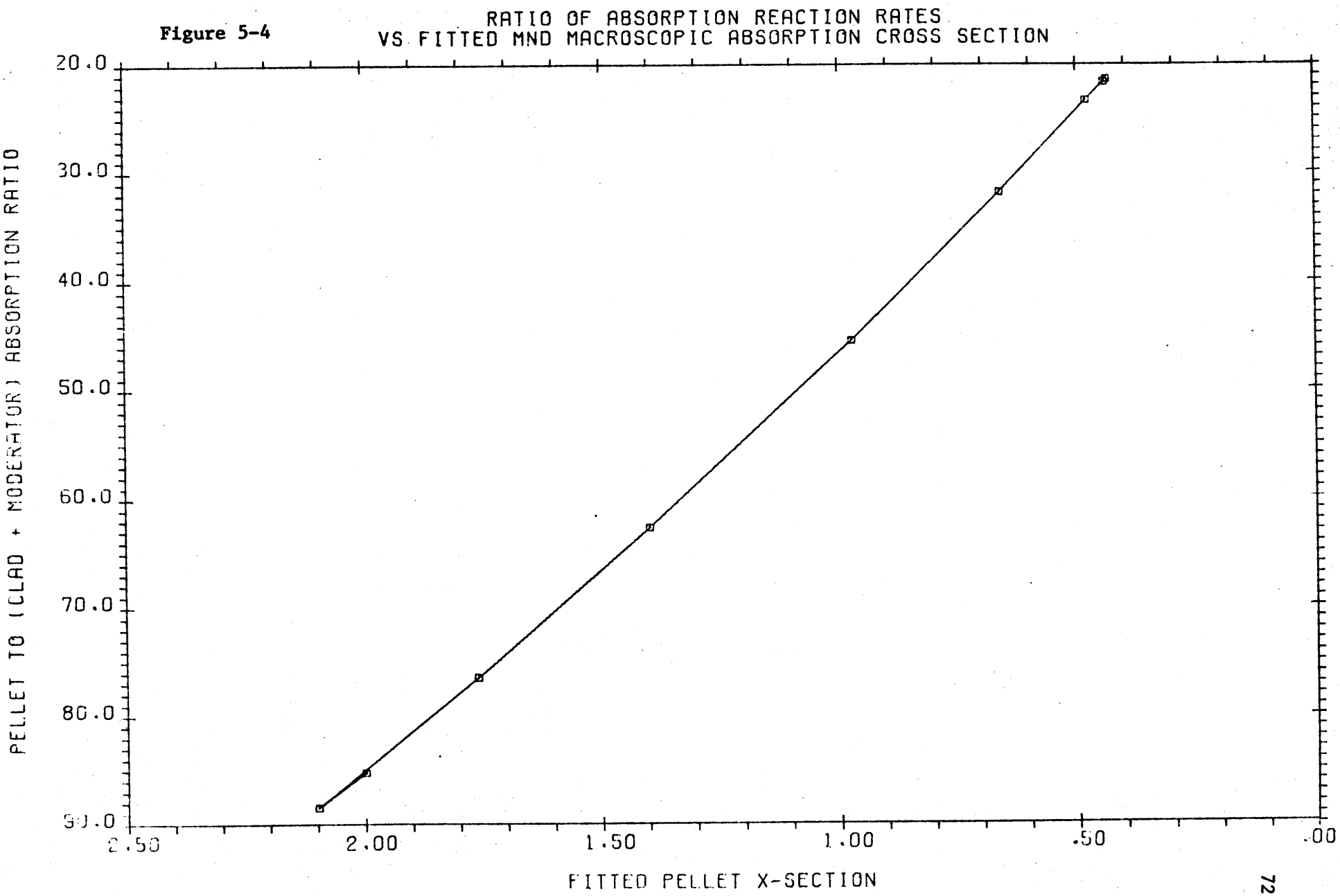
RATIO OF ABSORPTION REACTION RATES
VS FITTED MND MACROSCOPIC ABSORPTION CROSS SECTION
PELLET TO (CLAD + MODERATOR) ABSORPTION RATIO
20.0
30.0
40.0
50.0
60.0
70.0
80.0
90.0
2.50
2.00
1.50
1.00
.50
.00
FITTED PELLET X-SECTION

Figure 5-5

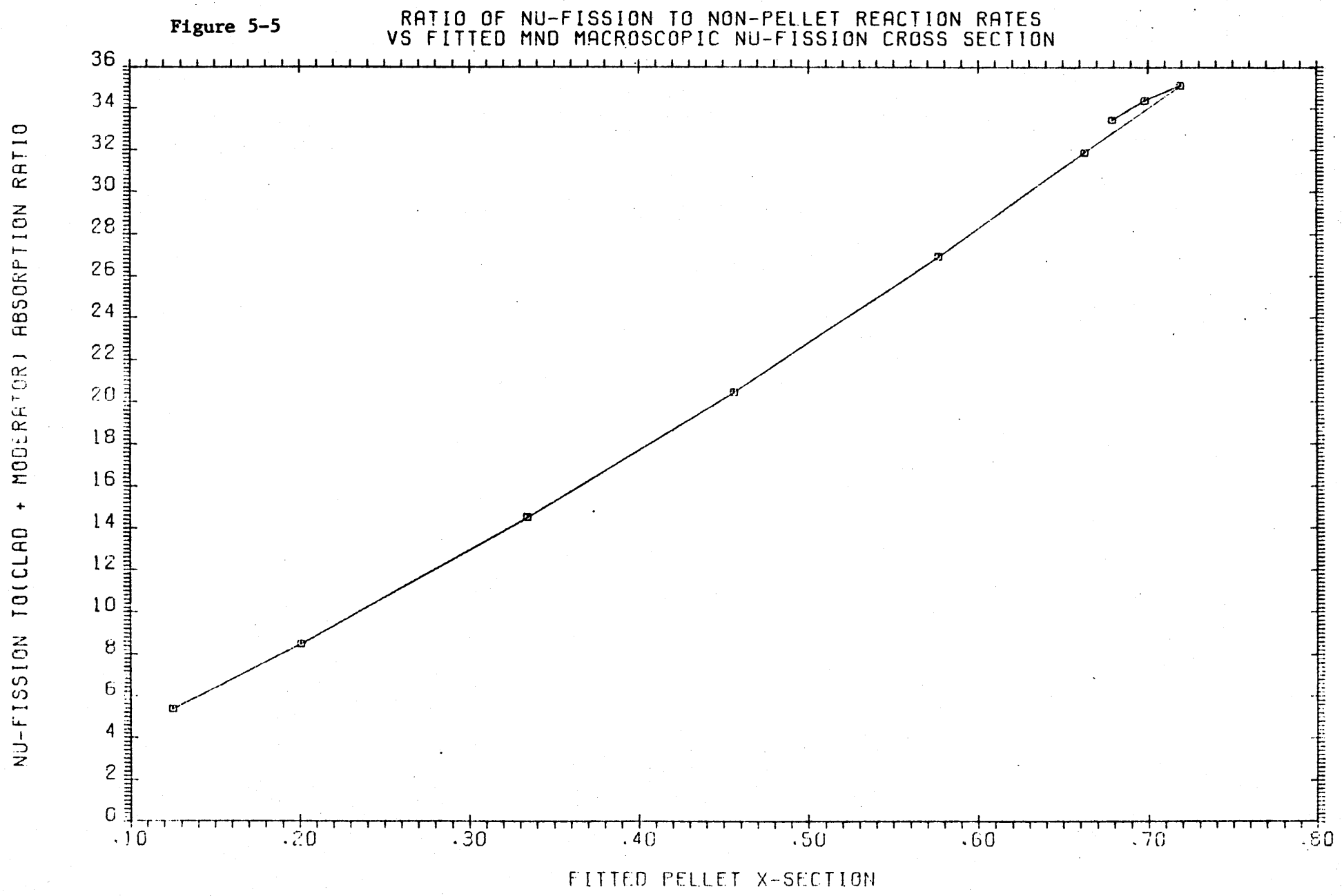
RATIO OF NU-FISSION TO NON-PELLET REACTION RATES
VS FITTED MND MACROSCOPIC NU-FISSION CROSS SECTION
NU-FISSION TO(CLAD + MODERATOR) ABSORPTION RATIO
0
2
4
6
8
10
12
14
16
18
20
22
24
26
28
30
32
34
36
.10
.20
.30
.40
.50
.60
.70
.80
FITTED PELLET X-SECTION

Figure 5-6

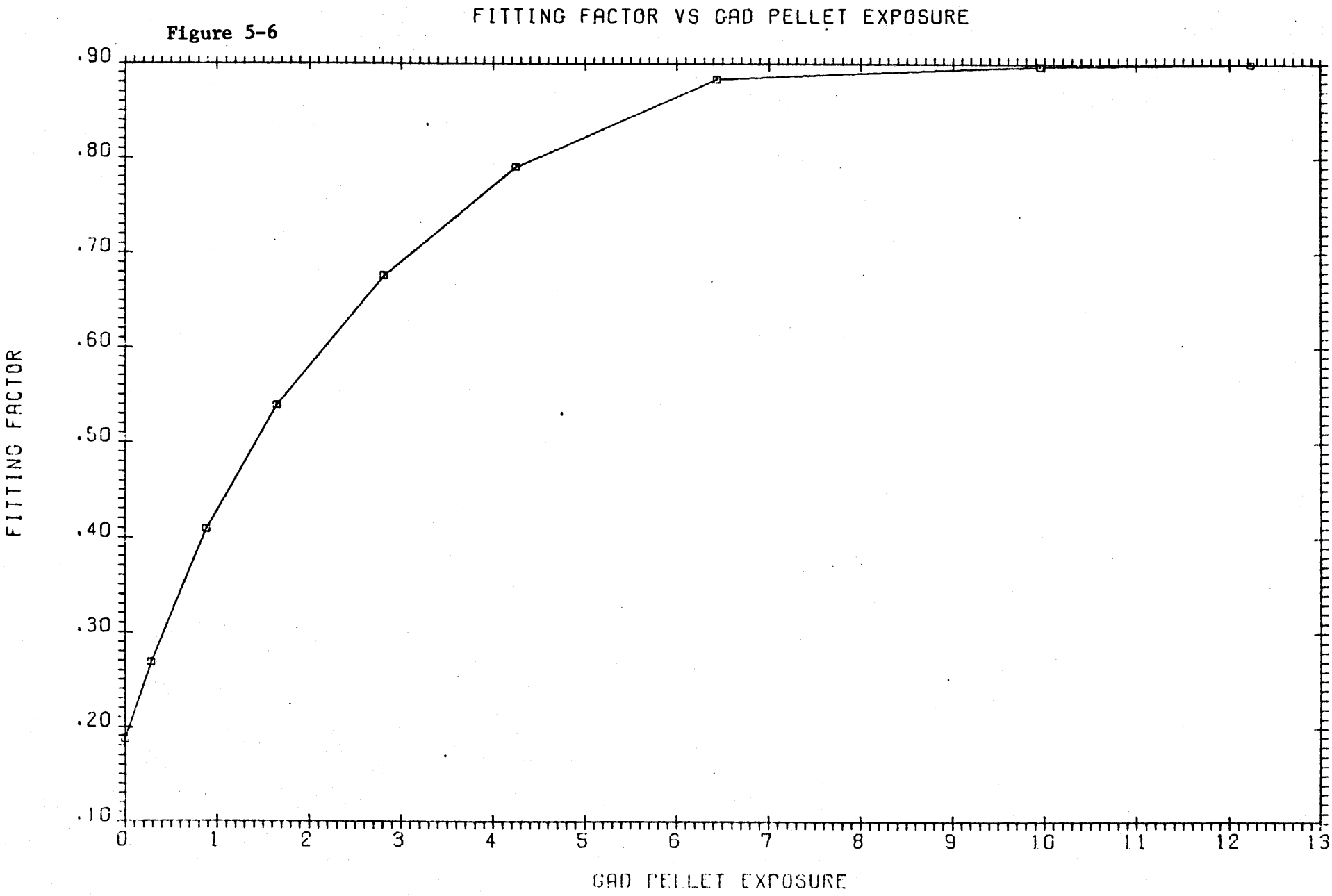
FITTING FACTOR VS GAD PELLET EXPOSURE
FITTING FACTOR
.90
.80
.70
.60
.50
.40
.30
.20
.10
0
1
2
3
4
5
6
7
8
9
10
11
12
13
GAD PELLET EXPOSURE

Figure 5-7 FITTED MACROSCOPIC FAST ABSORPTION X-SECTION FOR GAD PELLET

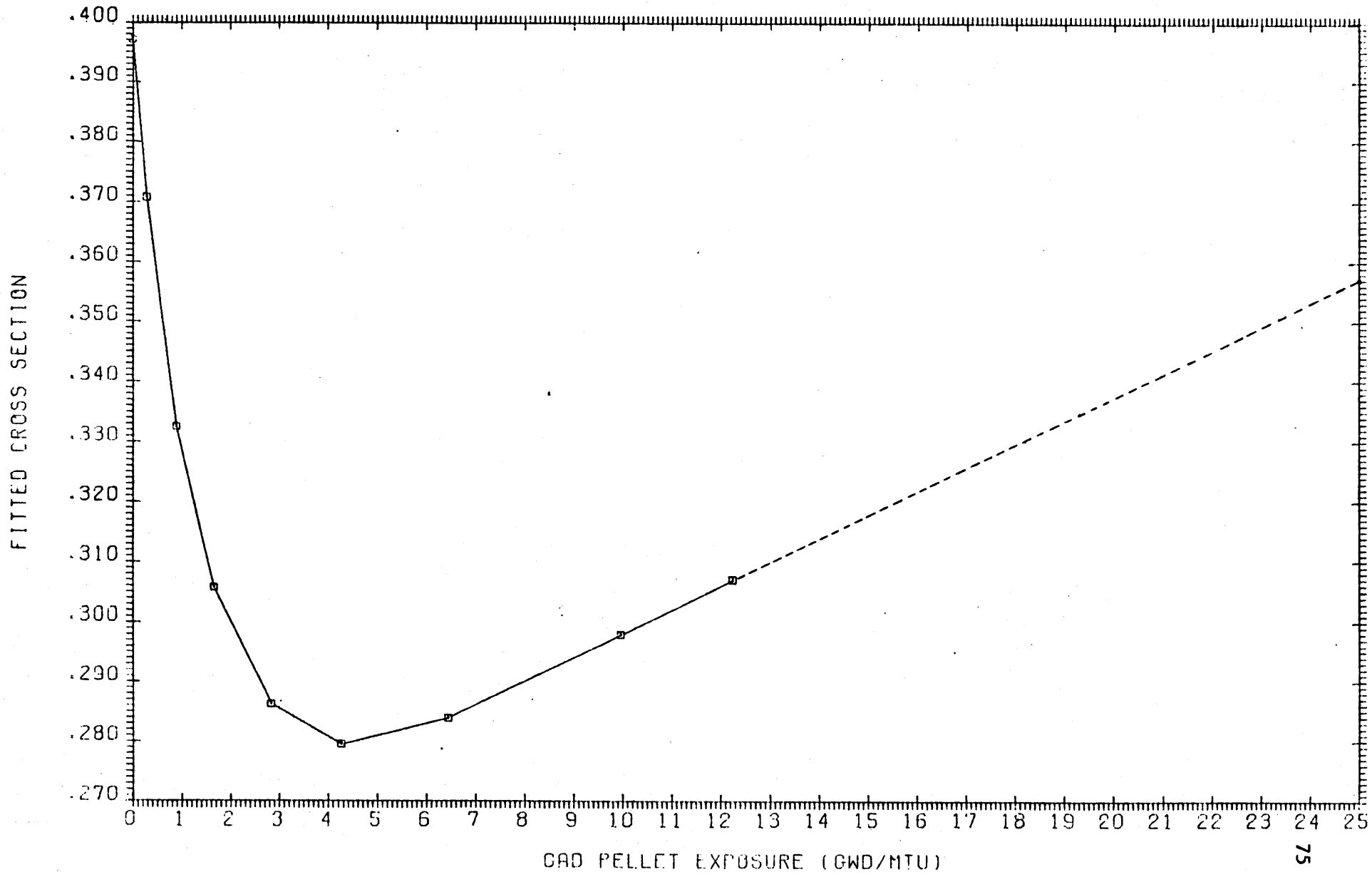

Figure 5-8 FITTED MACROSCOPIC FAST NU FISSIONX-SECTION FOR GAD PELLET

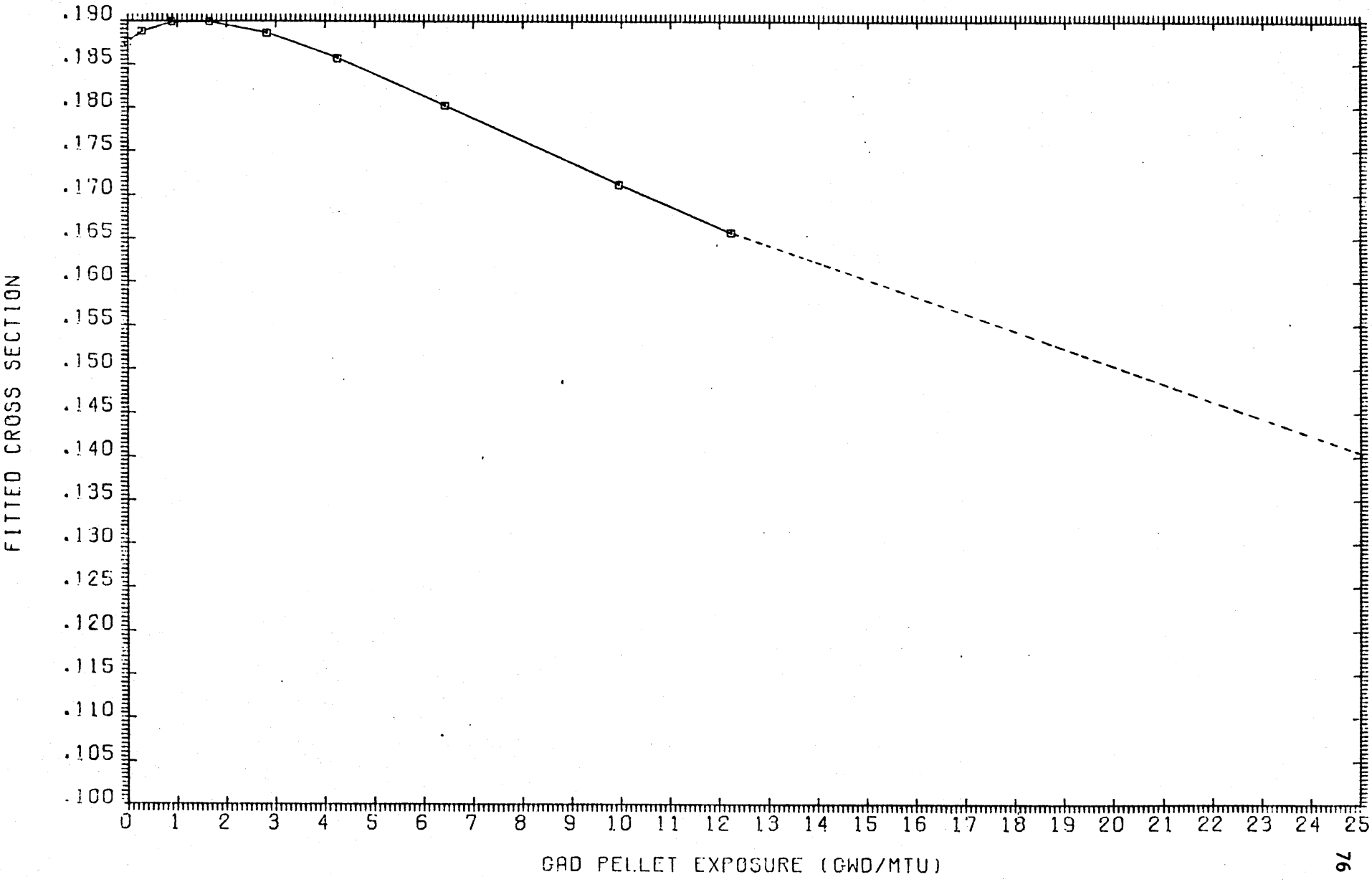

Figure 5-9 FITTED MACROSCOPIC FAST K FISSION X-SECTION FOR GAD PELLET

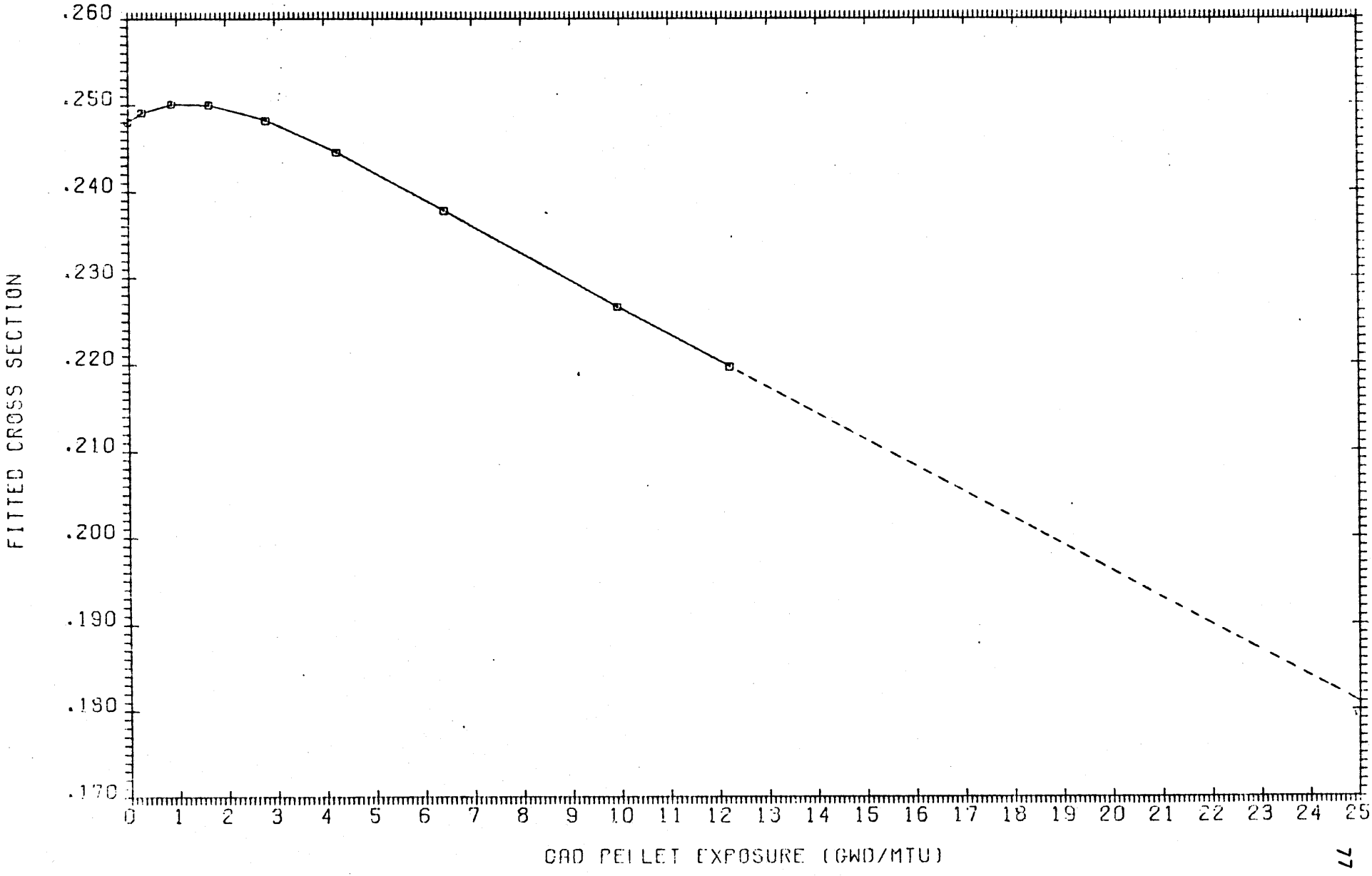

Figure 5-10 FITTED MACROSCOPIC MND TRHNSPORT X-SECTION FOR GAD PELLET

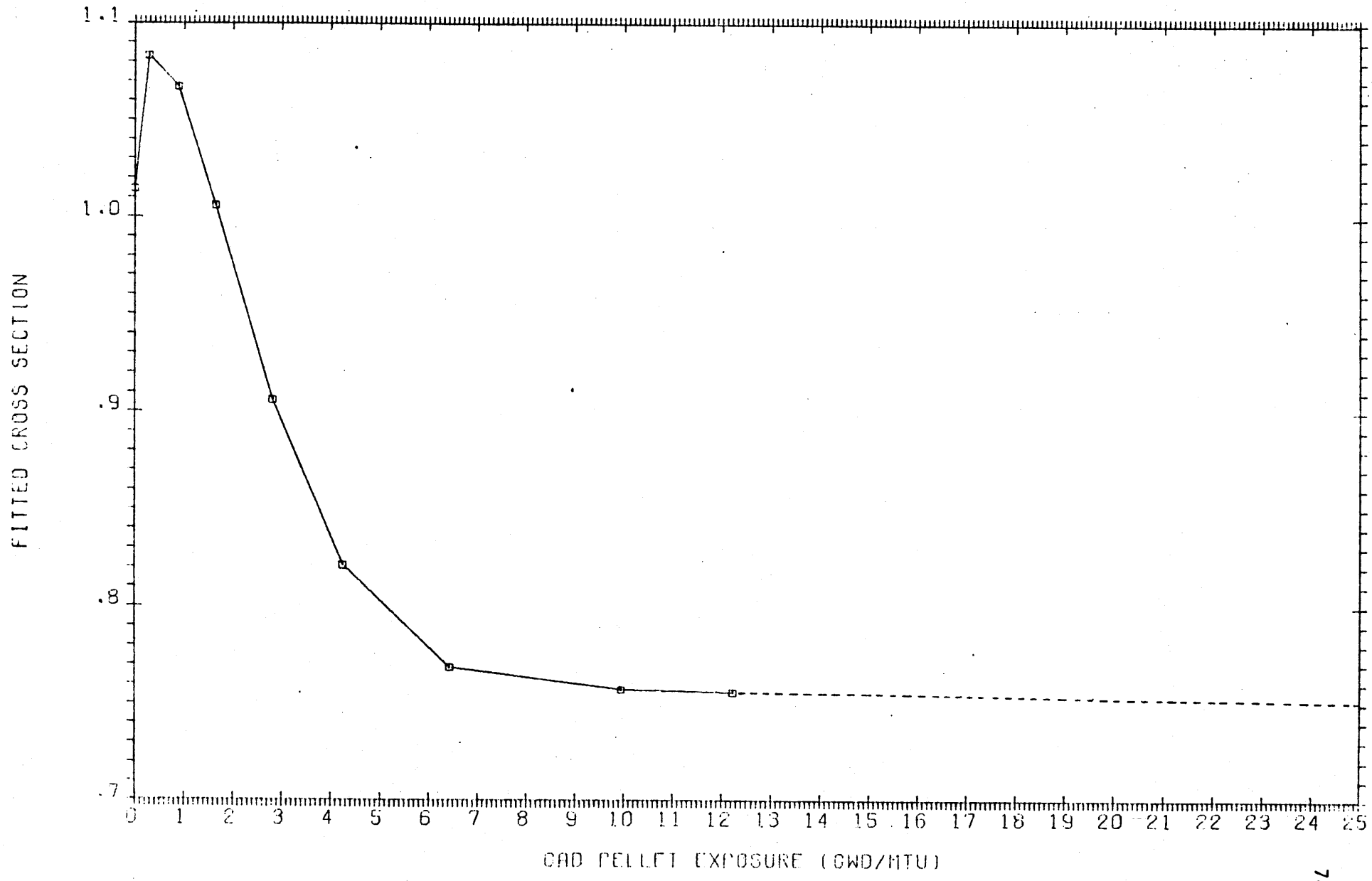

Figure 5-11 FITTED MACROSCOPIC MND ABSORPTION X-SECTION FOR GAD PELLET

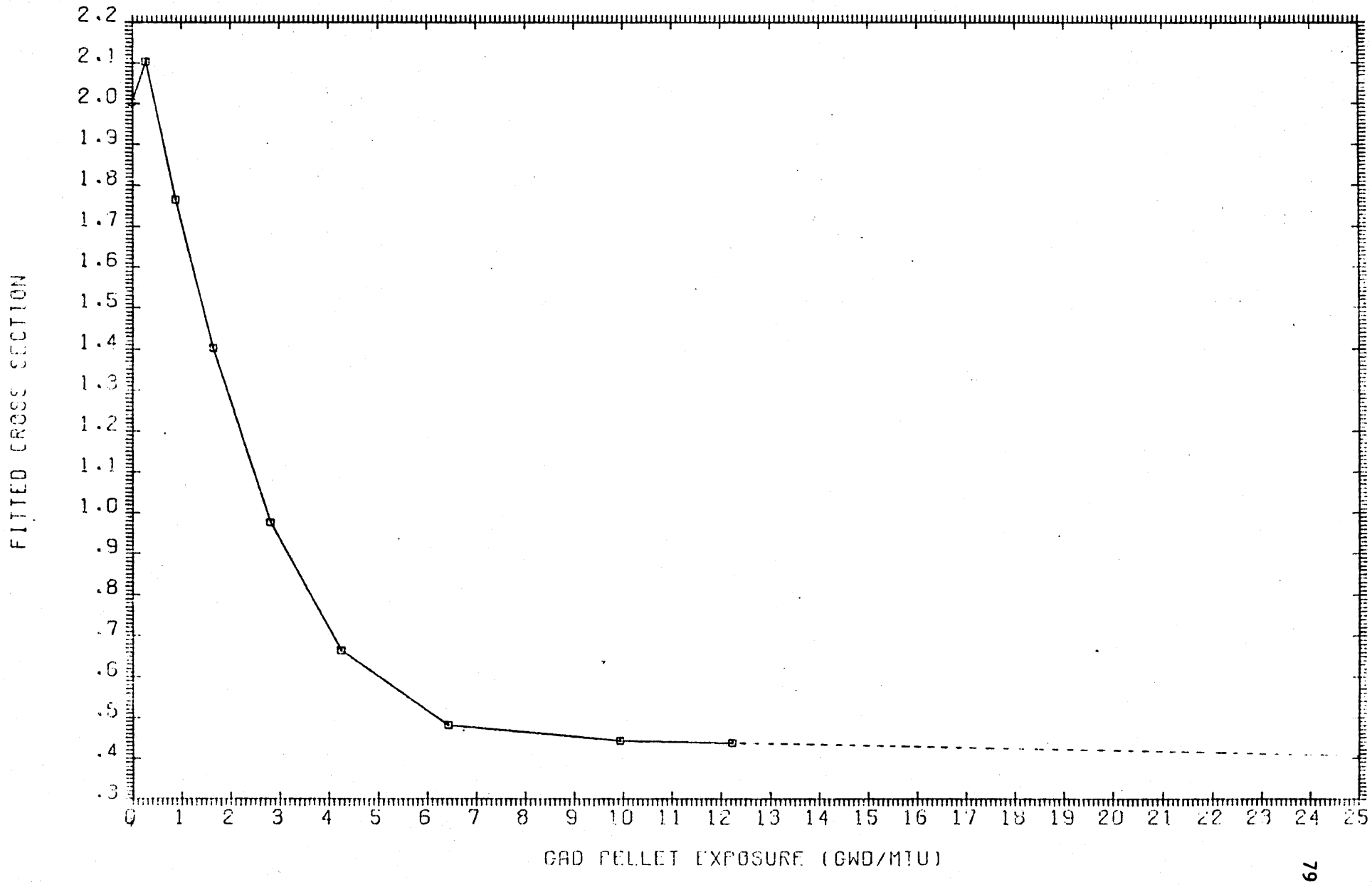

Figure 5-12 FITTED MACROSCOPIC MND NU FISSION X-SECTION FOR GAD PELLET

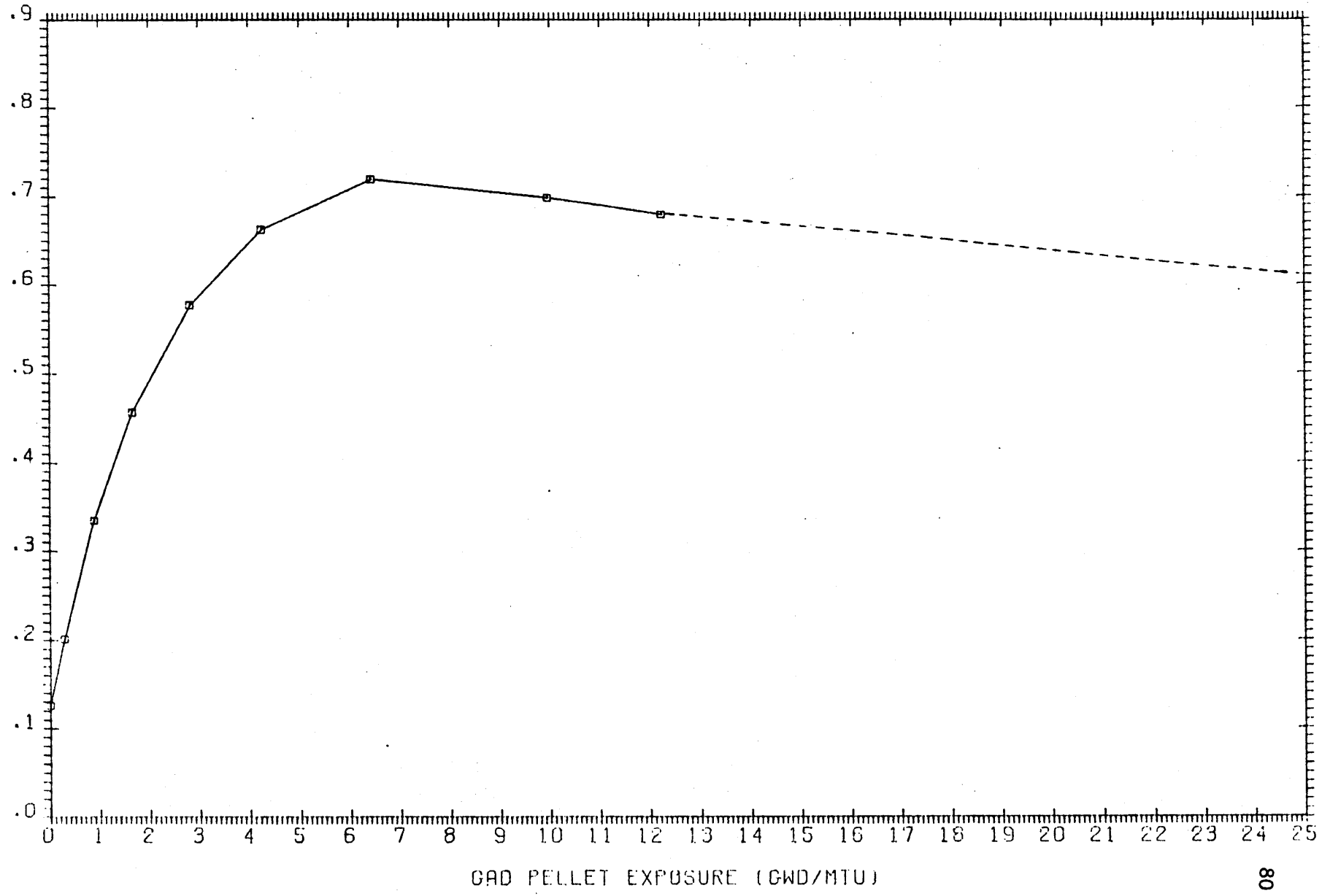

Figure 5-13 FITTED MACROSCOPIC MND K FISSION X-SECTION FOR GAD PELLET

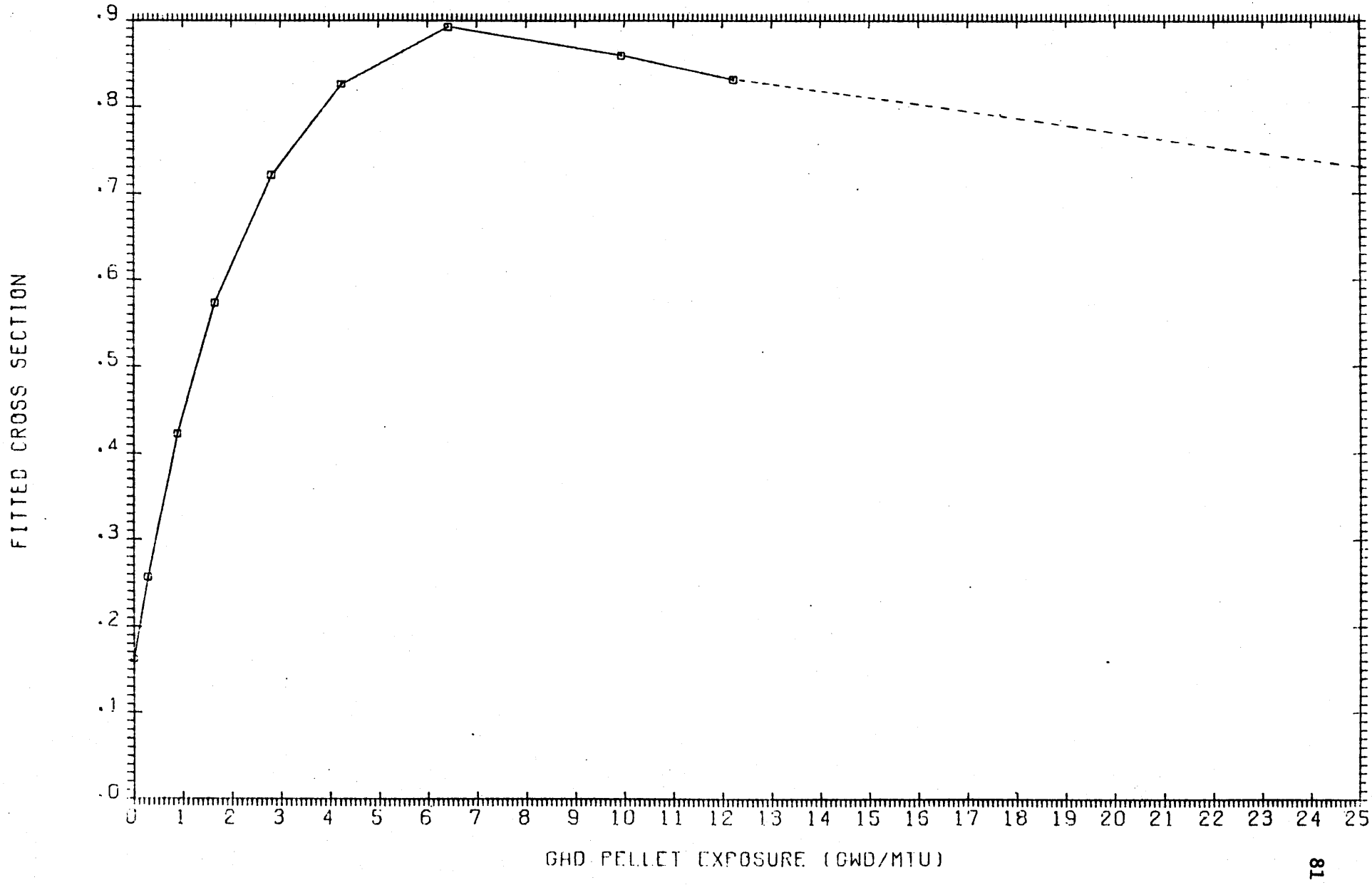

6.0 TREATMENT OF CONTROL RODS

6.1 Introduction

Figure 6-1 is a detailed drawing of a VY control rod blade, its characteristics and dimensions. This cruciform control rod contains 84 vertical stainless steel tubes filled with boron carbide (B_4C) powder, compacted to approximately 70% of theoretical density. The 30 percent free volume is used to accommodate helium which is generated by the B^{10} (n,α) Li reaction. The tubes are held in a cruciform array by a stainless steel sheet extending the full length of the control rod. The sheet has holes which allow water to enter the region between the boron carbide tubes and the sheet to cool the boron carbide tubes heated by the neutron absorption reactions. The inside and outside diameters of the stainless tube are 0.138 and 0.188 inches respectively, and the overall width and thickness of the cruciform control rod are 9.75 and 0.312 inches.

6.2 Difficulties in the Treatment of Cruciform Control Rods with a Round Tube Structure

A treatment which will reproduce what takes place neutronically within a cruciform control rod is extremely difficult to perform, since some neutrons can pass through the rod and not see the absorber material. The transmission of these neutrons through the rod is certainly not due to transparency of the absorber which is black to thermal neutrons, but is due to the slit represented by the clad. Furthermore, some neutrons may scatter off the sheet structure and never reach the black absorber.

Then, treating the rod as a set of solid slabs (as necessary for a 2-D diffusion representation) will overestimate the worth of the

control rod. Therefore, it is important to use Monte Carlo or some form of transport theory in a full rodded bundle calculation. Furthermore, since boron has a large cross section epithermally as well as thermally, the flux must be computed accurately in all energy ranges. Since both methods are very expensive, an alternative approach has been taken. The effect of absorber distribution and of structural materials, such as the stainless steel tubing and sheath, on the relative control worth was estimated by General Electric Company(32) based on the results of blackness tests on samples of control rods with B_4C filled tubes in a critical assembly facility. The results were compared with the measured worth of bare B_4C slabs for several boron surface densities. The plot of the comparison is reproduced in Figure 6-2. As seen from Figure 6-2 and stated in Reference 32, the worth of a cruciform control rod is lower by an almost constant ratio, than the worth of a bare B_4C slab with the same boron surface density. Therefore, the worth of a bare B_4C slab, which can be calculated by using PDQ, must be reduced by a factor which can be estimated from Figure 6-2 for the given configuration and boron surface density of the cruciform rod.

In this study, the calculation of two-group diffusion theory constants for the cruciform control rods has been performed in the following steps.

1) The cruciform control rod was transformed to a continuous bare slab absorber by preserving the surface density of boron and the thickness of the control rod. Then, a reactivity worth reduction factor for the bare B_4C slab was obtained

from Figure 6-2 for the specific configuration and boron surface density of the VY cruciform control rod.

2) Two-group constants for the equivalent bare slab absorber were computed by using the RODWORTH code. These constants were corrected to account for the number of internal mesh points and for the MND scheme used in the PDQ rodded bundle calculation.

   Since the stainless steel central structure was explicitly represented in PDQ, two-group constants were computed by using LEOPARD for this homogeneous region.

3) Using these constants in PDQ, the reactivity worth of the equivalent bare slab absorber was calculated and then decreased by the reduction factor obtained in step one, to yield the reactivity worth of the cruciform control rod.

4) A series of PDQ calculations was run changing the MND macroscopic absorption cross-section of the equivalent slab absorber until it matched the predicted reactivity worth of the control rod. This fitted MND macroscopic absorption with the other slab constants constitutes the two-group control rod diffusion constants which predict the reactivity worth of the control rod.

6.2.1 Transformation of Cruciform Control Rod to Continuous Bare Slab Absorber

This transformation of geometry was performed by preserving the surface density of boron and the thickness of the control rod. That is, the density of B_4C for the bare slab geometry was adjusted to yield the same boron surface density as the cruciform control rod.

The overall thickness of the cruciform rod was preserved in the slab geometry for the purpose of representing the volume of "non-control" regions correctly.

The adjusted density of B_4C in the bare slab was calculated from:

$$\rho_a = \rho_s / x_o \qquad (6.1)$$

where ρ_a = adjusted density of B_4C in the bare slab, g/cc;

ρ_s = surface density of B_4C in the cruciform rod, g/cm^2;

xo = half-thickness of the cruciform rod, cm.

The "surface density of B_4C in the cruciform rod" is defined as the total amount of B_4C in the control rod divided by the area of the outer surface of the sheet, not considering the outer surface occupied by the stainless steel central structure which was represented explicitly in PDQ, since in Reference 32 nothing is stated about the effect of the hub.

Using the notation and data presented in Figure 6-1:

$\rho s = 0.1645\ g/cm^3$ (6.2)

$\rho a = 0.4152\ g/cm^2$ (6.3)

The boron surface density, ρs_∞ used as a base value in Figure 6-2 was $0.1288\ gm/cm^2$.

In Figure 6-2, the No. 5 curve represents the Vermont Yankee cruciform control rod more closely than any other curve in the figure because it has approximately the same stainless steel clad and sheath thickness (the reactivity worth reduction factor is very sensitive to both thicknesses). Using the No. 5 curve, one obtains the following

reactivity ratio of the cruciform rod to the equivalent bare slab absorber:

$$\frac{\text{Cruciform rod}}{\text{Bare slab absorber}} = \frac{1.109}{1.205} = 0.9203 \qquad (6.4)$$

6.2.2 Constants for the Bare Slab Absorber and the Stainless Steel Hub

The calculation of two-group constants for the bare slab absorber was carried out by using the RODWORTH code.

Cruciform slab geometry with a total thickness 0.312 in. was used. The two macro-group average values of α and β were obtained by averaging the macro group values over the spectrum determined by a BOL LEOPARD assembly supercell, 2.19 w/o U-235 at 40% voids.

The required boron-10 number density within the slab absorber was calculated as:

$$N^{B_{10}} = \frac{\rho_a W^B W^{B_{10}}}{10.0}\left(0.6025\right) = 0.003873 \text{ atoms/b-cm}$$

where W^B is the weight fraction of boron in B_4C, 0.7828, and W^{B-10} is the natural abundance of B-10, 0.1978.

Figure 6-3 shows the bare slab absorber mesh overlay. Two internal mesh points were used within the half-slab in PDQ rodded bundle calculations (equivalent to three internal points in a full slab). As RODWORTH edits one-internal and zero-internal mesh point constants, the three-internal mesh point constants were hand-calculated using the following equations:

$$D = \frac{h(\alpha+\beta)}{2\sinh(Kh)}\tanh(KD) \qquad (6.5)$$

$$\Sigma_a = \frac{2D}{h^2}\left[\cosh(Kh)-1\right] \qquad (6.6)$$

where h is the mesh size, and:

$$K = \frac{1}{D} \ln \left[\frac{1 + (\alpha/\beta)^{1/2}}{1 - (\alpha/\beta)^{1/2}} \right] \qquad (6.7)$$

These equations have been derived by Gelbard and are also presented by Michelini (33).

We refer to three instead of two internal mesh point constants since these equations have been derived to account for the number of internal mesh points used in a finite difference solution of the "whole slab". From RODWORTH, the following two group, average values of α and β were obtained.

Group	α	β	
Fast	3346-1	8677+1	
Thermal	4962+0	5047+0	(6.8)

Using equations 6.5 to 6.7 with α,β given by 6.8 and h, D set equal to 0.19812 and 0.79248 cm. respectively, results in the following three-internal mesh point constants.

Group	D(3)	$\sum a(3)$	
Fast	3433200+1	8454600-1	(6.9)
Thermal	5414700-1	2997119+1	(6.10)

Using D(3), $\Sigma_a^{Th}(3)$ given by 6.10 and taking $(1/v)^{WW}$ from the LEOPARD problem used to obtain the flux spectrum, results in the following MND constants for the bare slab absorbers.

	D(3)	$\Sigma a(3)$	
MND Constant	9377900-1	5190814+1	(6.11)

Thus, (6.9) and (6.11) were the two group constants used for the bare slab absorber in PDQ.

The two group constants for the homogeneous stainless steel hub structure were calculated as:

$$\Sigma = N_o \sigma \qquad D = 1/(3\Sigma_{TR}) \qquad (6.12)$$

where N_o is the LEOPARD basic number density of SS-304 (0.08807 at/b-cm) and σ represents the SS-304 microscopic cross sections (except the removal), obtained from the preceeding LEOPARD run. The SS-304 microscopic removal cross section was not obtained from LEOPARD because it gives a negative value.

As the SRT is inadequate to use because there is no hydrogen associated with this region, the SS-304 microscopic removal cross section was determined by atom averaging the σ_R of the individual elements which constitute the SS-304 (68.6% Fe, 9.5% Ni; 19.0% Cr; 2.0% Mn) where σ_R of the elements was calculated by using Treatment 2 obtaining the group fluxes from the preceding LEOPARD.

Thus, the two group constants shown in Table 6-1 were obtained for the stainless steel central structure.

6.2.3 Reactivity Worth of the Control Rod

The reactivity worth of the bare slab absorber was calculated by:

$$\Delta\rho^{SLAB} = \frac{k_\infty^{OUT} - k_\infty^{IN}}{k_\infty^{OUT}\, k_\infty^{IN}} \qquad (6.13)$$

where:

k_∞^{OUT} is the multiplication factor from the PDQ calculation of the unrodded fuel bundle;

k_∞^{IN} is the multiplication factor from the PDQ calculation of the fuel bundle containing the control slab.

The PDQ calculations were carried out as explained in Chapter 7. The result for the unrodded fuel bundle (discussed more fully in Chapter

8) is a k_{∞}^{OUT} of 1.10305, and the fuel bundle with control slab results in a k_{∞}^{IN} of 0.8043. By equation 6.13, this gives a slab reactivity worth of:

$$\Delta\rho^{SLAB} = 0.3367$$

Reducing this by the factor of 0.920 from Figure 6-2, yields a control rod reactivity worth of 0.3099.

6.2.4 Determining the Effective Control Rod Constants

This was accomplished by running a series of PDQ two dimensional fuel bundle calculations with differing MND microscopic absorption cross sections for the bare slab region until one matched the predicted reactivity worth of the control rod. Table 6-2 shows the resulting reactivity worth as a function of the MND absorption cross section of the bare slab region.

Figure 6-4 shows the reactivity worth of the control rod as a function of the control rod MND macroscopic absorption cross section. Since the true reactivity worth of the cruciform rod is 0.3099, the interpolation of the above data gives 245+1 cm^{-1} for the MND macroscopic absorption cross section of the cruciform control rod. Thus, the final set of two group constants of the Vermont Yankee cruciform control region is as shown in Table 6-3.

Figure 8-11 shows the local power peaking for the rodded fuel bundle calculated by using PDQ with these constants.

TABLE 6-1

Two Group Constants for the Control Rod Hub

	D	Σa	ΣR
Fast	10291+1	34841-2	11926-2
MND	51137+0	26313+0	0+0

TABLE 6-2

Slab Reactivity Worth as a Function of MND Absorption Cross Section

MND Absorption Cross Section (cm^{-1})	Reactivity Worth ($\Delta\rho$)
5.1908	0.3367
4.1527	0.3290
3.0	0.3169
2.0	0.3004
1.0	0.2689

TABLE 6-3

Final Cross Sections for Control Rod

	D	Σa	Σ_R
Fast	3433+1	84546-1	0+0
MND	93779-1	245+1	0+0

Figure 6-1
Control Blade Model

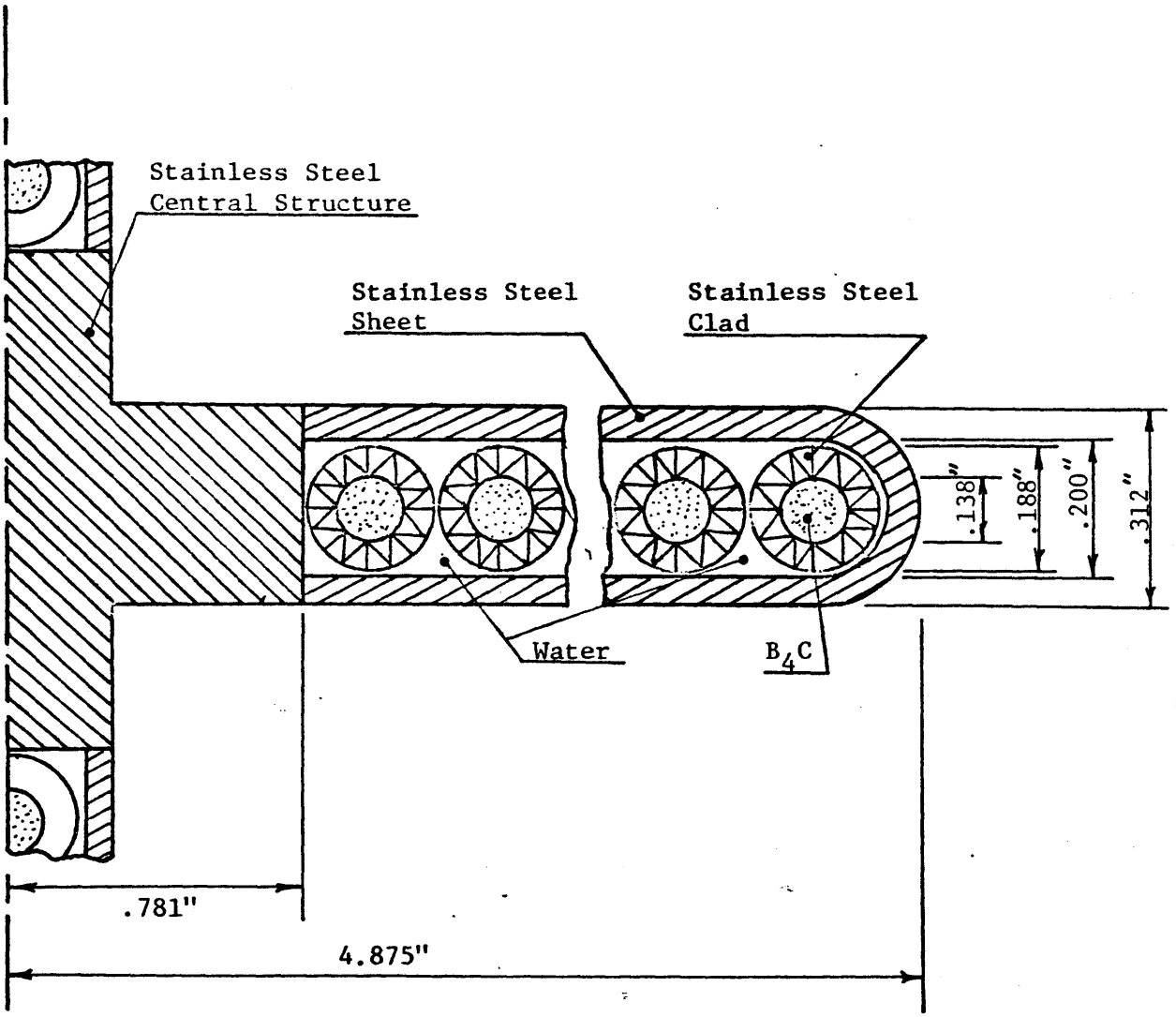

Parameters

Control Rod Pitch	12.0
Poison Length	143.0
Number of Poison Tubes per BladeWing	21
B_4C Theoretical Density, G/cc	2.504
B_4C Percent of Theoretical Density	70

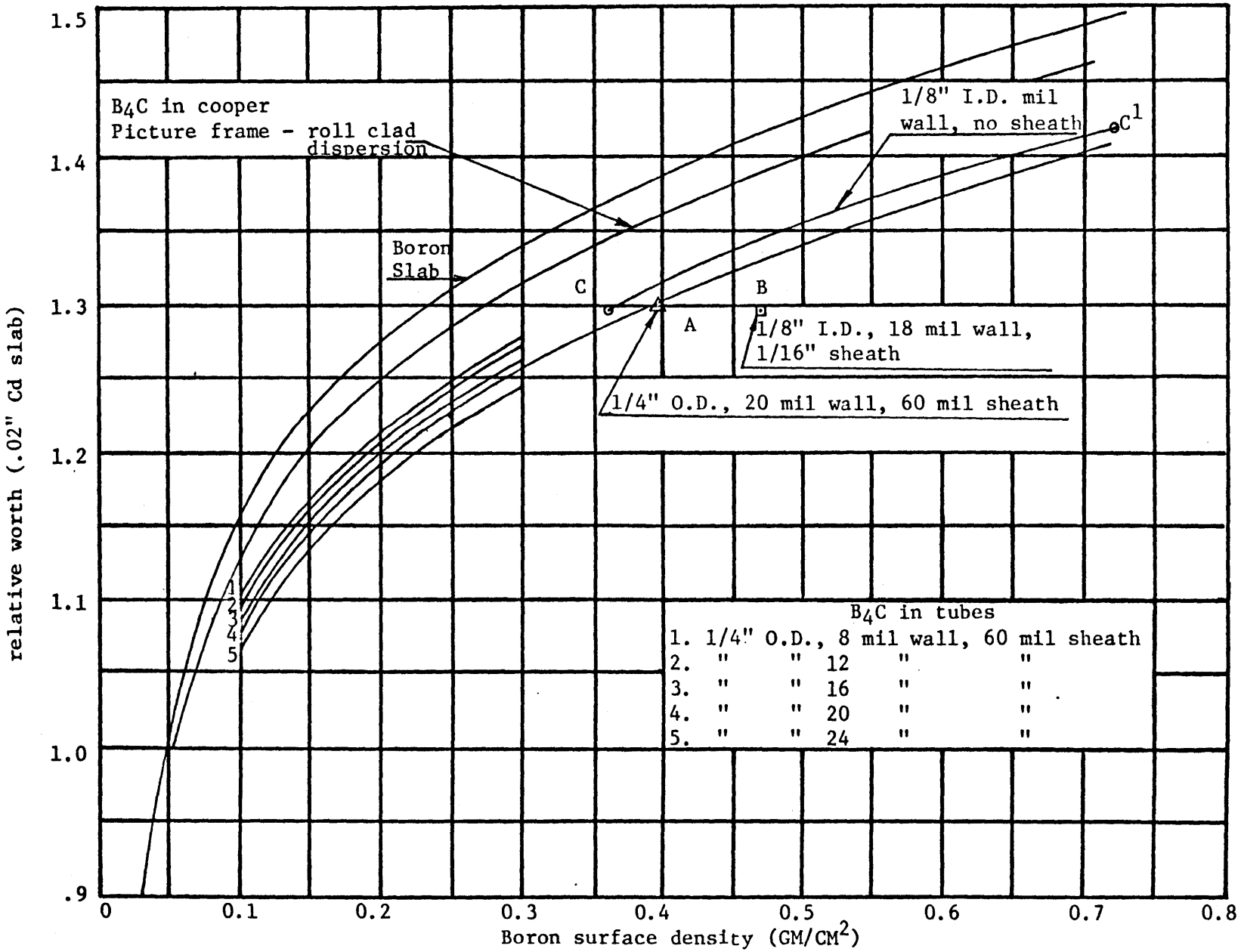

FIGURE 6-2 RELATIVE WORTH VS. SURFACE DENSITY FOR B_4C

Figure 6-3

Bare Slab Absorber Mesh Overlay

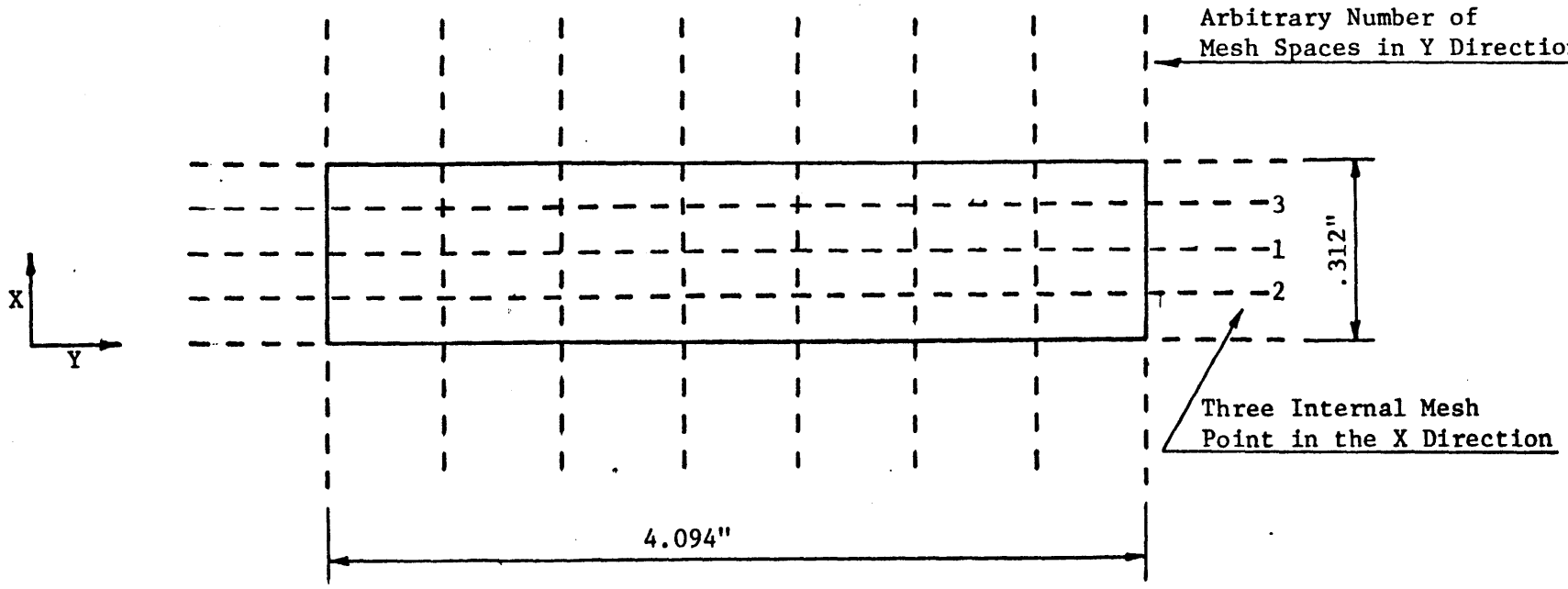

Figure 6-4 CONTROL ROD REACTIVITY WORTH VS MACROSCOPIC MND ABSORPTION CROSS SECTION

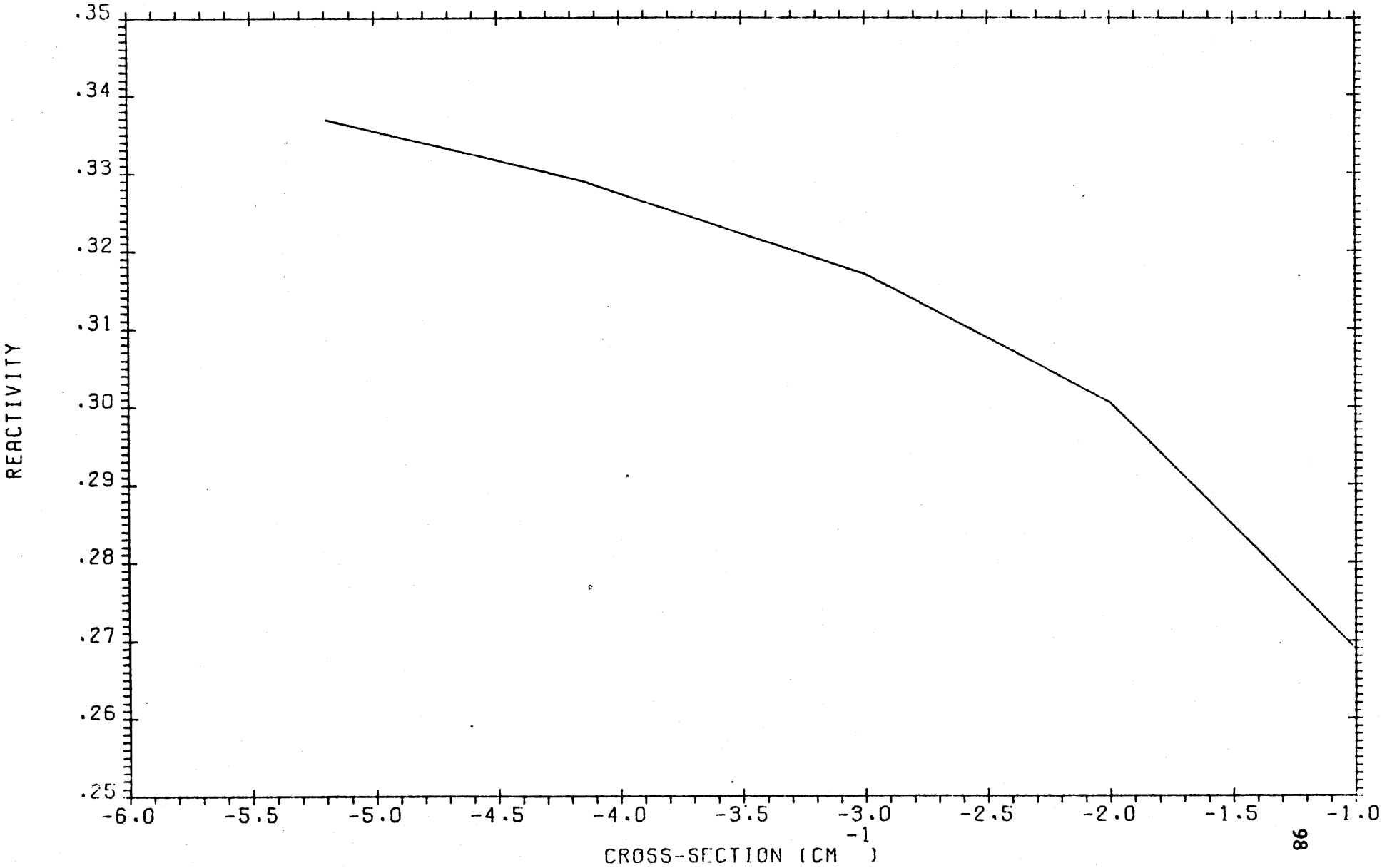

7.0 TREATMENT OF THE BUNDLE BY DIFFUSION THEORY

7.1 Introduction

This chapter describes the PDQ07-HARMONY model used in this study to perform bundle calculations of power distributions, burnups, lifetime and rod worths. A similar method has been used to analyze the Maine Yankee and Yankee Rowe PWR's and was found to give good results (Reference 34). All detailed discussions pertain to the model used for Vermont Yankee Reload 2 Fuel Bundle (2.19% average enrichment) at 40% voids.

PDQ07 is a diffusion theory code developed at Bettis Atomic Power Laboratory. It solves the diffusion equations in a finite-difference form that results from representing the fuel bundle by a set of discrete meshes. Few group cross-sections are assigned to each region defined by the grid of mesh points. Once the problem has been defined by the specification of the spatial relationships between the meshes and the cross-sections given for each region, a set of neutron fluxes is determined. This set of fluxes and the associated cross-sections will then yield all reaction rates of interest, such as absorption or fission rates.

The HARMONY program, also a Bettis product, is the mechanism for storing cross section data and making it available to the PDQ07 program. The cross-sections used are calculated by the LEOPARD, NUCELL and RODWORTH programs. The CHIMP-II program was used to automatically transfer cross-sections from LEOPARD to HARMONY. HARMONY also solves the depletion equations that describe the fuel bundle and keeps track of each nuclide concentration as depletion proceeds. The program is very flexible in the method of cross-section

storage and nuclides allowed, so that it can be tailored to fit many reactor types.

7.2 The PDQ Representation

7.2.1 Solution Geometry

The geometry used was a full bundle 2-D representation, since diagonal symmetry is not allowed as an option. The rectangular mesh grid had 35 points (34 mesh intervals) on each side. The planar mesh intervals reflect hot rather than cold dimensions (1.6256 cm fuel rod pitch, cold vs. 1.62814 cm hot).

Figure 7-1 shows the general layout. There are 44 regions with composition correspondence to region one-to-one, since the largest composition and planar region numbers are equal. The problem is divided into the 33 regular fuel cells, the 2 clad-moderator regions for the gadolinia pins, the water tube cell, the voided film, the Zr-4 channel, the water gaps (narrow and wide separately), the control rod, the stainless steel central structure and the 2 gadolinia fuel bearing pellets. Except for the case of the gadolinia fuel, the details of each fuel cell such as the fuel pellet, clad and moderator are not shown. Rather the fuel pin and the moderator are homogenized. A reflection (zero current) boundary condition was used at the four sides of the layout shown in Figure 7-1.

7.2.2 Edit Geometry

The following edit sets were selected:

1) All regular fuel an edit set;
2) The two gadolinia pellets an edit set;
3) The bundle an edit set;
4) Each region an edit set.

The two first were selected to calculate the evolution of the fuel isotopic compositions with the burnup, the third to calculate the bundle critical buckling, the migration area and the two-group constants, and the fourth to check the gadolinia densities and regular fuel isotopic compositions versus burnup.

7.2.3 Power and Depletion Intervals

A power level is input to the PDQ problem as well as a time interval. The power level given is the number of watts the PDQ represents. For a 2-D problem, the axial direction is assumed to be 1 cm high. Therefore, a fuel bundle 2-D problem would represent the following power:

$$\text{PDQ Power} = \frac{1\ \text{cm}\ (\text{Bundle Ave. Power (watts)})}{\text{core height (cm)}} \tag{7.1}$$

Using equation 8.1, the PDQ bundle power at hot conditions was calculated as:

$$\text{PDQ Power} = \frac{1593\ (10^6)}{368\ (144.666)\ (2.54)} = 11780.6\ \text{watts} \tag{7.2}$$

where 1593 is the Full Core Power in MWth

144.666 is the fuel height at hot conditions

This power value is used to determine the neutron flux level for depletion purposes. The input time interval specifies how long the bundle is to operate at the given power level. To account for the

high burnup rate of the 155 and 157 gadolinium isotopes, i.e., the fast variation of the MND macroscopic absorption and fission cross-sections of the gadolinia fuel pellet with the burnup, time steps of 500 MWD/MTU were taken up to 10,000 MWD/MTU (when the gadolinia is gone) the depletion being followed until 32,500 MWD/STU by using 6 further steps - three of 2500 and another three of 5000 MWD/STU. Two initial steps of 100 and 400 MWD/STU were used to accurately represent the Xe-135 and Sm-149 buildup at the start of the calculation. Thus, a total of 27 time steps was run in this study to reach the end of life of the bundle. Since PDQ requires the time (in hours) at the beginning and at the end of the depletion calculation, the selected burnup steps (in MWD/STU) were transformed by the equation

$$T(\text{hrs}) = \frac{(\text{MTU/cm bundle})(0.9072)}{(\text{Input watts/cm})\,10^{-6}} \qquad (7.3)$$

where 0.9072 is the conversion factor to pass from MT to ST. Flux renormalization during a depletion step was not used.

The basic scheme used in a PDQ depletion calculation is as follows. First, the fluxes are calculated for the initial nuclide concentrations. This set of fluxes is then used in the depletion part. However, there is another time interval to be considered, the cross-section re-evaluation interval. This is the interval at which cross-sections that depend on nuclide concentrations are re-evaluated. The interval may be different for each data type and for each nuclide. This interval is part of the cross-section data itself.

Once a total depletion step has been finished, we arrive at new nuclide concentrations. Then we can calculate a new set of fluxes and

are ready to begin the depletion process again. In this manner, the bundle is depleted from beginning-of-life to end-of-life.

There are two depletion options in PDQ, pointwise depletion and blockwise depletion. In pointwise depletion, concentrations are calculated for each small area surrounding each point. This method gives the greatest detail of depletion effects. In blockwise depletion, concentrations are calculated for each block defined by a final figure number, region number pair. This method is faster running but less explicit. Since great detail of local depletion effects is required to calculate good local peaking factors versus burnup, the pointwise depletion option was selected.

7.2.4 Axial Buckling

To account for neutron leakage out of the bundle in the axial direction (and in the radial), a buckling value can be input. Since we were only interested in the variation of K_∞, M^2 and the local peaking factors with the burnup, a value of 0+0 was input for the two groups and the 44 compositions.

7.2.5 Files

Much of the output of the PDQ program can be saved on tape or disk files. These include fluxes, power values, nuclide concentrations, details of geometry and reaction rates. PDQ was always requested to save flux, concentration and partition power files on tape and disk after every depletion time step. In the first step, it was asked to save the geometry file, which was then used in all the other depletion steps. Since PDQ purges the geometry and partition power files of the preceding step, the geometry file of the first step and the concentration files of each time step were saved on tape and disk,

allowing in this way the possibility of performing restart calculations.

7.3 Harmony

7.3.1 Cross-Section Definition

The PDQ program accepts as input, macroscopic cross-sections for each region. When the calculation of the fluxes is done, there is no distinction made between nuclides, only a single value of $\Sigma a, \Sigma f$, etc. for each group is given. HARMONY keeps track of each nuclide's contribution and sums them for use by the PDQ. Values of the interpolating cross-sections are given for a discrete set of concentrations known as mask tables. The mask tables are used in conjunction with the interpolating tables, i.e., the mask forms the abscissa values while the interpolating tables make up the ordinate values. Non-interpolating data does not depend on any nuclide concentration. It is a constant value. For example, σa of Pu-242 for the thermal group may be considered a constant value. U-235 concentration, Pu-240 concentration, fission product concentration, and gadolinium pellet burnup make up the four mask tables used in this study.

In the model used for VY Reload 2 fuel bundle, there were three types of treatment for cross-sections. Two for fueled regions (one for regular fuel regions and another for gadolinia fuel regions) and one for non-fueled regions. In the non-fuel region, it is assumed that no depletion occurs, i.e., the nuclide inventory stayed constant.

7.3.2 Tablesets for Non-Gadolinia Bearing Fuel

The regular fuel tablesets contain all the cross-section data for the representation of the non-gadolinia fuel used in the PDQ. Table 7-1 shows the cross section to Table assignment and the LEOPARD burnup steps used in CHIMP to obtain the cross-sections of the regular fuel tablesets. The master cross-sections were obtained from a middle of life step (14,000 MWD/MTU). Additionally, the values of Kappa and Nu for each fissionable nuclide were assigned as master micro, except that the Kappa for Pu-240 fuel was assigned as reversed micro interpolating table due to its 50% variation with the burnup. All the interpolating data was constructed with the U-235 mask, except the reversed micro interpolating σ_a of Pu-240 for the fast group and σ_a of the FP nuclide for both groups, which were correlated to Pu-240 and F.P. masks, respectively. The CHIMP-II program set up all but the mask cards for a HARMONY tableset input. The mask values themselves are the fuel pin cell number densities obtained from the depletion LEOPARDS for the fourteen burnup steps under consideration for the regular fuel regions. When table assignment number five is chosen in the CHIMP input, the cross sections are placed in reversed order, with the last time step first.

7.3.3 The Gadolinia Fuel Pellet Tableset

The gadolinia tableset contains all the cross-section data for the gadolinia pellet representation used in the PDQ. The data used to formulate the tableset were obtained from the fitting procedure discussed in Chapter 5. There are two types of data used, master macro and macro interpolating tables. The master macro data are the fast macroscopic transport and removal constants given in Chapter

5 . The macro-interpolating data consists of the MND macroscopic transport and the macroscopic absorption, nu-fission and kappa-fission for both groups. These cross-sections were given as a function of a dummy isotope concentration which equals the gadolinia pellet burnup (MWD/MTU). Figures 5-7 to 5-13 show the variation of these cross-sections with the mask. Since the gadolinia pellet burnup has an increasing value with time, the dummy mask and its associated cross-sections were input in reverse order.

To create the gadolinia pellet burnup counter (MWD/MTU), two chains and another dummy isotope were associated with the gadolinia pellet regions as will be shown in 7.3.6.

7.3.4 Nuclides and Chains

The reactions taking place in the fuel bundle were restricted to 14 nuclides. This is a simplification since there are actually more than 200 nuclides present, many created in the fission process. This simplified model is a good approximation.

The values of kappa and nu were taken from LEOPARD at middle of life. The kappa value includes most forms of energy from the fission process, the kinetic energy of the fission fragments and neutrons, heat of decay products, and gamma absorption energy. The energy of neutrinos is lost. Before they are assigned to a master micro table, CHIMP converts them to effective values by dividing by the fraction of total power generated directly in fission. In this way, the PDQ bundle power is calculated based on the total reactor power, i.e., without removing the fraction of the power produced by α, β and γ decay (3%).

Shown below are the depletion and fission product chains used. The applicable chains are assigned to each region. The following characters are used:

a = absorption

f = fission

d = decay

1. Depletion chain for U-235, U-236

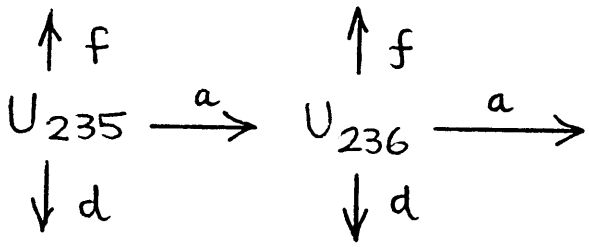

2. Depletion chain for U-238, and Pu-239, Pu-240, Pu-241, Pu-242

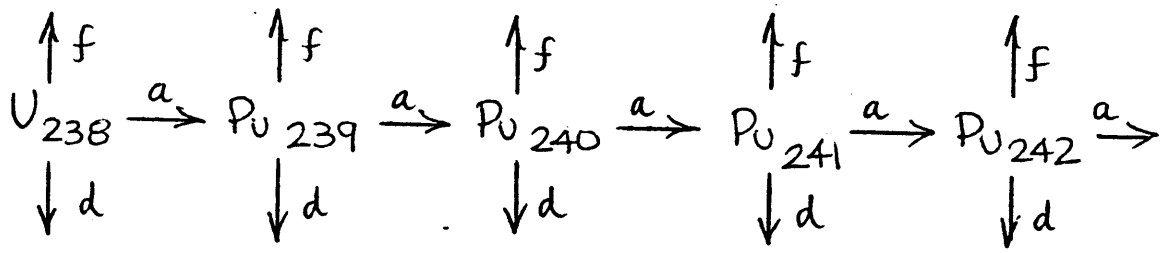

3. Fission product chain for I135 and XE135

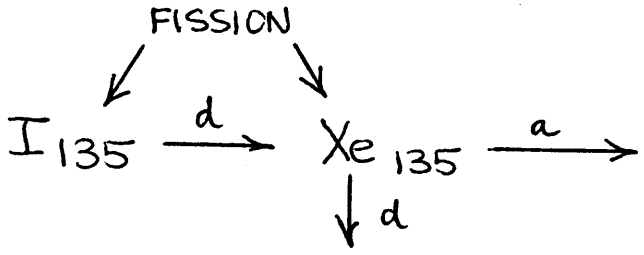

4. Fission product chain for PM149 and SM149

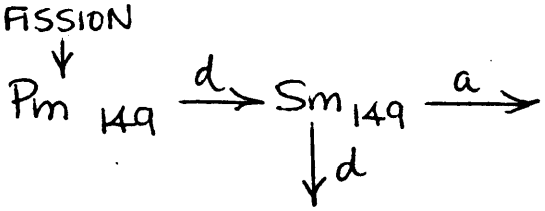

5. Fission product chain for F.P. nuclide (accounts for fission products except I135, XE135, PM149 and SM149).

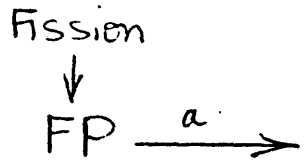

6. Depletion Chain for KAPF nuclide, parent of MWD/MTU nuclide

(Non-Depleting)

7. Fission Product Chain for MWD/MTU nuclide

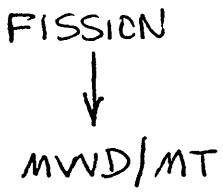

The MWD/MTU nuclide is a measure of the gadolinia fuel pellet burnup. This quantity was used as mask table to correlate the macro interpolating cross-sections in the gadolinia fuel pellet tableset. In the PDQ, it is calculated as a fission product of a non-depleting nuclide (KAPF), which has a constant concentration. A fast (MND) microscopic fission cross-section equal to the fast (MND) macroscopic kappa fission cross-section of the gadolinia fuel pellet is given to the parent nuclide, which has a concentration of 1-29 (at/b-cm) and a

negligible decay constant (1-20 sec^{-1}). This small concentration was used to avoid any contribution of the parent nuclide to the total kappa fission reaction rates in the gadolinium fuel pellet.

7.3.5 Control Rod Constants

The same set of rod constants was used for all calculations. They were described in Chapter 6. The cross section values were given in Table 6-3.

TABLE 7-1

Cross Section to Table Assignment

Isotope

LEOPARD Index	HARMONY Index	Element	Σ_{tr1}	Σ_{a1}	Σ_{r1}	Σ_{f1}	Σ_{tr2}	Σ_{a2}	Σ_{f2}
1	1	Hydrogen	2	2	2	1	2	2	1
2	2	Oxygen	2	2	2	1	2	2	1
3	3	Zirconium-2	2	2	2	1	2	2	1
18	235	Uranium-235	2	4	2	4	2	4	4
19	236	Uranium-236	2	4	2	3	2	4	1
20	238	Uranium-238	2	4	2	3	2	4	1
21	239	Plutonium-239	2	4	2	4	2	4	4
22	240	Plutonium-240	2	5	2	3	2	4	3
23	241	Plutonium-241	2	4	2	4	2	4	4
24	242	Plutonium-242	2	4	2	3	2	3	1
26	1492	Samarium-149	2	3	2	1	2	4	1
27	1352	Xenon-135	2	3	2	1	2	4	1
28	900	Fission Products	2	5	2	1	2	5	1

Burnup steps to be used (MWD/MTU)

0, 100, 500, 1000, 2000, 4000, 6000, 8000, 10000, 14000, 18000, 22000, 26000, 30000 (limited to 14 burnup steps)

14000 was used to obtain the Master Tables

Table Assignment Number	Table
1	Master Macro
2	Macro Interpolating
3	Master Micro
4	Micro Interpolating
5	Reversed Micro Interpolating

Figure 7-1.
PDQ Bundle Geometry

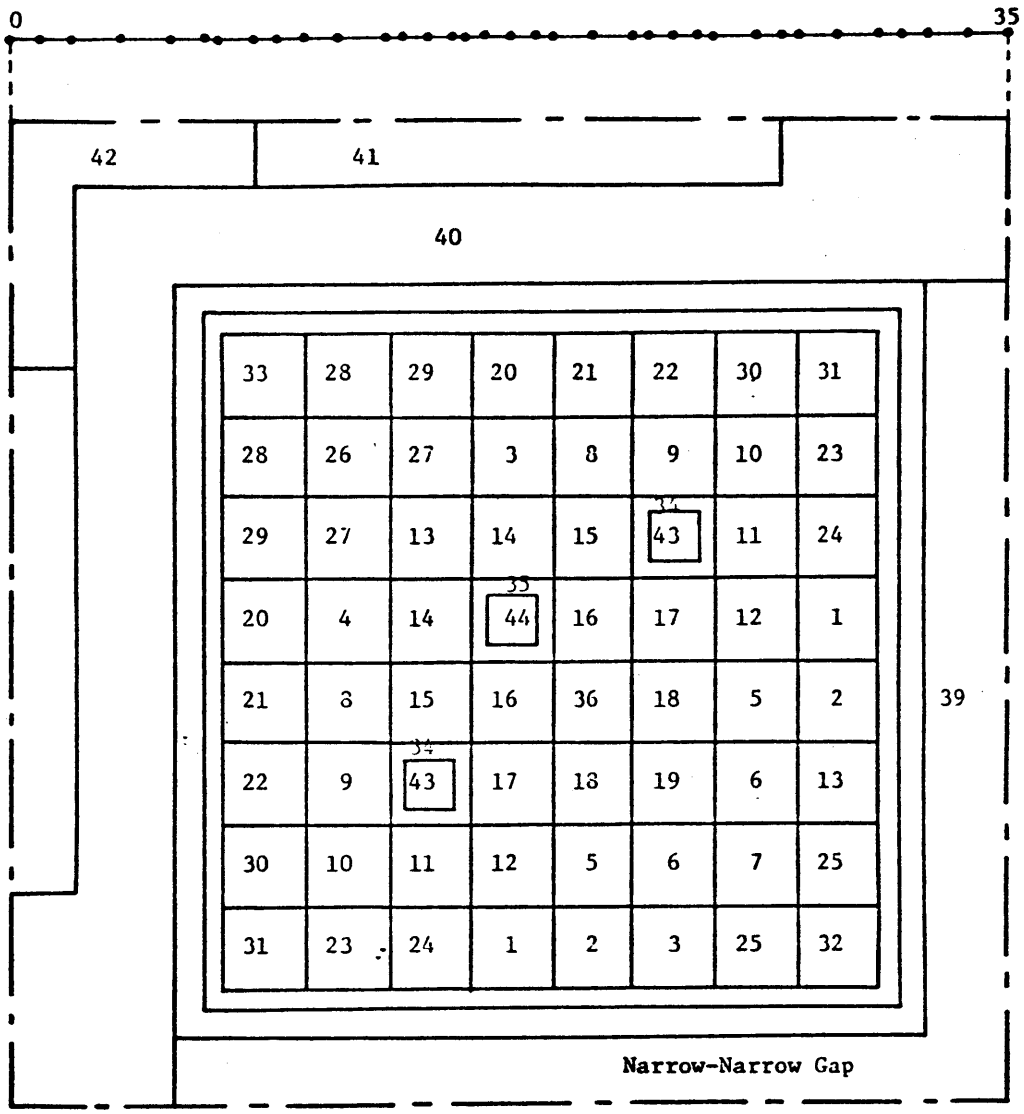

Non-Gadolinium Fuel Receiving Regions

1 to 19: 2.50% Fuel Cell
20 to 27: 1.90% Fuel Cell
28 to 32: 1.49% Fuel Cell
33: 1.18% Fuel Cell

Gadolinium Bearing Fuel Regions

43 to 44: Gadolinium Fuel Pellets

Non-Fuel Regions

34 to 35: Gad Clad + Mod Regions
36: Water Tube Cell
37: Voided Flux
38: Zr-4 Channel
39: Narrow Water Gap
40: Wide Water Gap
41: Control Rod 1
42: SS-304 Central Structure

8.0 RESULTS

8.1 Summary of Cases Calculated

The model described in Chapter 7 has been applied to the 8D219 bundle described in Chapter 2. Four bundle depletions were performed under various control conditions:

- Case X. Unrodded depletion to 27.5GWD/STU
- Case A. Depletion to 4 GWD/STU with control rod alternately inserted for 1 GWD/STU, then removed for next 1 GWD/STU, etc.
- Case B. Depletion to 4 GWD/STU with control rod alternately removed for first 1 GWD/STU, then inserted for next 1 GWD/STU, etc. This is the reverse of Case A.
- Case C. Depletion to 22.5 GWD/STU with control rod alternately inserted for 1 GWD/STU, and removed for 3 GWD/STU.

Case X is the simplest kind of bundle depletion which could be performed. Cases A and B were performed to estimate the sensitivity of bundle rod-out characteristics to depletion history.

Case C represents a more or less realistic approximation to the control history seen by a bundle operating in the core. The control rods available to the core are usually divided into four groups, which are used sequentially for about 1 GWD/STU each to control the core.

8.2 Infinite Multiplication Factor

Figure 8-1 compares the values of k_∞ from PDQ depletions of the bundle under the control rod out condition (Case X), control rod out with no-gad condition (Case Y), and control rod inserted for one out of every four GWD/STU condition (Case C). For Case C, the values of k_∞ have been plotted only for those exposures where the control rod

was not inserted, so that a meaningful comparison can be made with Cases X and Y. The results in Figure 8-1 show that:

- After the gad burns out, the k_∞ of the gad bundle approaches that of the bundle with no gad, when both depletions are performed with no control rod insertion.
- The effect of control rod insertion during part of the depletion is to raise the unrodded k_∞ of the bundle. This effect may initially be due to changes in the burnout rate of the gadolinia because of the flux tilt induced by control rod insertion. However, Figure 8-1 shows that the effect appears to be permanent; it remains even after the gadolinia has burned out.

As a check on this effect, the values of k_∞ from the PDQ depletion of the bundle without gadolinia (Case Y) were compared with those from a LEOPARD depletion of the same bundle. Figure 8-2 shows that good agreement is obtained between the two calculations, although one might expect some difference simply because the LEOPARD depletion contains great detail in energy but little detail in space, whereas the PDQ is just the reverse.

Further indications of this effect are shown in Figure 8-3, which presents details of the k_∞ values from Cases X and C, as well as k_∞ values from Cases A and B, in which the bundle was depleted for alternate periods of 1 GWD/STU in the rodded and unrodded configuration.

The BOL value of k_∞ for the rodded condition is 0.8225. This yields a BOL Δk of 0.281 due to control rod insertion.

8.3 Burnup of Gadolinia

The effect of control rod insertion on gadolinia burnup may be observed in Figures 8-4 and 8-5, which compare the power in the gad fuel rods as a function of exposure for Cases X, A, B and C. It is apparent that control rod insertion somewhat hastens the burnup of gadolinia. This may be seen, too, from Figures 8-6 and 8-7, which show the burnup of the gadolinia pins in comparison to that of the bundle for the various cases.

8.4 Local Peaking

Figures 8-8 through 8-10 show the local power distribution as a function of exposure for Case X, the unrodded depletion.

Figure 8-11 shows the BOL local power distribution for the rodded bundle. The upper set of numbers represents the final results for this condition after the diffusion theory constants for the control rod have been iterated to adjust the control rod worth by the factor shown in Figure 6-2. The increase in power of the gadolinia bearing pins, relative to the unrodded case, is apparent here.

The effect of control rod insertion history on maximum local peaking is shown in Figures 8-12 and 8-13. Figure 8-12 compares the maximum local peak vs. exposure for the rod-out depletion (Case X) and Case C. Like k_∞, the maximum local peaking for the rod-out condition appears to be influenced by the control rod insertion history. This is further illustrated in Figure 8-13, where the rod-out peaking vs. exposure is plotted for Case X, Case C, and from the manufacturer's calculations.

8.5 Parameters for the Homogenized Bundle

Diffusion theory parameters for the homogenized bundle are useful in setting up nodal representations of a full BWR core. Two group, diffusion theory parameters for Case X are plotted in Figure 8-14 through 8-24. The effect of the gadolinia is particularly apparent in the thermal MND parameters. Some effect is also observable in the fast removal cross section.

Figure 8-1 BUNDLE INFINITE MULTIPLICATION FACTOR VS EXPOSURE FROM PDQ to 22.5 GWD/ST

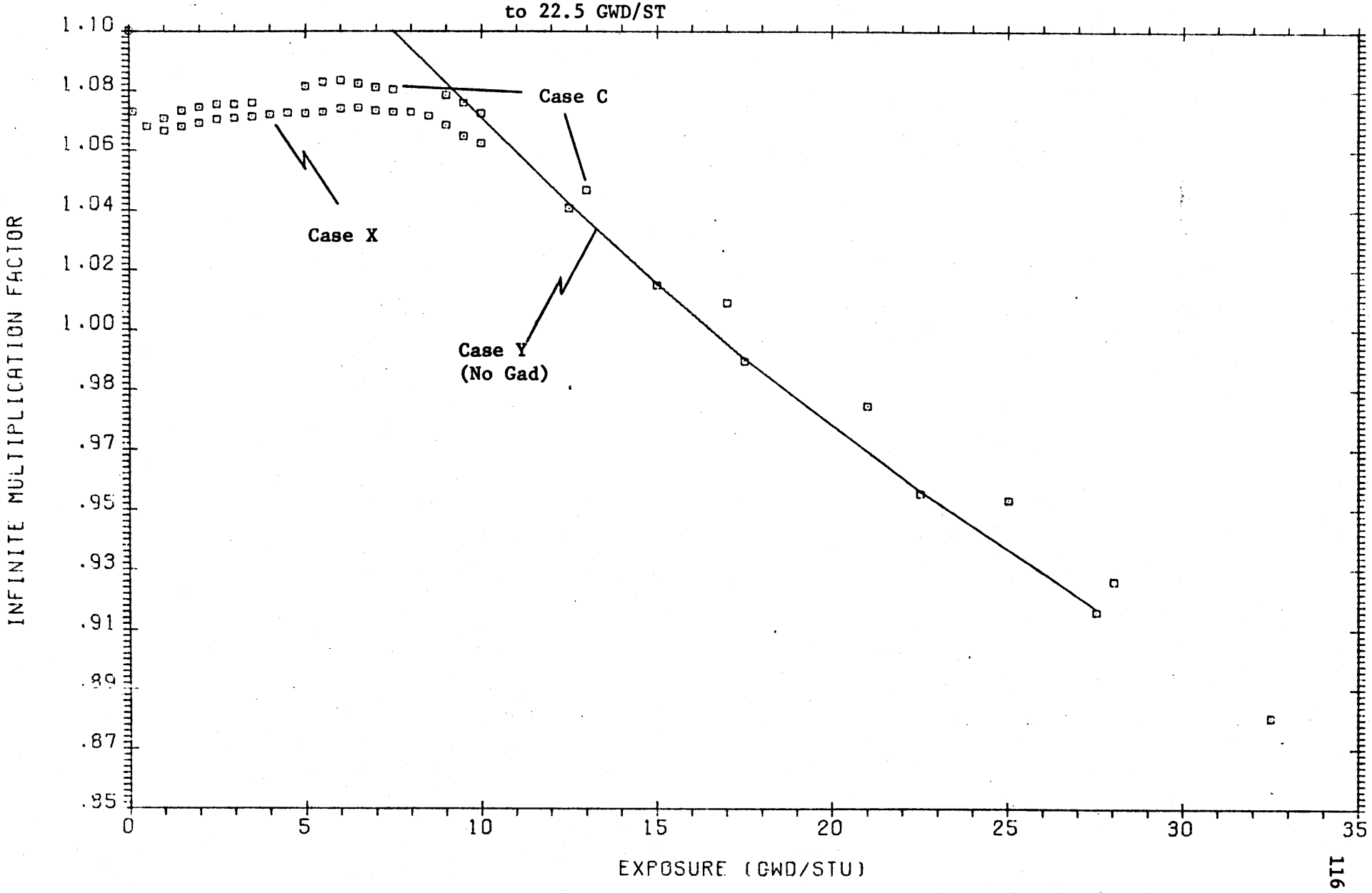

Figure 8-2 BUNDLE (NO GAD AND CR OUT) INFINITE MULTIPLICATION FACTOR VS EXPOSURE

PDQ and LEOPARD Depletions

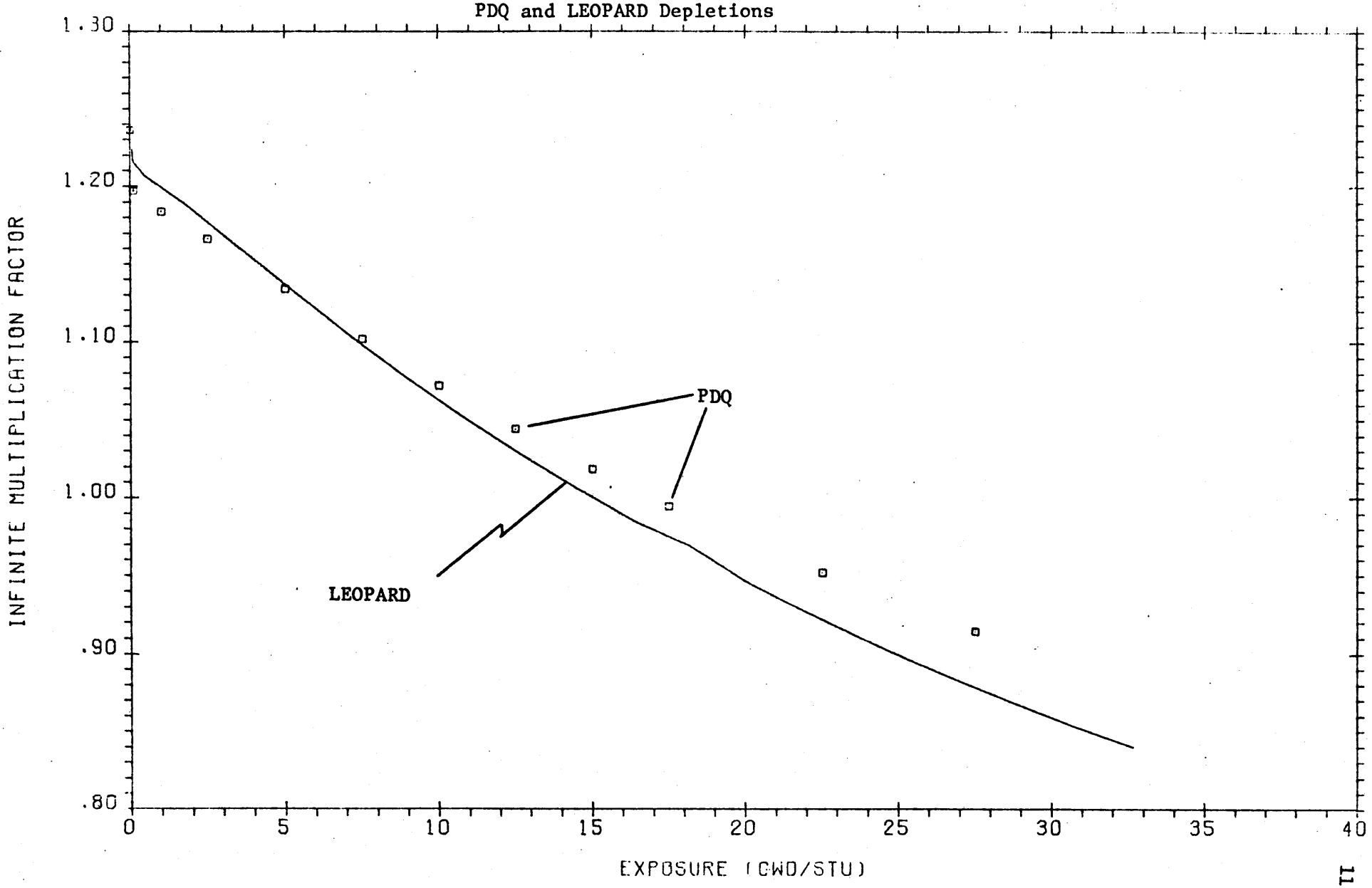

Figure 8-3 BUNDLE INFINITE MULTIPLICATION FACTOR VS EXPOSURE FROM PDQ to 4 GWD/ST

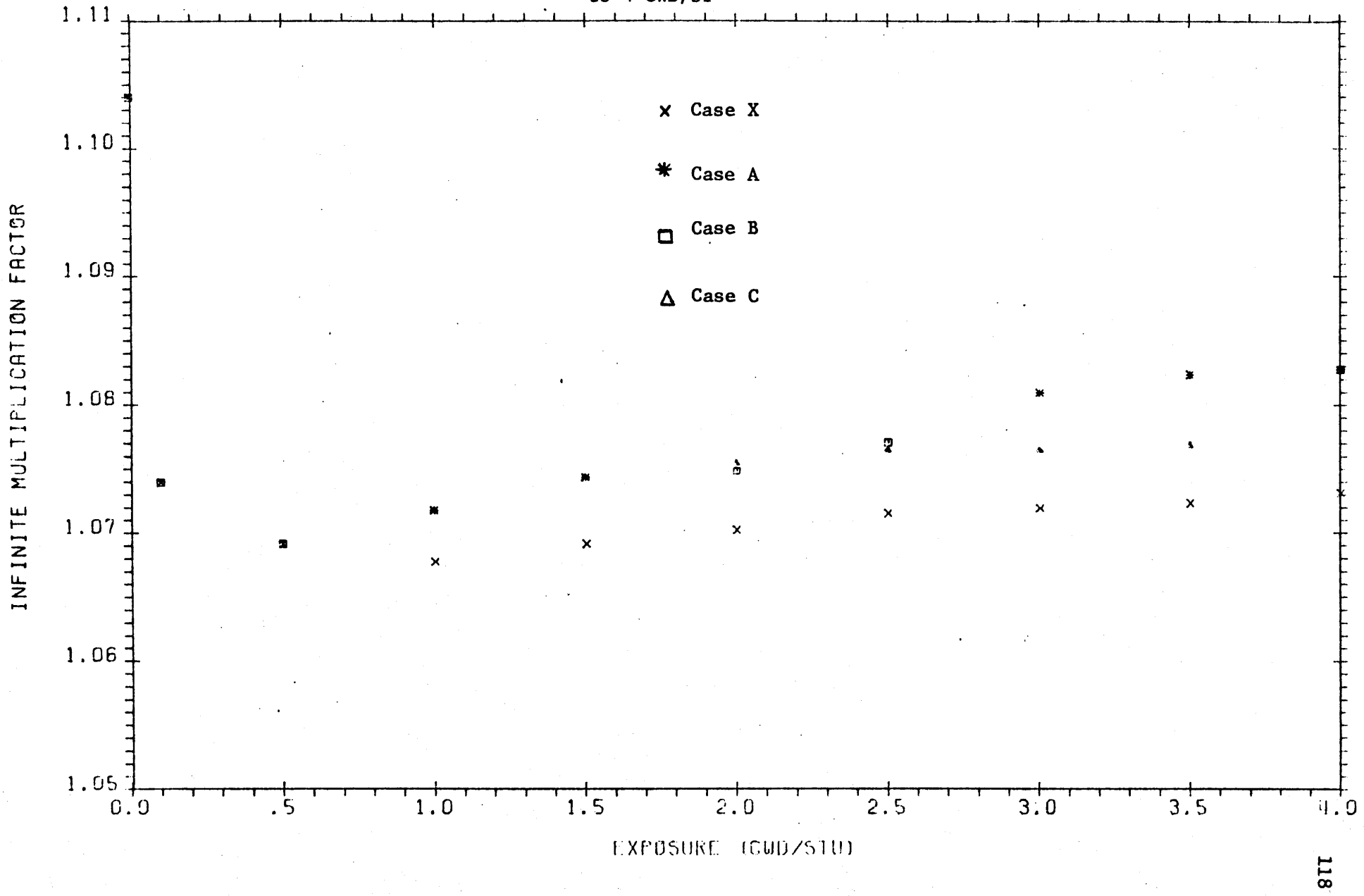

Figure 8-4

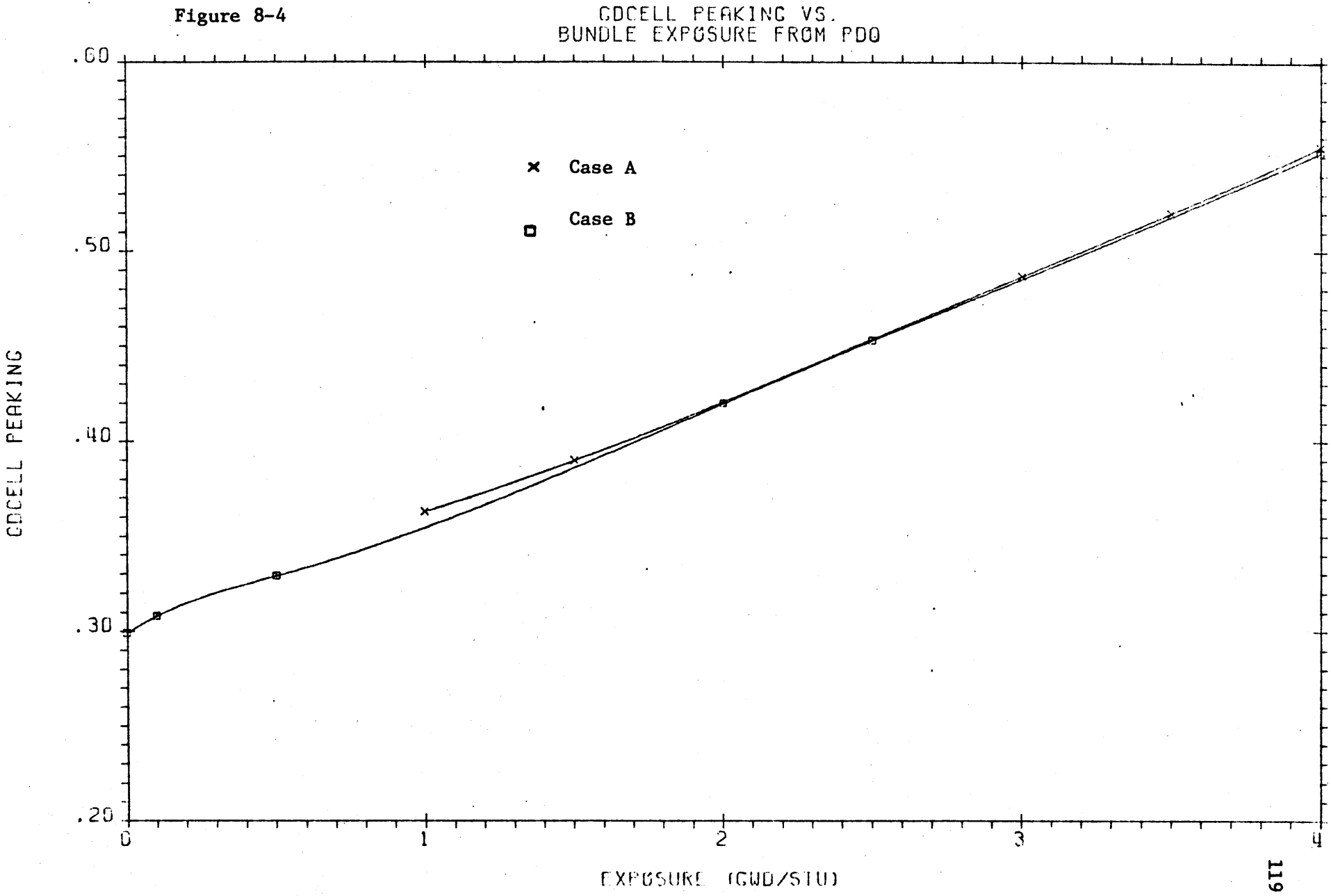
CDCELL PEAKING VS.
BUNDLE EXPOSURE FROM PDQ
Case A
Case B
CDCELL PEAKING
.60
.50
.40
.30
.20
0
1
2
3
4
EXPOSURE (GWD/STU)

Figure 8-5

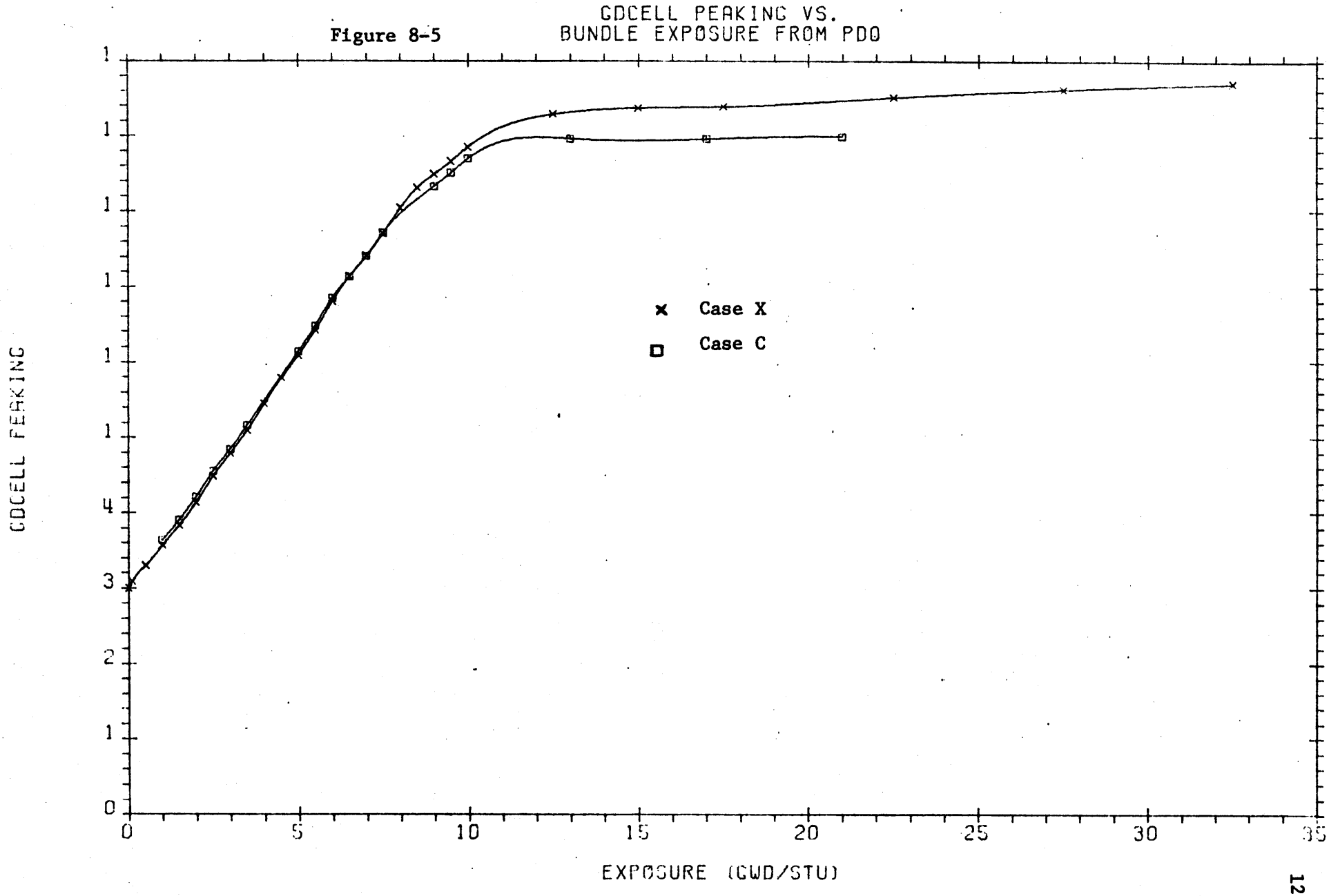
GDCELL PEAKING VS.
BUNDLE EXPOSURE FROM PDQ
GDCELL PEAKING
EXPOSURE (GWD/STU)
Case X
Case C
0
5
10
15
20
25
30

Figure 8-6

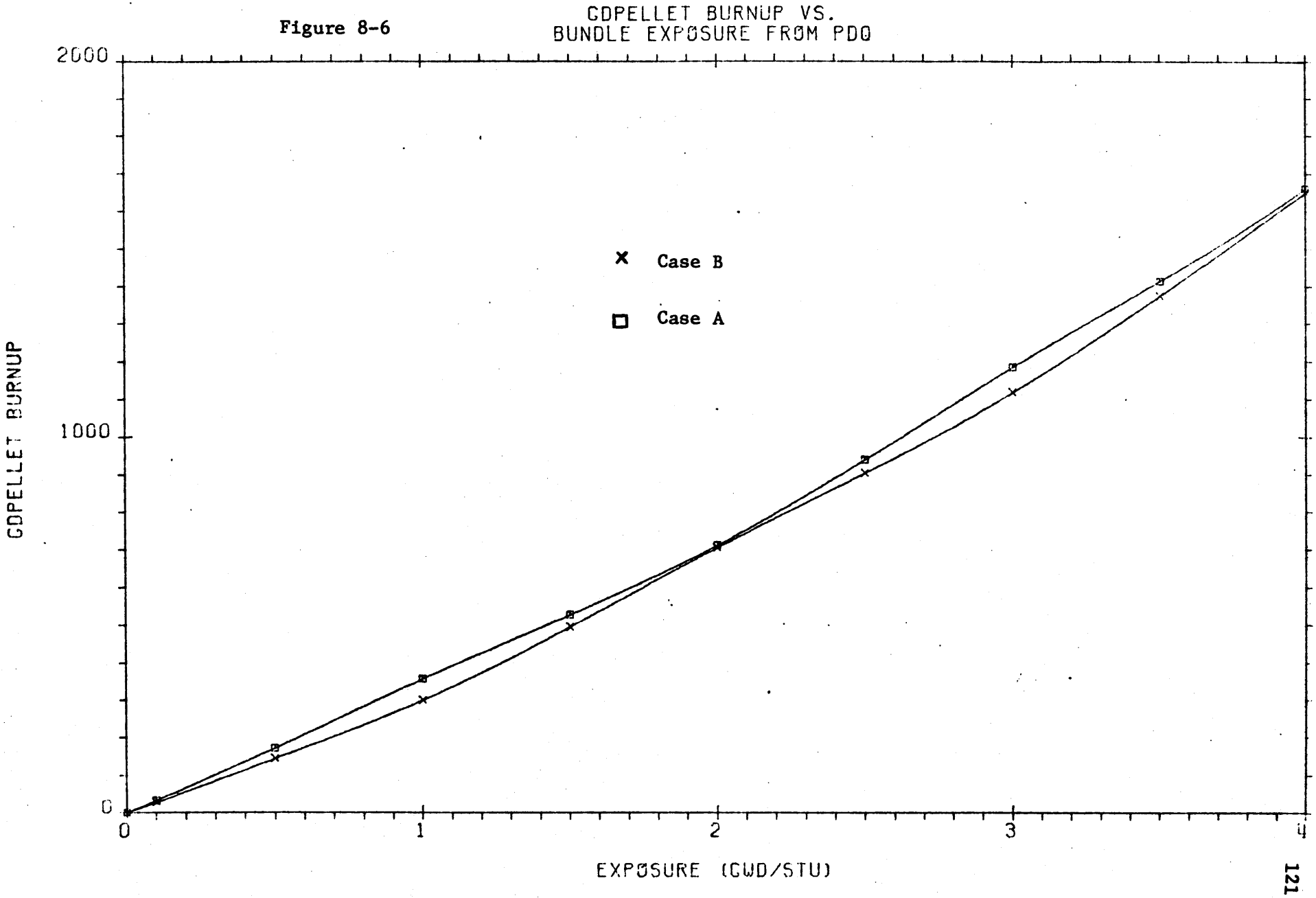
CDPELLET BURNUP VS.
BUNDLE EXPOSURE FROM PDO
2000
1000
0
CDPELLET BURNUP
Case B
Case A
0
1
2
3
4
EXPOSURE (GWD/STU)

Figure 8-7

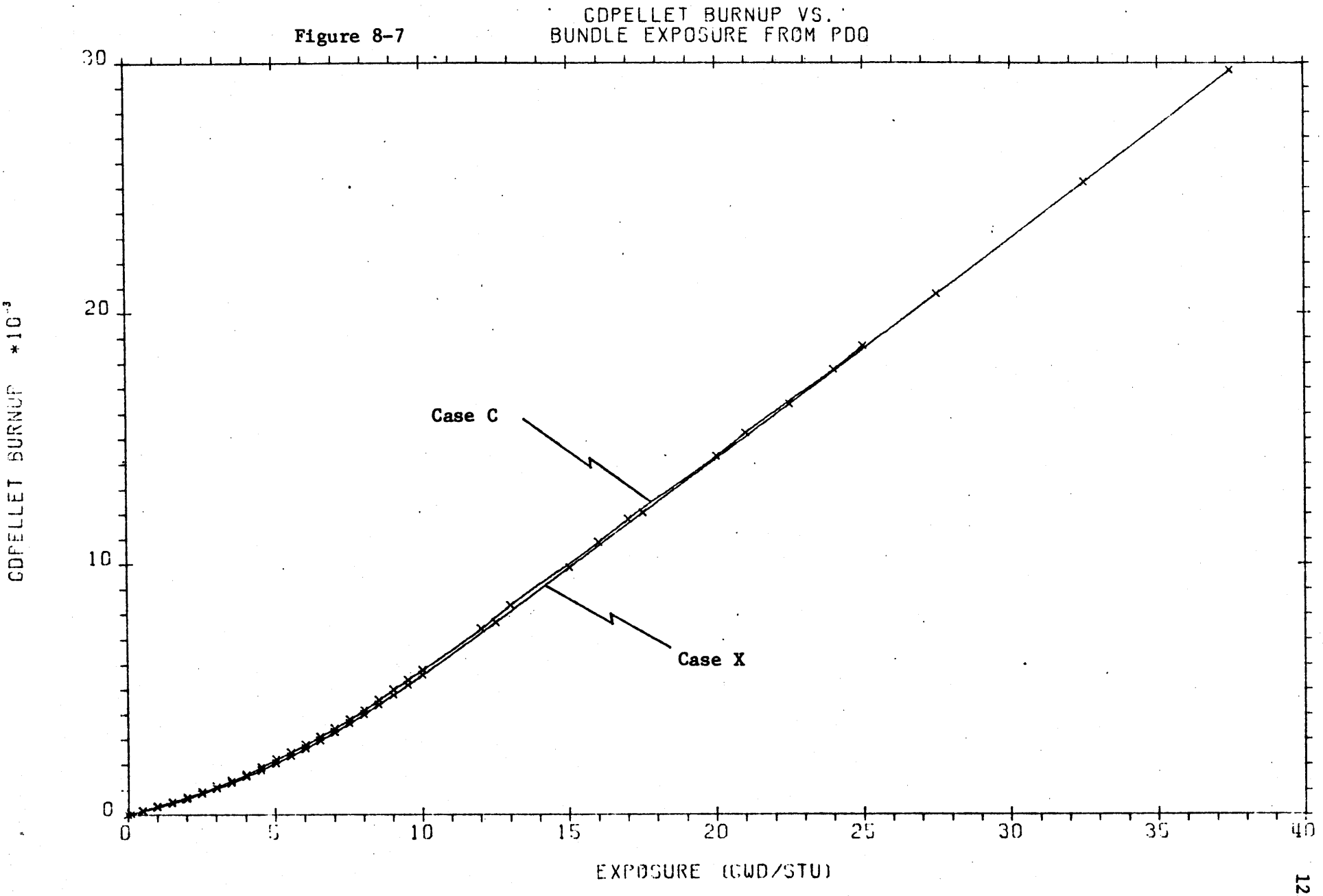
CDPELLET BURNUP VS.
BUNDLE EXPOSURE FROM PDQ
CDPELLET BURNUP *10⁻³
30
20
10
0
0
5
10
15
20
25
30
35
40
EXPOSURE (GWD/STU)
Case C
Case X

Figure 8-8

Wide-Wide Corner

1.043 1.054 1.080	1.119 1.124 1.132	1.009 1.013 1.023	1.153 1.154 1.151	1.113 1.115 1.114	1.126 1.129 1.128	0.974 0.980 0.993	1.072 1.079 1.092
	1.140 1.139 1.136	0.990 0.989 0.990	1.128 1.123 1.112	1.064 1.060 1.052	1.059 1.057 1.048	1.186 1.184 1.173	1.114 1.116 1.115
		1.042 1.037 1.026	0.904 0.901 0.893	0.848 0.846 0.841	0.302 G 0.312 0.369	0.993 0.990 0.983	0.984 0.986 0.987
			G 0.293 0.308 0.346	0.809 0.809 0.805	0.843 0.842 0.837	0.957 0.953 0.949	1.164 1.162 1.151
				WS	0.916 0.914 0.910	0.979 0.975 0.970	1.157 1.154 1.145
		G			0.953 0.949 0.944	1.026 1.021 1.015	1.203 1.280 1.189
						1.120 1.115 1.107	1.037 1.038 1.039
							0.945 0.950 0.964

Key Pin Relative Power @

XXX	0 GWD/ST
XXX	0.1 GWD/ST
XXX	1.0 GWD/ST

Local Peaking and Bundle Characteristics vs. Exposure

Figure 8-9

Wide-Wide Corner

1.087 1.050 1.028	1.118 1.080 1.046	1.022 1.006 2.983	1.131 1.098 1.070	1.102 1.079 1.058	1.115 1.092 1.069	1.001 1.996 0.987	1.092 1.069 1.043
	1.111 1.068 1.031	0.982 0.967 0.955	1.092 1.070 1.052	1.045 1.041 1.037	1.048 1.053 1.054	1.154 1.128 1.103	1.102 1.078 1.056
		1.014 1.006 1.004	0.903 0.928 0.953	0.861 1.903 0.941	0.488[G] 0.698 0.866	0.988 1.000 1.008	0.987 0.983 0.979
			0.457[G] 0.644 0.818	0.830 0.879 0.922	0.854 0.889 0.919	0.949 0.954 0.950	1.129 1.102 1.082
				WS	0.911 0.917 0.924	0.962 0.952 0.947	1.120 1.089 1.067
		G			0.953 0.927 0.923	0.999 1.977 0.962	1.157 1.115 1.085
						1.081 1.043 1.014	1.027 1.003 0.985
							0.970 0.950 0.947

Key Pin Relative Power @

XXX	3.0 GWD/ST
XXX	6.0 GWD/ST
XXX	9.0 GWD/ST

Local Peaking and Bundle Characteristics vs. Exposure

Figure 8-10

Wide-Wide Corner

1.007 1.013 1.046	1.019 1.011 1.024	0.984 0.991 1.008	0.146 1.032 1.026	1.040 1.030 1.027	1.049 1.035 1.030	0.987 0.996 1.015	1.022 1.017 1.032
	0.995 0.970 0.935	0.949 0.946 0.943	1.033 1.014 0.989	1.029 1.014 0.992	1.042 1.023 0.996	1.069 1.035 0.909	1.039 1.030 1.027
		1.001 0.994 0.980	0.972 0.980 0.978	0.967 0.978 0.979	0.950 G 0.963 0.988	1.009 1.004 0.990	0.988 1.001 1.013
			0.907 G 0.922 0.942	0.953 0.969 0.975	0.946 0.963 0.973	0.969 0.978 0.979	1.071 1.065 1.053
				WS	0.940 0.957 0.969	0.954 0.967 0.974	1.058 1.057 1.051
		G			0.935 0.953 0.966	0.962 0.972 0.975	1.068 1.062 1.051
						0.988 0.992 0.983	0.988 0.997 1.012
							0.954 0.974 1.002

Key Pin Relative Power @

XXX	15.0 GWD/ST
XXX	22.0 GWD/ST
XXX	27.5 HWD/ST

Local Peaking and Bundle Characteristics
BOL
CR Inserted

Figure 8-11

Wide-Wide Corner

.477 .405	.549 .506	.554 .517	.688 .645	.722 .680	.810 .765	.811 .778	1.024 1.002
	.690 .655	.692 .668	.872 .849	.894 .875	.964 .948	1.181 1.169	1.171 1.168
		.854 .840	.834 .830	.857 .859	.388 G .394	1.130 1.140	1.134 1.147
			.366 G .372	.936 .950	1.027 1.046	1.191 1.215	1.448 1.477
				WS	1.183 1.211	1.286 1.319	1.511 1.551
		G			1.271 1.305	1.389 1.428	1.619 1.666
						1.538 1.585	1.408 1.452
							1.285 1.326

Key

XX
XX

Iterated
Non-interated

Figure 8-12 BUNDLE MAXIMUM LOCAL PEAKING VS EXPOSURE

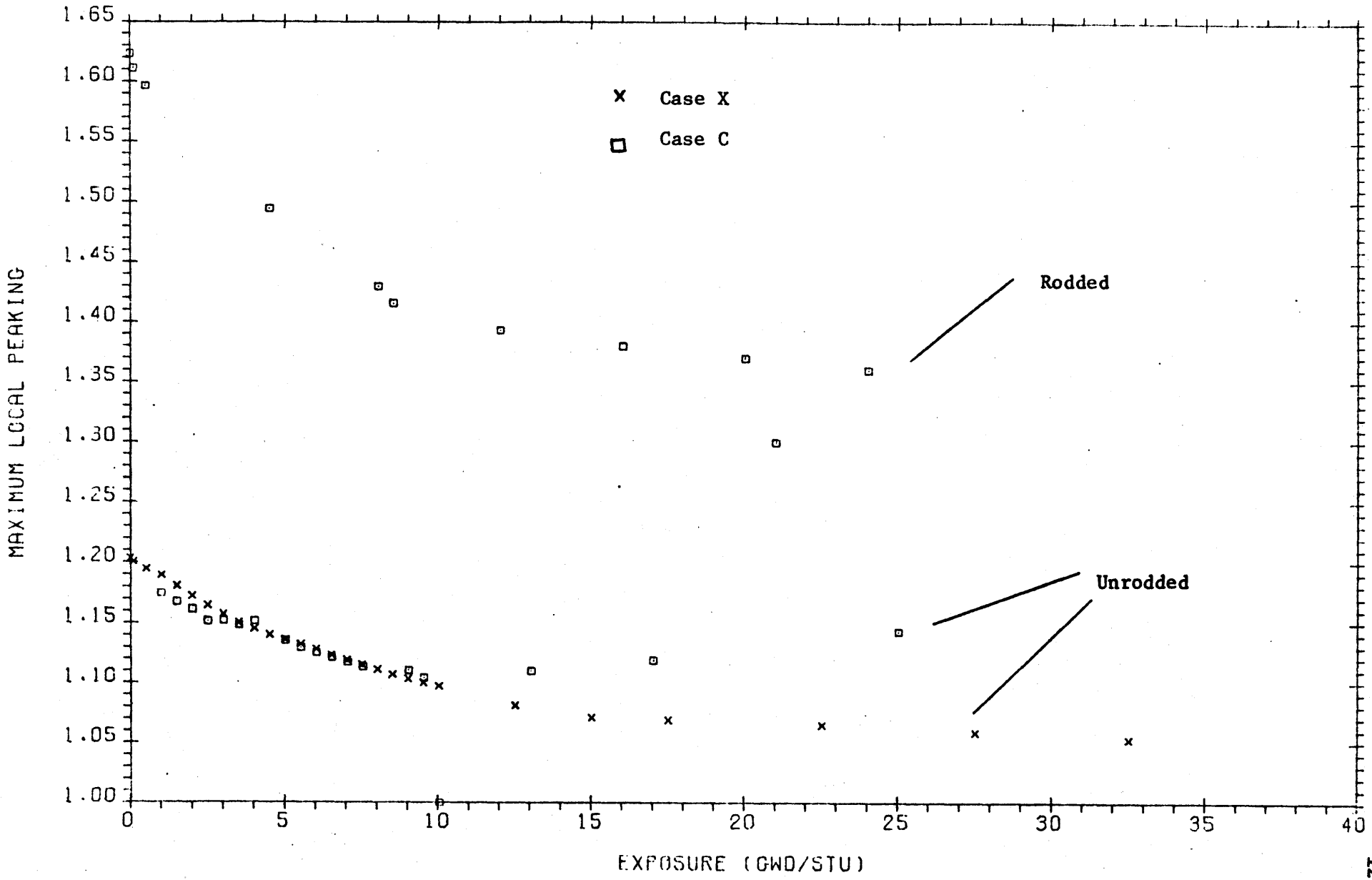

Bundle
Maximum Local Peaking
vs. Exposure

Figure 8-13

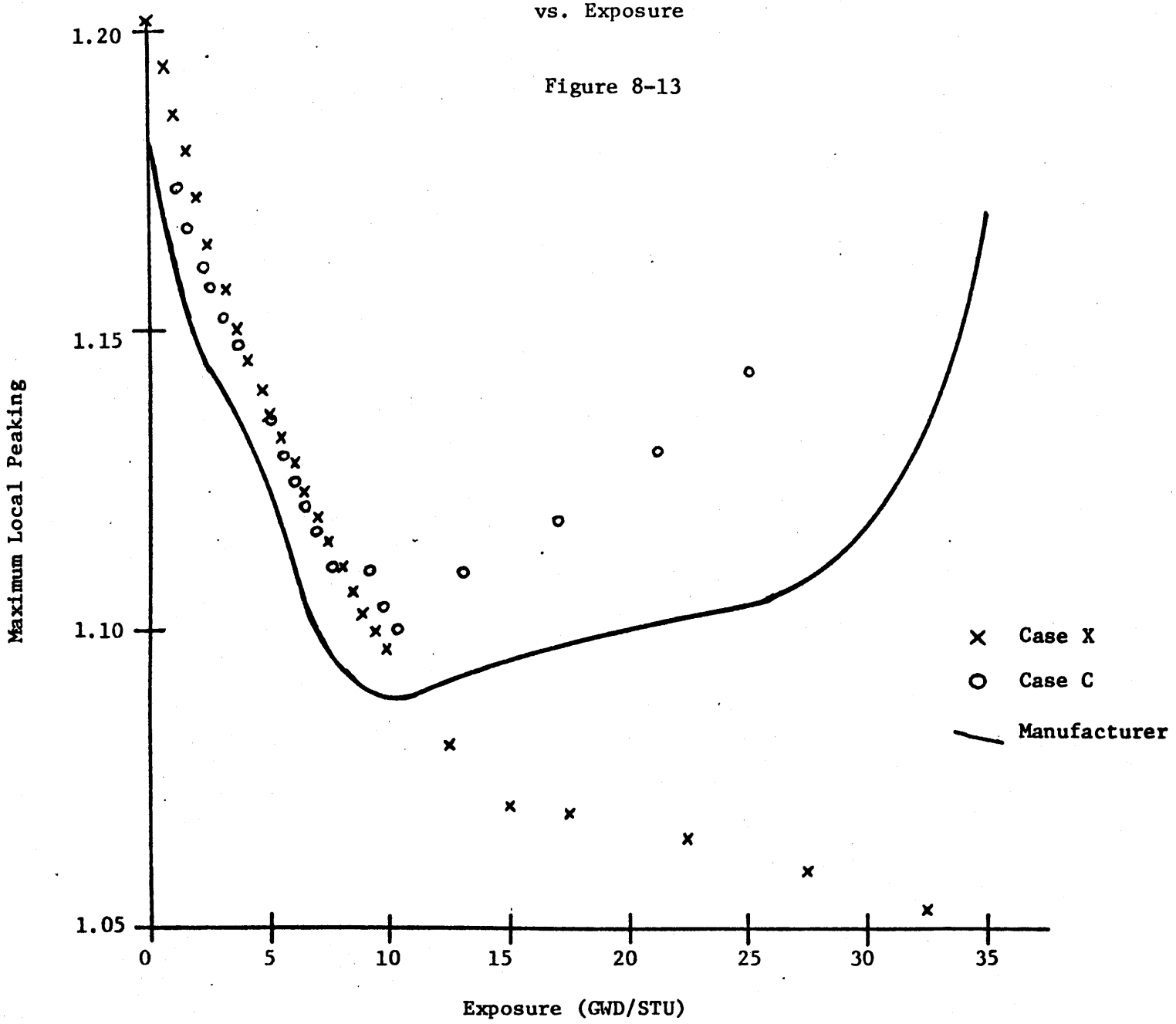

Figure 8-14

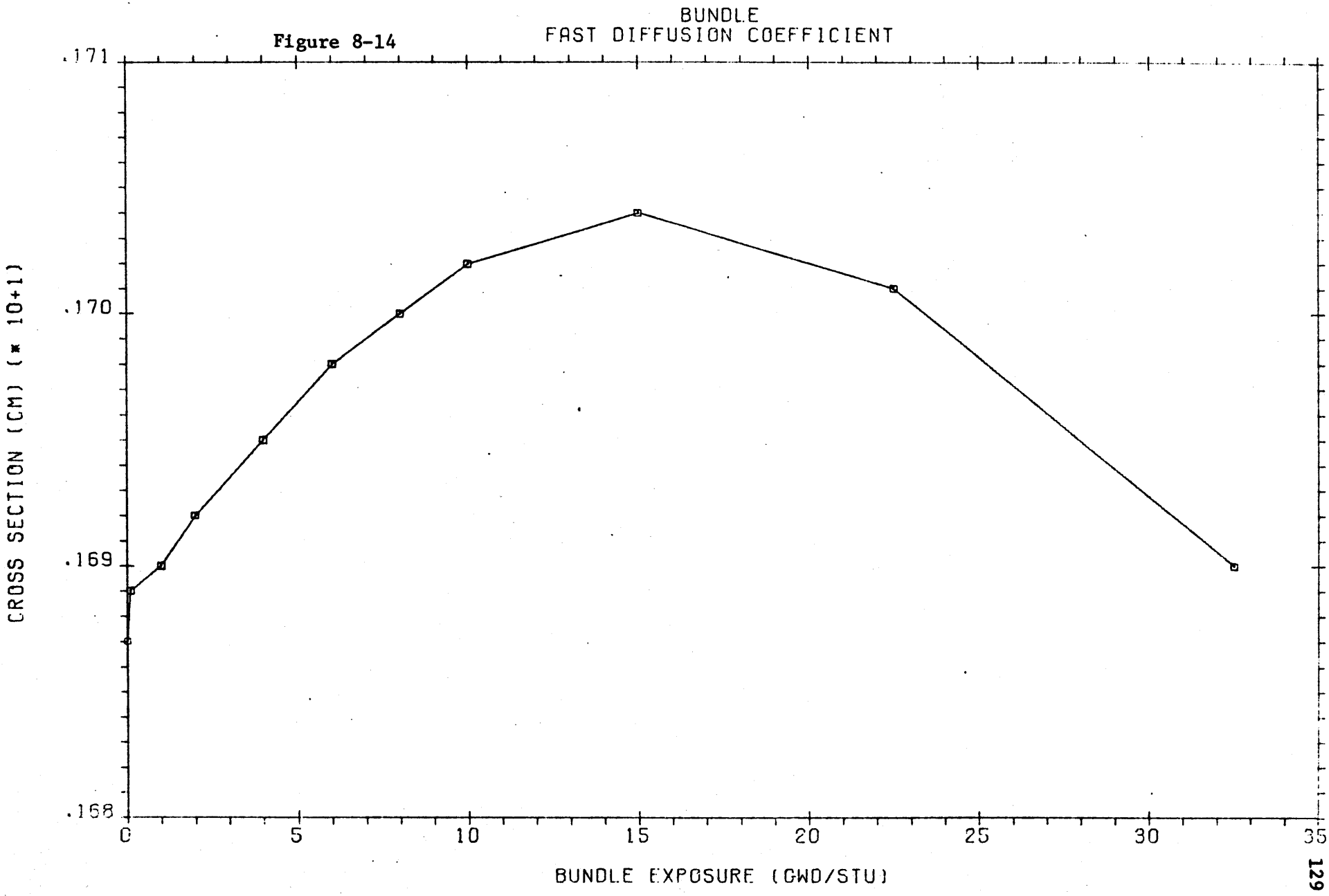
BUNDLE
FAST DIFFUSION COEFFICIENT
.171
.170
.169
.168
CROSS SECTION (CM) (* 10+1)
0
5
10
15
20
25
30
35
BUNDLE EXPOSURE (GWD/STU)

Figure 8-15

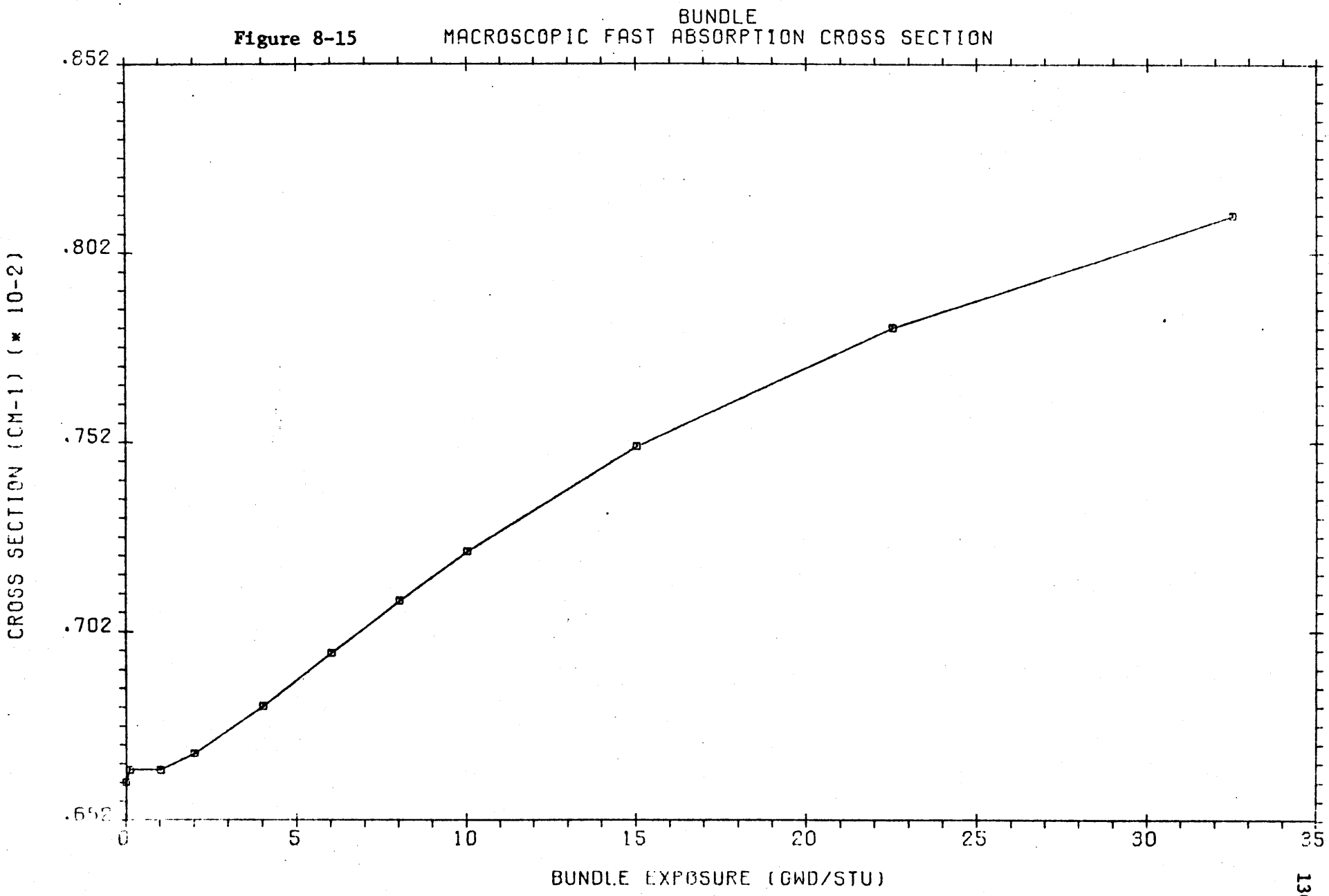
BUNDLE
MACROSCOPIC FAST ABSORPTION CROSS SECTION
.852
.802
.752
.702
.652
CROSS SECTION (CM-1) (* 10-2)
0
5
10
15
20
25
30
35
BUNDLE EXPOSURE (GWD/STU)

Figure 8-16

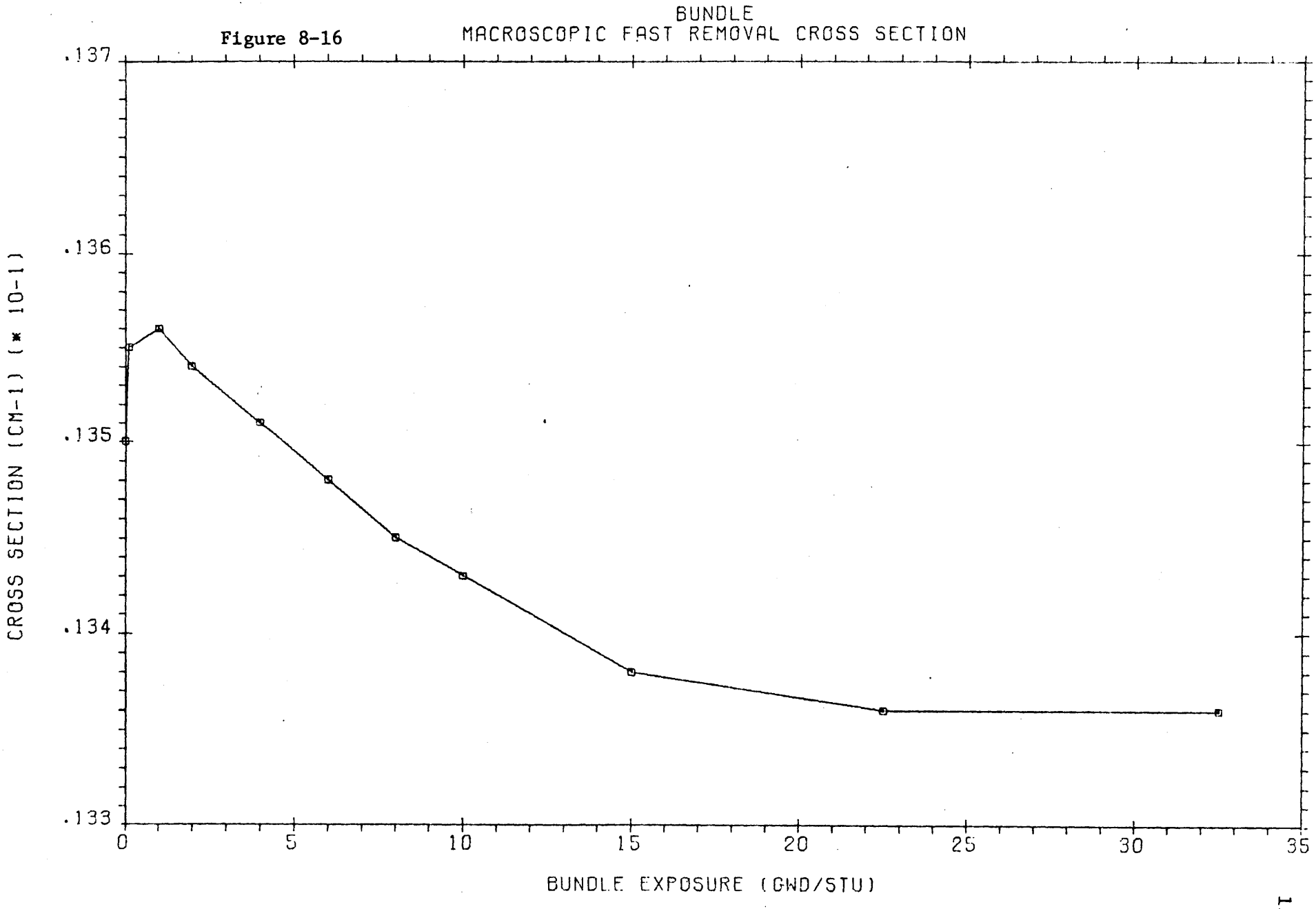
BUNDLE
MACROSCOPIC FAST REMOVAL CROSS SECTION
.137
.136
.135
.134
.133
CROSS SECTION (CM-1) (* 10-1)
0
5
10
15
20
25
30
35
BUNDLE EXPOSURE (GWD/STU)

Figure 8-17

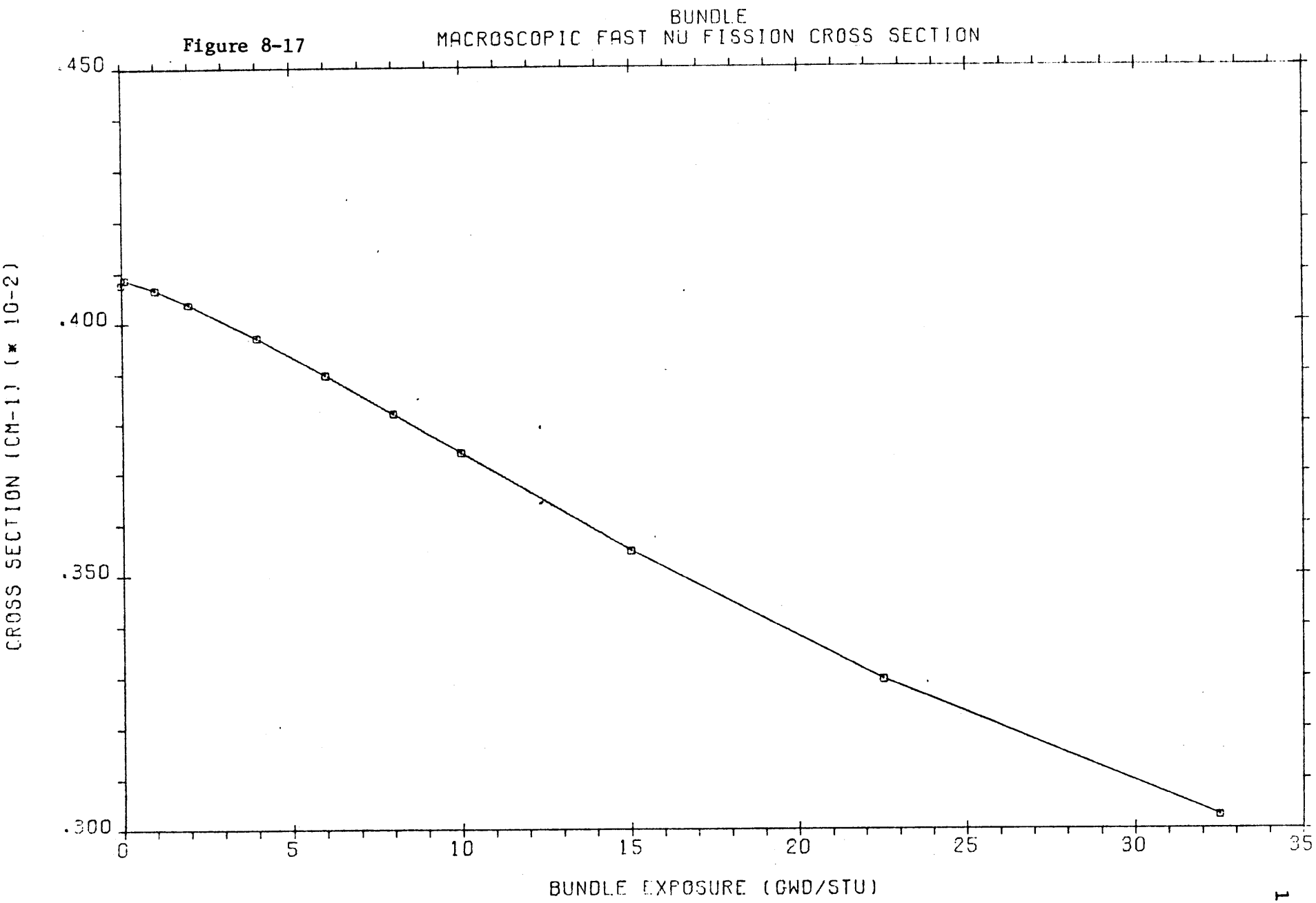
BUNDLE
MACROSCOPIC FAST NU FISSION CROSS SECTION
.450
.400
.350
.300
CROSS SECTION (CM-1) (* 10-2)
0
5
10
15
20
25
30
35
BUNDLE EXPOSURE (GWD/STU)

Figure 8-18

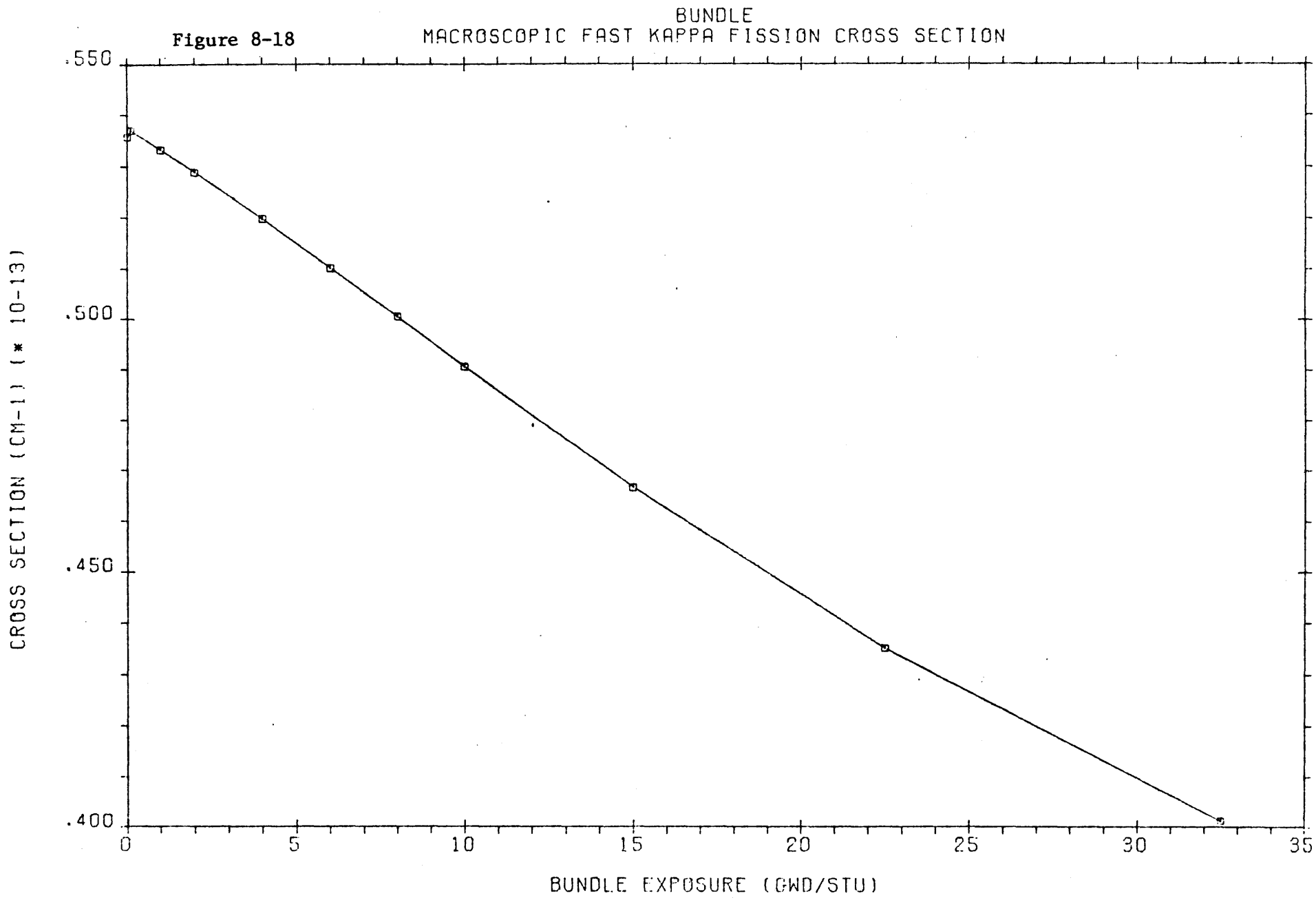
BUNDLE
MACROSCOPIC FAST KAPPA FISSION CROSS SECTION
.550
.500
.450
.400
CROSS SECTION (CM-1) (* 10-13)
0
5
10
15
20
25
30
35
BUNDLE EXPOSURE (GWD/STU)

Figure 8-19

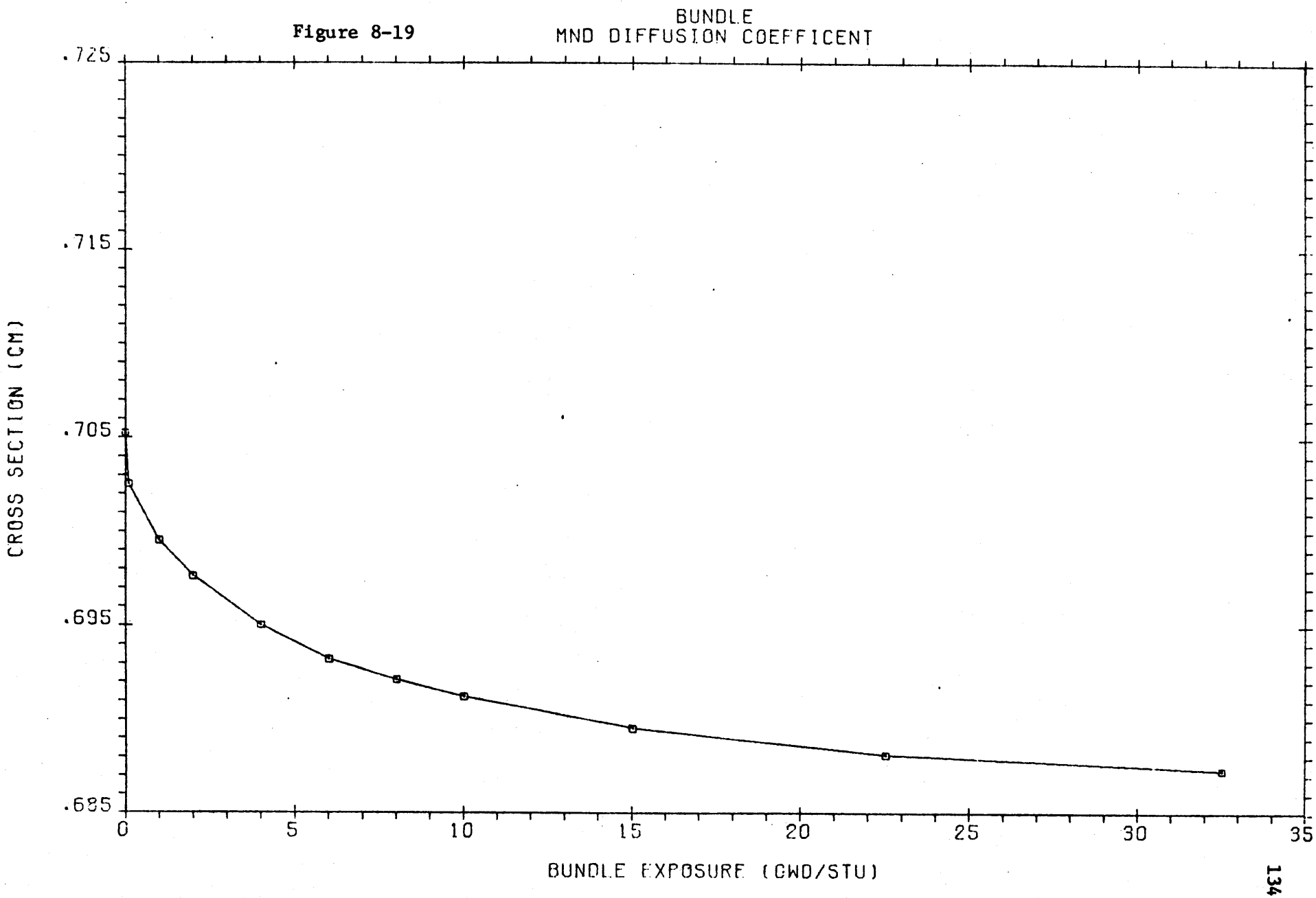
BUNDLE
MND DIFFUSION COEFFICENT
.725
.715
.705
.695
.685
CROSS SECTION (CM)
0
5
10
15
20
25
30
35
BUNDLE EXPOSURE (GWD/STU)

Figure 8-20

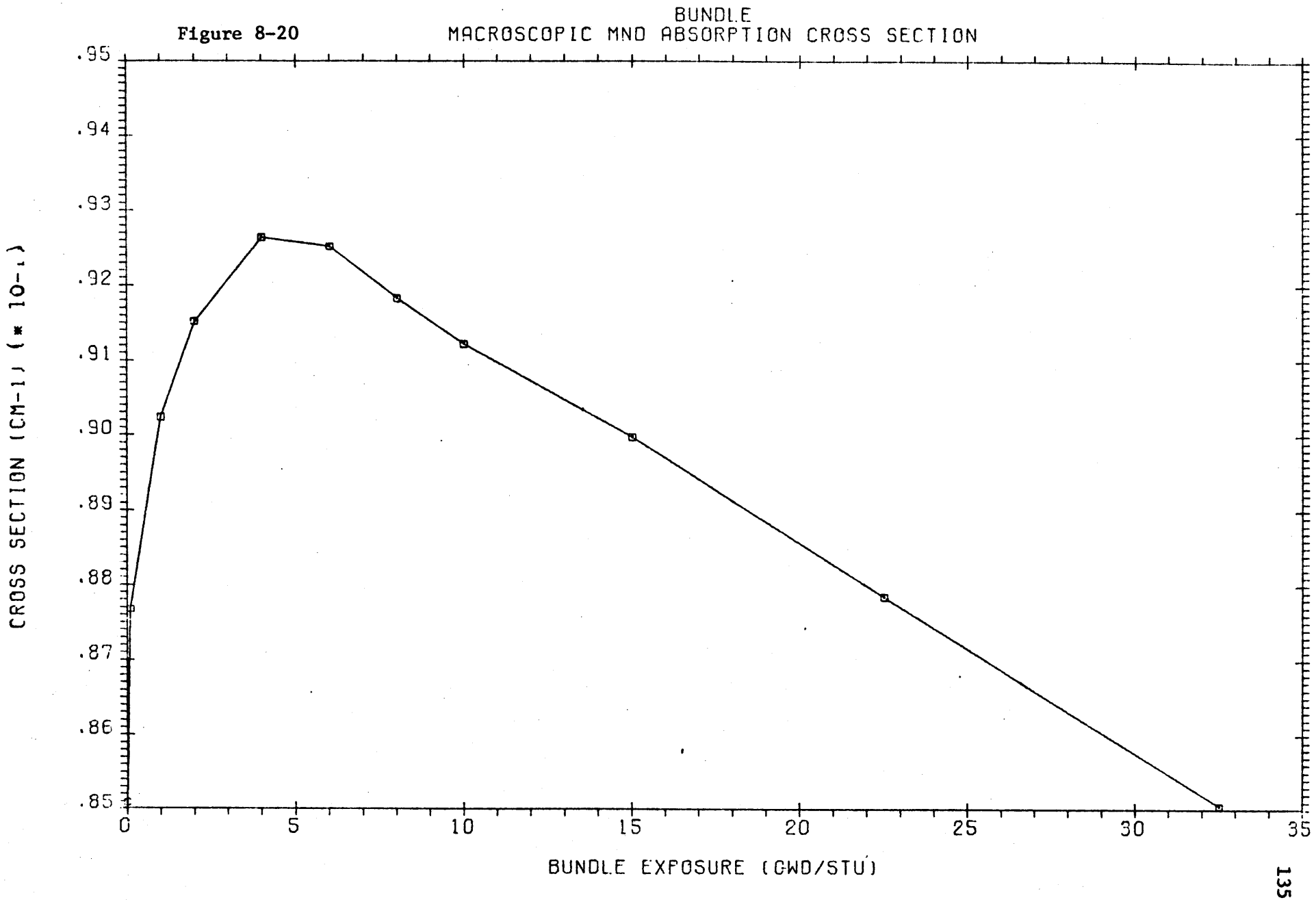

11/23/76

Figure 8-21

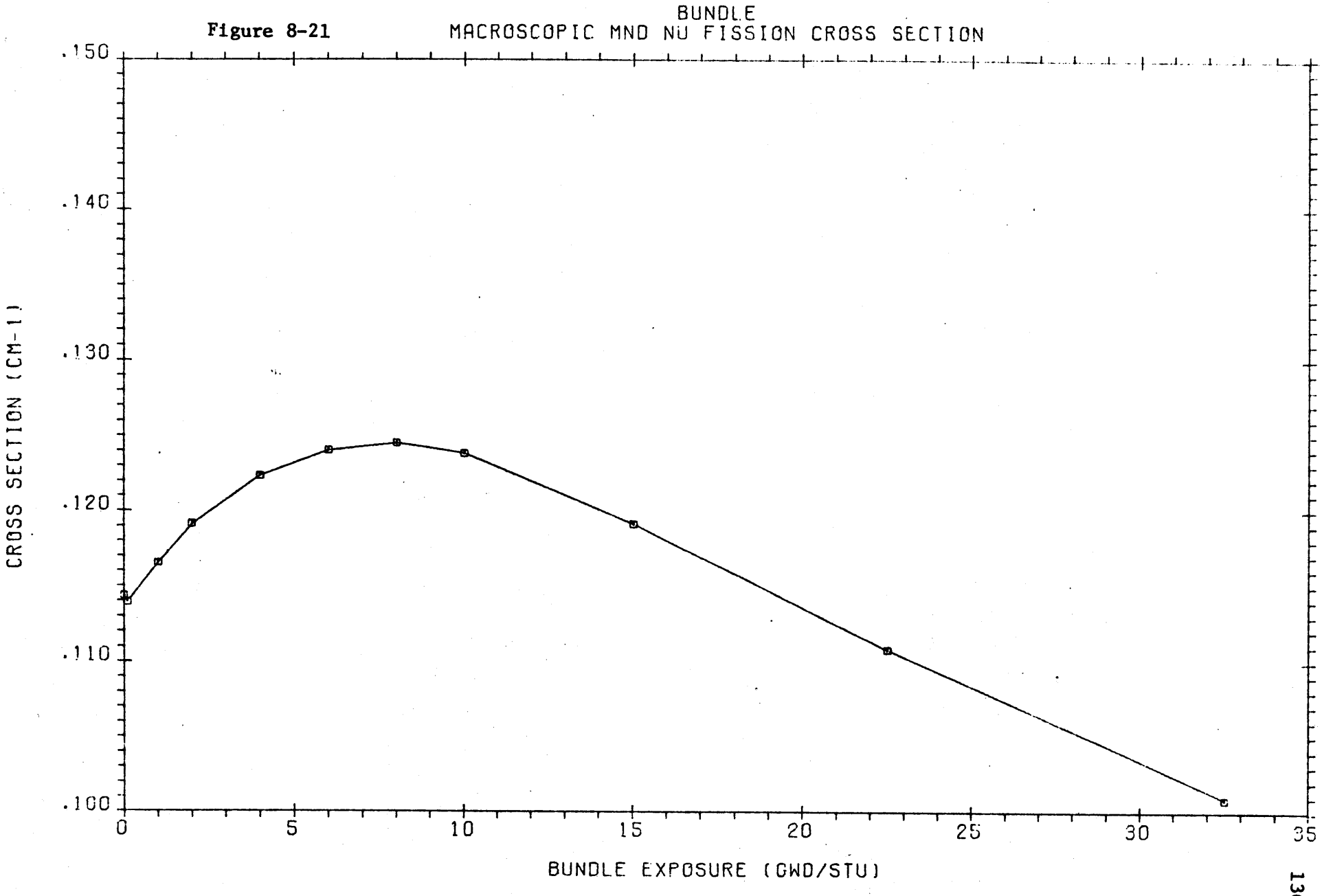
BUNDLE
MACROSCOPIC MND NU FISSION CROSS SECTION
.150
.140
.130
.120
.110
.100
CROSS SECTION (CM-1)
0
5
10
15
20
25
30
35
BUNDLE EXPOSURE (GWD/STU)

Figure 8-22

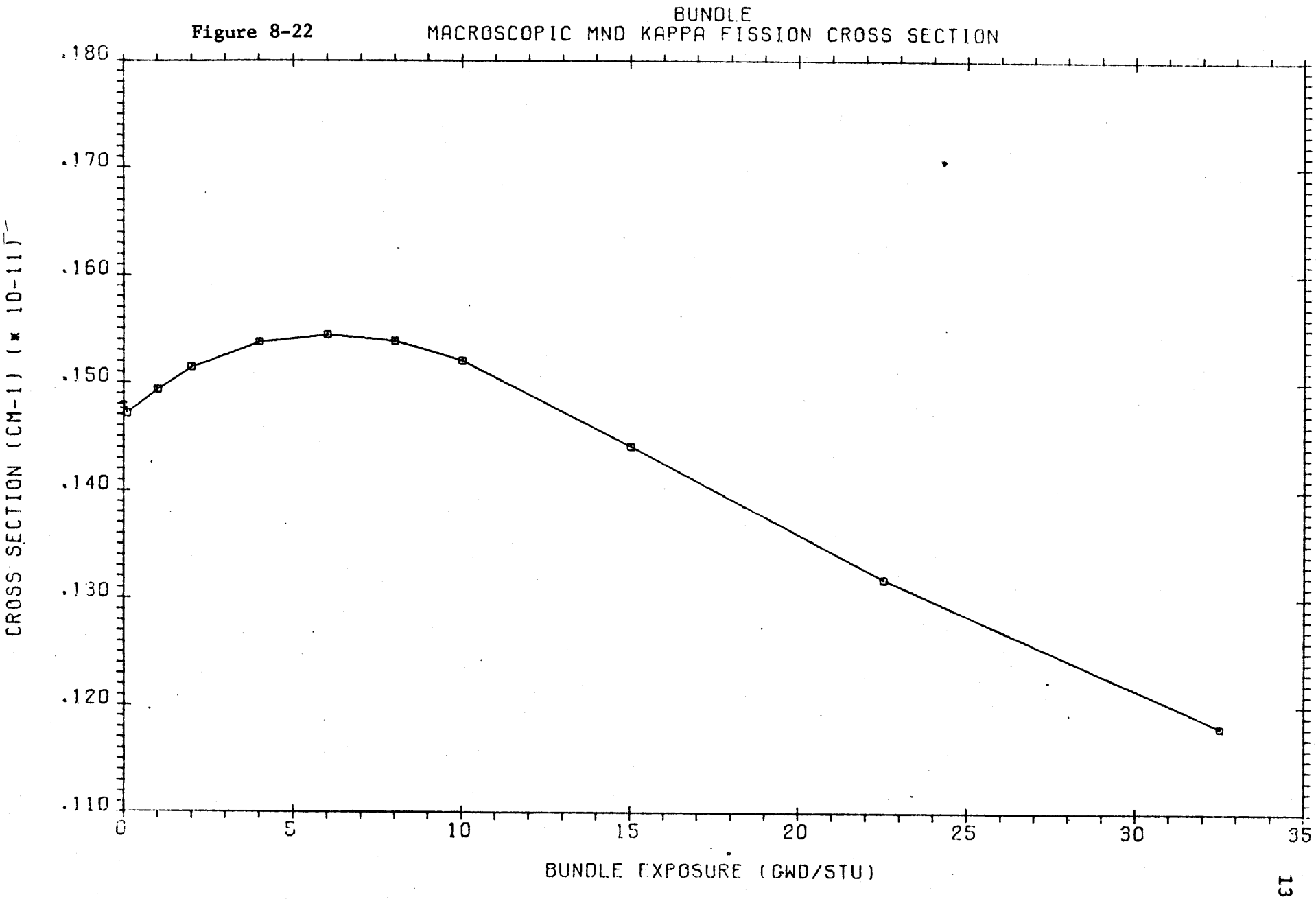
BUNDLE
MACROSCOPIC MND KAPPA FISSION CROSS SECTION
.180
.170
.160
.150
.140
.130
.120
.110
CROSS SECTION (CM-1) (* 10-11)
0
5
10
15
20
25
30
35
BUNDLE EXPOSURE (GWD/STU)

Figure 8-23

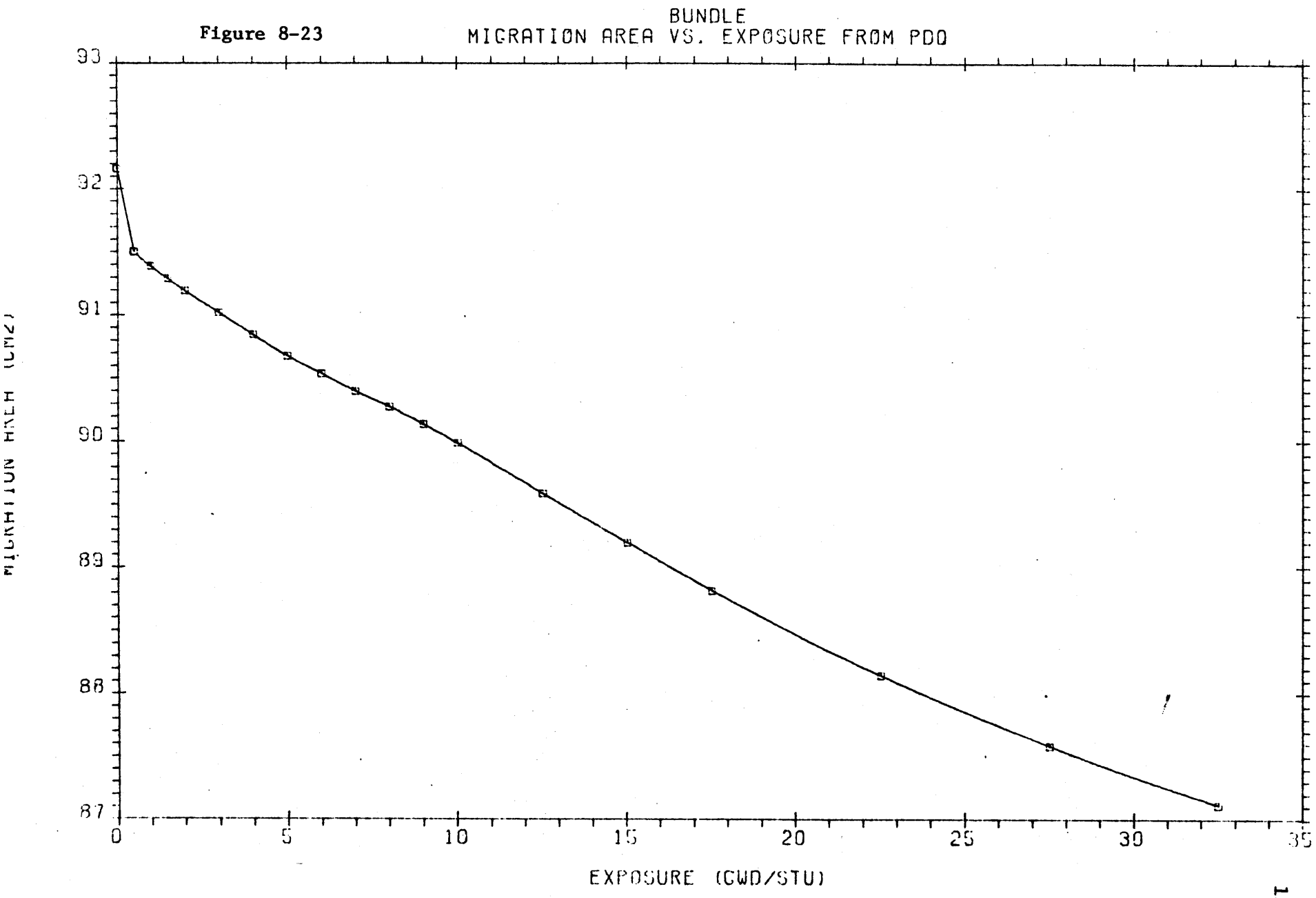
BUNDLE
MIGRATION AREA VS. EXPOSURE FROM PDO
93
92
91
90
89
88
87
0
5
10
15
20
25
30
35
EXPOSURE (CWD/STU)

Figure 8-24 BUNDLE CRITICAL BUCKLING VS. EXPOSURE FROM PDQ

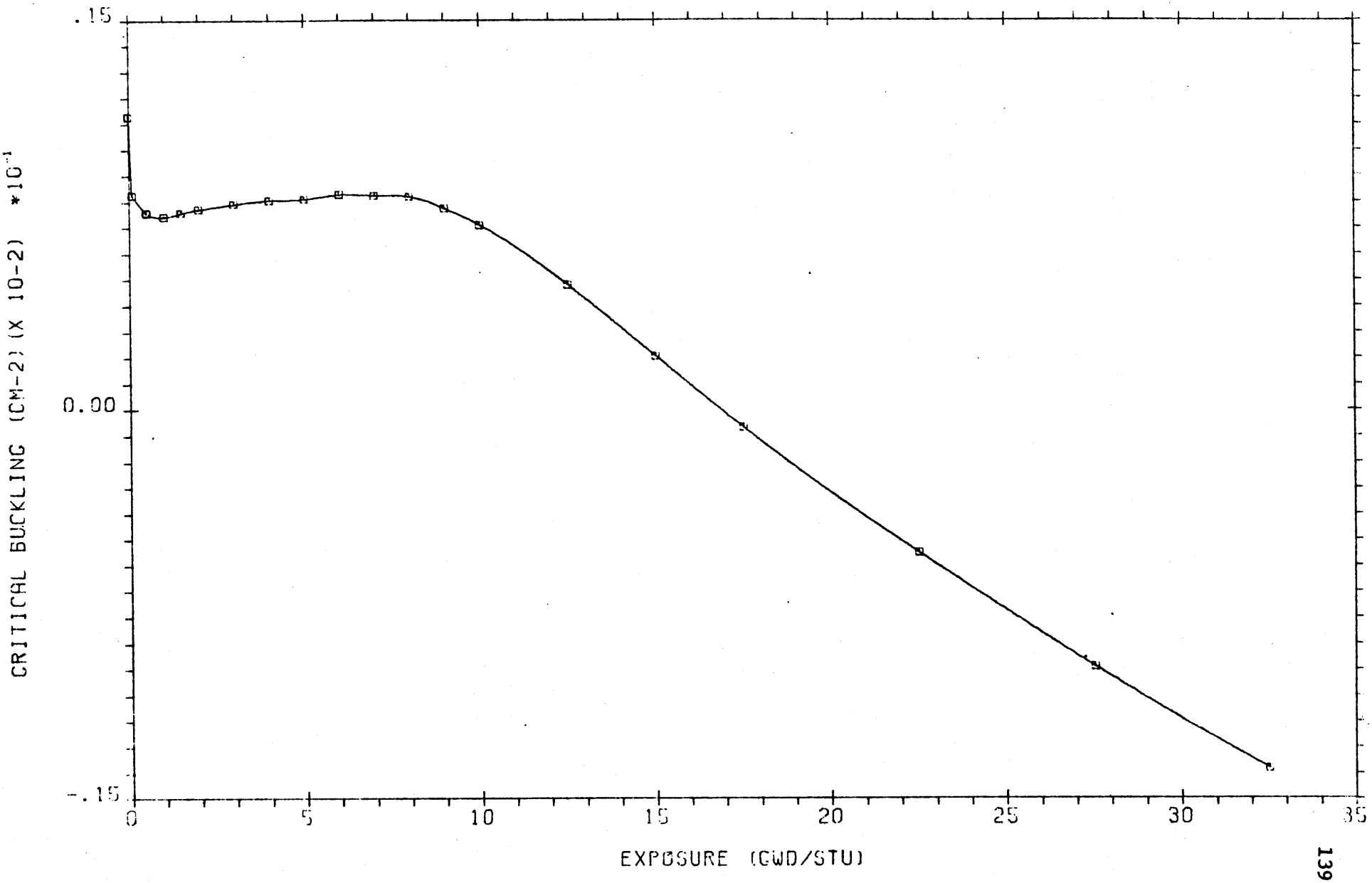

9.0 CONCLUSIONS AND RECOMMENDATIONS FOR FURTHER WORK

Discussions with personnel at Yankee Atomic indicate that the results presented in Chapter 8 are in reasonable agreement with the values they use for the Vermont Yankee core. The good agreement (within a few percent) between the exposure dependent maximum local peaking factor as calculated here and as shown by the fuel supplier (see Figure 8-13) is further indication of the usefulness of the present simple procedure for BWR bundle calculations.

This procedure has been used to examine the dependence of k_∞ and local peaking on control rod insertion history. Variations of about one percent in k_∞ and several percent in local peaking appear to be attainable. The precise extent of these variations may be subject to further revision as improvements are made in the calculational model.

Such improvements and extensions of the model include:

1. Extension of the model to 3 or 4 energy groups.
2. Extension to a four bundle, rather than a single bundle model. This would allow a more realistic treatment of effects due to control rod insertion and non-identical neighbor bundles.
3. Application to the case of varying void history.
4. Assessment of the effect of control rod insertion on cross sections for fuel unit cells. This is ignored in the current model.
5. Development of a method to calculate cold k_∞'s as a function of exposure using isotopics generated in the hot depletions. This would be useful in calculating cold shutdown margins.

6. Use of the model to calculate void coefficients for BWR bundles.

References

1. Martin, C.L., "Lattice Physics Methods", GE Licensing Topical Report NEDO-20913, July, 1976.

2. Vermont Yankee Nuclear Power Station FSAR Docket No. 50-271.

3. Vermont Yankee Nuclear Power Station, Reload Application for 8x8 Fuel, NEDO-20558, July, 1974.

4. Barry, R. F., "LEOPARD - A Spectrum Dependent Non-Spatial Depletion Code for the IBM-7094", WCAP-3269-26, September, 1963.

5. BOHL, H., et.al., "MUFT-4 Fast Neutron Spectrum Code for the IBM-704", WAPD-TM-172, July, 1957.

6. Amster, H. and R. Suarez, "The Calculation of Thermal Constants Averaged Over a Wigner-Wilkins Flux Spectrum: Description of the SOFOCATE Code", WAPD-TM-39, January 1957.

7. Strawbridge, L.E., and R. F. Barry, "Criticality Calculations for Uniform, Water Moderated Lattices", NSE, 23, p. 58, September, 1965.

8. Weinberg, A. M., and E. P. Wigner, The Physical Theory of Neutron Chain Reactors, p. 302, University of Chicago Press, (1958).

9. Amouyal, A., P. Benoist, and J. Horowitz, "New Method of Determining the Thermal Utilization Factor in a Unit Cell", J. Nuclear Energy, 6, (1957).

10. Wigner, E. P., and J. E. Wilkins, Jr., "Effect of the Temperature of the Moderator on the Velocity Distribution of Neutrons, with Numerical Calculations for H as Moderator", AECD-2275, September, 1948.

11. Stamm'ler, R. J. J. et. al., "Neutron Thermalization in Reactor Lattice Cells", IAEA Technical Report Series, No. 68, October, 1966.

12. Poncelet, C. G., "LASER - A Depletion Program for Lattice Calculations Based on MUFT and THERMOS", WCAP-6073, April, 1966.

13. Honeck, H., "THERMOS, A Thermalization Transport Theory Code for Reactor Lattice Calculations", BNL-5826 (1961).

14. Brown, H., and D. St. John, "Neutron Energy Spectrum in D_2O", DP-33 (1954).

15. Koppel, J. U., and J. A. Young, "Neutron Scattering by Water Taking into Account the Anisotropy of the Molecular Vibrations", Nuclear Science and Engineering 19:412, August, 1964.

16. Nelkin, M., "Scattering of Slow Neutrons by Water", Physical Review 119 (2):714, July, 1960.

17. Honeck, H. C., "Some Methods for Improving the Cylindrical Reflecting Boundary Condition in Cell Calculations of the Thermal Neutron Flux", Trans. ANS 5(2):350, November, 1962.

18. Moller, Shore, Sailor, "Low Energy Neutron Resonances in Erbium and Gadolinium", NSE, 8, 183-192 (1960).

19. Henry, A. F., "A Theoretical Method for Determining the Worth of Control Rods", WAPD-218, August, 1959.

20. Cadwell, W. R., et. al., "The PDQ-5 and PDQ-6 Programs for the Solution of the Two-Dimensional Neutron Diffusion-Depletion Problem", WAPD-TM-477, January, 1965.

21. Varga, R. S., Matrix Iterative Analysis, Prentice Hall, (1962).

22. Hageman, L. A., and C. J. Pfeifer, "The Utilization of the Neutron Diffusion Program PDQ-5", WAPD-TM-395, January, 1965.

23. Breen, R., O. J. Marlowe, C. J. Pfeifer, "HARMONY-System for Nuclear Reactor Depletion Computation", USAEC Report WAPD-TM-478, 1965.

24. Celnik, J., J. R. Tomonto, J. S. Tulenko, "Repressurization of Fission Products in Thermal Power Reactors Containing UO_2 and Plutonium Recycle Fuel", Trans. Am. Nucl. Soc., 10, 516 (1967).

25. Rampolla, D. S., "Adjusting Absorption Cross Sections in Transport Calculations to Achieve Specified Region Capture Integrals", NSE, 31, 396-414 (1968).

26. Radkowsky, A., ed., "Naval Reactors Physics Handbook", Vol. I, pp. 454-457, TID-7030, (1964).

27. Henry, A. F., Nuclear Reactor Analysis, MIT Press, 1976.

28. Klotzken, G., "A Method of Monte Carlo Fitting", NSE, 57, 218-247, (1975).

29. Mertens, P. G., "Analysis of Conventional and Recycle Unit Assemblies for the Yankee (Rowe) PWR", MIT-134, (Draft Report), Department of Nuclear Engineering, Massachusetts Institute of Technology, (1971).

30. Momsen, B. F., "An Analysis of Plutonium Recycle Fuel Elements in San Onofre-I", MITNE-161, Department of Nuclear Engineering, Massachusetts Institute of Technology, June, 1974.

31. Wagner, M., "Spatial Distribution of Resonance Absorption in Fuel Elements", NSE, 8, p. 278, September, 1960.

32. Williamson, H. E., F. H. Megerth, "Economic Evaluation of Control Rod Materials and Fabrication Processes", GEAP-4013, May, 1962.

33. Michelini, M., "Neutron Transmission Probabilities Across Control Blades Filled with Round Tubes: Formulation and Accuracy", NSE, 42, 162-170, (1970).

34. Denver, D. J., E. E. Pilat, R. J. Cacciapouti, "Application of Yankee's Reactor Physics Methods to Maine Yankee", YAEC-1115, Yankee Atomic Electric Company, October, 1976.